Nanostructured oxide semiconductors grown on fabric for wearable thermoelectric power generator with UV shielding

DOCTORAL THESIS

Nanostructured oxide semiconductors grown on fabric for wearable thermoelectric power generator with UV shielding

Pandiyarasan Veluswamy

(55445023)

Graduate School of Science and Technology,

Educational Division

Department of Nanovision Technology

Shizuoka University

June 2017

Acknowledgement

Three years flew by just as some short months, and I feel very prosperous to have carried out my Ph. D. research work at Shizuoka University, Hamamatsu. This memory would live with me forever just like the blemish on my face which, coincidently, was the start to this delightful and extremely pleasing three-year trip. The completion of my research thesis would not have been possible without the help and support of others. I would like to express gratitude to those who have contributed their time and knowledge to guide me along the way.

First and foremost, I would like to express my deepest gratitude to my supervisor, Associate Professor Hiroya Ikeda for his supervision and advice throughout my research. I want to thank him for believing in me and providing me the opportunity to work at Nanodevice, Shizuoka University as a Ph.D. candidate. He patiently provided the vision, timely encouragement and valuable advice necessary for me to proceed through the doctoral program and to complete my thesis. Furthermore, under his guidance I have developed myself to be an independent researcher, I have gained new knowledge and learned a lot from him.

It is my pleasure to pay tribute also to Prof. Yasuhiro Hayakawa for giving me the opportunity to work in his lab. I learnt a lot with healthy discussions we had regarding my work that helped me grow in my research area. I also would like to express my heartfelt thankfulness to the other committee members, Professor Hirokazu Tatsuoka and Professor Akihiro Ishida for their supports, motivation and helpful suggestions on this thesis.

Abstract

Clothing and textile materials are the elements that are almost always present and is customizable to each human being. In the last few years, the smart textiles feature such as stain resistance, antimicrobial, superhydrophobic/ super-hydrophilic, antistatic, sensors, power generators, electromagnetic/ ultraviolet interference shielding, wrinkles resistant, and shrink-proof abilities. Since the energy and environmental efficiency governance are becoming the demand, there is a need for alternate renewable energy conversion system that will reduce the greenhouse gases emission and improve the energy competence.

The eco-friendly renewable energy source for smart textile from various environmental origin such as photovoltaic (PV) utilizing the light source, thermoelectric (TE) employs temperature difference, piezoelectric (PE) proving kinetic energy from vibrations or shocks and radio frequency (RF) energy were accepting moving waves of electric and magnetic together. The ability of harvest energy from ambient sources enables the lifetime of battery-operated for wearable devices. The human body is a constant heat source, and typically a temperature difference exists between body skin and the environment. Even in a scenario where the wearer located in a dark room or stationary or presence in air condition room, energy can be produced. Because the thermoelectric generates electrical power from heat flow across a temperature gradient, and it is based on the solid-state technology with the principle of Seebeck effect. As the heat flows from hot to cold, free charge carriers (electrons and holes) in the material are driven, and the resultant voltages. Similarly, depending on power generator size, place, and activity of human body is suitable for harvesting energy in the range of microwatts to hundreds of milliwatts.

The performance of wearable thermoelectric power generator (WTPG) material is closely related to the dimensionless figure-of-merit (zT), $zT=[(S^2\sigma)/\kappa]$ T, where S represents as thermopower (Seebeck coefficient), σ represent as electrical conductivity, κ represent as thermal conductivity, and T is the temperature respectively. Since the advent of nanostructured power generation materials exhibits high zT owing to the maximization of power factor ($S^2\sigma$) and reduction in κ. Throughout the literature, the nanometer-scaled crystalline structure can reduce κ by enhancing the boundary scattering of phonons, but it degrades the power factor, simultaneously. With the aim of bettering the power factor, an increment of thermopower is expected by tailoring the density of states through nano-structuration such as nanocomposites and superlattices and doping modulation.

Traditional materials for thermoelectric such as bismuth telluride have been studied and utilized commercially for the last half century, but recent advancements in materials selection are one of the principal function of the active thermoelectric device as it determines the reliability of the fabrication regarding technical and economic aspects. Recently, many researcher's efforts have been made to utilize oxide nanomaterials for WTPG applications which may provide environmental stable, mechanical flexibility, and light weight with low cost of manufacturing. In precise, fabric containing oxide metals have shown great promise as P-/ N-type materials with improved transport and UV shielding properties. On the other hand, we have focused on ZnO and rGO nanostructures as a high-efficiency WTPG material because they are non-toxic to skin, inexpensive and easy to obtain and possess attractive electronic properties, which means that they are available for clothing with low-cost fabrication. To our observation, we are reporting

about the thermoelectric properties of ZnO and rGO nanostructures coated cotton/ carbon fabric via the solvothermal method for the first time.

In this work, we have shown that enhanced UV shielding of 183.34 and thermoelectric power factor of 22 µW/mK^2, respectively by ZnO mixed nanostructures on cotton fabric (CF) through solvothermal method. It demonstrated that ZnO with mixed nanorods and nanosheets structure could significantly improve its thermoelectric power factor through lower resistivity and higher Seebeck coefficient. After successfully obtaining mixed nanostructures of ZnO, we investigated Ag- and Sb- in ZnO composite through two-step solvothermal method. In composites lead to a high thermopower value of 471.9 µV/ K^{-1} and enhanced UV shielding with a value of 83.96. we consider that this is mainly due to the growth process of ZnO is disrupted, when the Ag composites are introduced, and the growth process is again favored when enough Ag have recombined with the Zn material which may cause the positive effect on the charge separation efficiency. Then the higher value due to the intergranular crystal structure which plays a significant role in charge transport. To take the benefits from reduced graphene oxide (rGO), i.e., lower thermal conductivity due to oxide deficiency defects and high power factor arising from efficient graphene sheets and therefore, the obtained thermopower value of 32 µV/ K^{-1}. Lastly, the carbon fabric coated with ZnO different morphology through ultrasonication assisted solvothermal method was about -0.04 ~ 0.054 µV/K and for bare carbon fabric it was found to be about 0.08 µV/K. In addition to the carrier concentration, it is important to note that there was a change of carrier type from P-type to N-type resulting due to the coating of ZnO on carbon fabric. We understand that these values can be further improved by optimizing composite and improving the surface texture of the carbon fabric.

Contents

Page

CHAPTER 1

Introduction & Literature review

1.1 Background

Turning textile fibers into progressively challenging and innovative product have seen manifold development in the last decade. The most promising characteristics of fibers drive the development of a wide range of fibrous products enabling digital components and electronics to be embedded in them known as smart clothing or smart textiles or smart fabrics. Adopting the new technology of smart fabrics is advantageous since they are relatively lightweight, comfortable, soft, and biodegradable. The move towards function-focus fibrous structures in pavement and embankment reinforcement may seem more appropriate, it implies technological applications such as stain resistance, antimicrobial, superhydrophobic/ super-hydrophilic, antistatic, sensors, power generators, electromagnetic/ ultraviolet interference shielding, wrinkles resistant, and shrink-proof abilities.

Among modern perspective, the wearable devices used to monitor a variety of health and environmental measures are becoming popular, and those devices requires capable of functioning autonomously for extended periods without replacing or recharge of batteries, but it is not practically impossible or ineffective. Since time immemorial, technology focuses to decrease the power consumption of devices so that the battery lasts for years. It has been done long ago, e.g., in watches. Low power consumption devices are developing gradually and that today offers provide opportunities for yesterday's dreams [1-6].

The main drawbacks are to supply power stable and reliable to commercialize wearable devices, the efforts are being made to explore alternative energy sources for recharging of batteries is performed on a regular or occasional basis using the auxiliary power source of energy harvesting modules such as photovoltaic cells or thermoelectric devices, which are also known as renewable energies. The renewable energy sources, being clean energy sources, noiseless, have an extreme

advantage over conventional energy resources from an environmental point of view. The photovoltaic cells are variable power supply, dependent on sunlight, which could lead to an energy shortage if too much of a region's power comes from photovoltaic cells. Therefore, photovoltaic cells fail to provide long-term autonomy sufficient power for portable devices. Fortuitously, the thermoelectric devices have attracted much attention due to their ability of direct conversion of heat to electricity. The performance of thermoelectric devices is recycling wasted heat energy, lower production cost, scalability, long-lived power source, no side effects or harm, free from gas emission, easy to dispose of and reliable source of energy [7-9].

1.2 Motivation

The body heat from the human is one of the source to harvest energy, which produces electricity from tiny energies in the environment that is called thermoelectric (TE) power generator as shown in Fig. 1.1 In this application, the power generator was designed in the form of textile, so-called wearable power generator (WPG). It is also made available in the form of curtain, tent, and umbrellas and therefore, it is useful not only for a daily life applications but for special applications such as natural disaster. TE materials have prominent aspects like reliability, environmental benignity, and easy incorporation into existing technologies. They can be used as long-life power sources and provide a long-lasting solution to the ever-growing demand for implantable medical devices. This increasing demands for lightweight, high flexible, stretchable, and washable presents critical challenges for the progress of WPG.

1.3 History of wearable power generators

♣ In 1821, the Thematron's technology developed watches at Centre electronique horloger (CEH) in Neuchatel, Switzerland. Basically, three different materials were used antimony,

bismuth, and tellurium. The generators composed of two metal sheets: red one on the watch back side (in contact with the wrist's skin) and a blue one at the top of the case (in contact with ambient air); it is based on "Seebeck effect" principle, which generates a voltage that supplies energy to the quartz caliber. They had very low conversion efficiency, and it could not hold the electrical load, thus the distribution was eventually stopped.
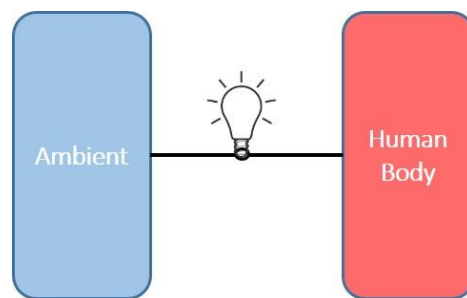
Fig. 1.1 wearable power generation on human body

♣ With not much achievement, several efforts followed, when finally, in the year 1988, Seiko developed another thermic watch; which was connected to a lithium-ion battery with a 10 months' power reserve. It has power saving mode, and it stopped when the watch was not being worn on hand to reduce energy consumption and save battery life.

♣ In 2010, Skinny Player was designed by Chinese engineers Chih-Wei Wang and Shou-His Fu; the player with a preloaded album onto it and to listen music you would simply stick the player onto your body; By sticking the player, it would gain power from its flexible battery charging device; it is eco-friendly and sustainable way; major issues with the player is when intended to exercise, the body is hot and usually sweats, however it was stuck on a sweating body for a long time.

♣ A tremendous achievement in the same year by Orange Power Wellies; Boots that converts heat from your feet into electrical power to charge your mobile phone; the battery gets

charged by twelve hours of walking but still its remarkable significant that the amount of energy can be harvested from the normal human activity; in order to decrease the charging period we should try more active duties like dancing or running; then the device contains pairs of p-type and n-type semiconductor materials forming a thermopile.

- In 2011, the first popular TE mobile developed by Nokia E-Cu designer Patrick Hilandom; the mobile would be able to heat-conductive charging system, being in your pocket and it creating a charger-free mobile phone future; the phone body is made up of copper on which are engraved heat sinks in the form of dried and cracked earth; basically, mobile phone chargers produce 51000 tons of emission of energy in the environment, in addition to greenhouse gases.

- In 2013, Fujifilm has developed the flexible polymer TE conversion module; it can able to generate milliwatt to microwatt power; it would be possible to operate the medium and low-temperature waste heat that surrounds us all in our daily lives; the power is generated by affixing a film substrate coated with organic materials on to a heating source, and the possible power can be generated in the temperature difference ambient and human body temperature of even 1°C.

- In 2016, developed by Sam Shames in Embr labs, Wristify is a heating and cooling bracelet that lets you make yourself comfortable by sending hot or cold pulses to a patch of skin on the wrist; it is more comfortable without changing your core temperature by focusing on the temperature at the skin, and sudden changing of the skin temperature can also notice immediately make you more comfortable.

1.4 Thermoelectric Materials

The performance of WPG is essential to develop high-efficient flexible TE materials. Theoretically, the efficiency of TE power generator rises monotonously with increasing dimensionless figure of merit, zT which is given by $zT=(S^2\sigma)/\kappa\,T$, where S, σ, κ, and T denote the thermopower (Seebeck coefficient), electrical conductivity, thermal conductivity, and temperature respectively. Henceforth, with the aim of improving the efficiency, an increase in Seebeck coefficient and a decrease in thermal conductivity are required. Traditional materials for TE such as bismuth telluride have been studied and utilized commercially for the last half century, but recent advancements in materials selection are one of the principal function of active TE device as it determines the reliability of the fabrication regarding industrial and economic aspects [10].

1.5 Nanostructuring an efficient approach

As a resolution of this purpose, the nanostructured materials are expected to enhance the Seebeck coefficient because of a carrier confinement effect and to lower the thermal conductivity because of an increase in the boundary scattering in phonon transport. The selection of the material has a significant role in the fabrication of high-performing TE materials. Owing to its flexible nature, conducting polymers (CPs) are favorable materials for the practical TE applications. Because of their high flexibility, environmental stability, and facile synthesis, they have the potential for use on human skin. However, most of the CPs such as polyaniline, polypyrrole, and poly(3,4-ethylenedioxythiophene) polystyrene sulfonate (PEDOT: PSS) are expensive and require complex treatments to achieve good electrical conductivity. Hence efforts have been made to find an alternative for fabricating flexible TE materials and composite materials have recently been attracting more and more attention since they possess many advantages including high thermopower, easy process-ability, and cost-effectiveness. Recently, many researcher's efforts

have been made to utilize oxide nanomaterials for WPG applications that may provide environmental stable, mechanical flexibility, and lightweight with low cost of manufacturing [11-13].

1.6 Conflicting wearable power generator

Human skin as one of its charge-collectors, converts muscle movements into enough power for small electronics which requires optimization of a variety of conflicting properties. At the same time, it should enhance the performance of the material and increase the zT for which characteristics such as high electrical conductivity, lower the thermal conductivity and a high thermopower (Seebeck coefficient) are required. The three parameters are strongly interdependent each other to makes the enhancement of zT highly challenging. Sometimes the nanomaterials coated fiber bond is not the strongest, so it wears down and wears off through use and another challenge, which is related conductive fibers is erosion over time. Various techniques have been considered owing to maximum performance in TE materials; a few examples of manipulation are described in the following sections [14-17].

1.6.1 Optimization of power generation on human body

Human body releases the thermal energy of about 2.4 to 4.8 watts, but more can be achieved by placing at different parts of the body. The ideal positions are indicated in Fig. 1.2. Similarly, the body heat trapping power may be enhanced by physical activity involved as shown in Table 1. Note, however, that energy harvested from the user may require considerable settings in position of the body. Most of the times it provides better expected results [18-22].
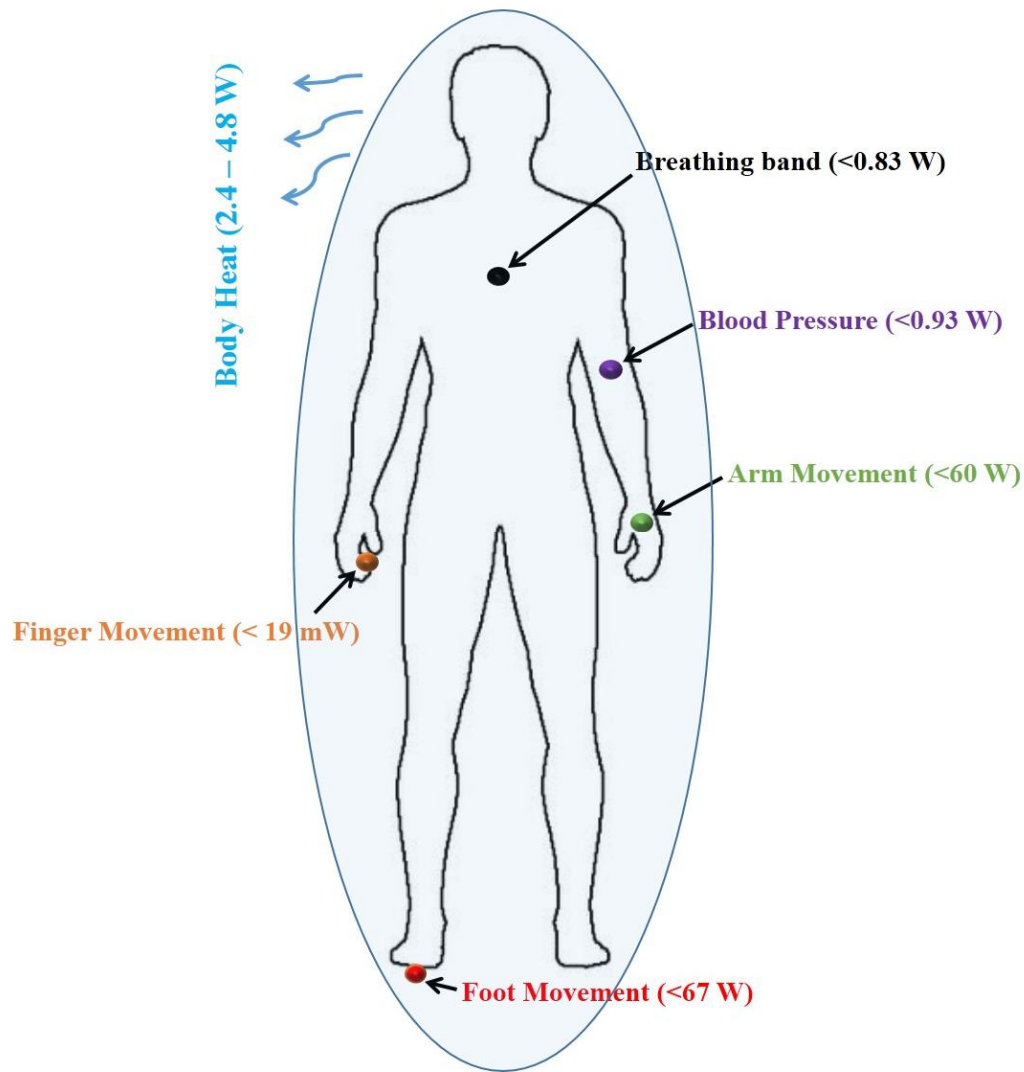
Fig. 1.2 WPG recovery from body in different places

Table 1.1: Power enhancement by movement of body

Activity	Sleeping	Sitting	Standing	Conversation	Eating	Driving	House Keeping	Swimming	Running
Watts	81	93	116	128	128	163	175	582	1048
Kilo cal/ hr	70	80	110	110	110	140	150	500	900

1.6.2 Optimization of coating techniques

On the other hand, we have focused on ZnO and rGO nanostructure composites as a high-efficiency WPG material because they are non-toxic to skin, inexpensive, available easily and possess attractive electronic properties, making them available for engineered clothing with low-cost fabrication. Up-to-date, several coating methods have been used to grow ZnO and rGO films for tuning its size and morphology, such as sol-gel method, solvothermal synthesis, chemical precipitation, microwave method, sonochemical route, chemical vapor deposition, vapor-phase method, sputtering, and electrochemical. Among these techniques, the solvothermal method is a promising method to synthesize nanostructures with high purity and isometric crystallization. As well as it improves a surface's strength and durability. Furthermore, a variety of nanostructures such as nanorods, nanoneedles, nanotube, nanosheets, nanoflakes, nanodiscs, and nanoflowers can be obtained by solvothermal method. In precise, fabrics containing ZnO and rGO have shown great promise as N-type and P-type materials with improved transport and UV shielding properties [23-26].

1.6.3 Optimization of composites

The thermopower can be enhanced in the presence of chemical composition and crystallinity of thermoelectric materials at nano-inclusion via engineering of multicomponent nanomaterials (nanocomposites), it has proven which can reduce the lattice thermal conductivity by promoting the phonon scattering at gain boundaries and simultaneously it enhances the power factor due to electron filtering at grain boundaries [27-30].

References

1. Xiaoming Tao, "Wearable electronics and photonics", CRC Press, Woodhead publishing limited, Cambridge, 2005.

2. J. McCann and D. Bryson, "Smart clothes and wearable technology", CRC Press, Woodhead publishing limited, Cambridge, 2009.

3. Gilsoo Cho, Seungsin Lee, and Jayoung Cho, "Review and Reappraisal of smart clothing", International Journal of Human-Computer Interaction, 25(6), 582 – 617, 2009.

4. Y. E. EI Mogahzy "Engineering Textiles – Integrating the design and manufacture of textiles products", CRC Press, Woodhead publishing limited, Cambridge, 2009.

5. Ssennoga Twaha, Jie Zhu, Yuying Yan, Bo Li, "A comprehensive review of thermoelectric technology: Materials, applications, modelling and performance improvement", Renewable and sustainable energy reviews, 64, 698 – 726, 2016.

6. X. F. Zheng, C. X. Liu, Y. Y. Yan, and Q. Wang, "A review of thermoelectrics research – research developments and potentials for sustainable and renewable energy applications", 32, 486 – 503, 2014.

7. J. Weber, K. Potje-Kamloth, F. Haase, P. Detemple, F. Volklein, T. Doll, "Coin-size coiled-up polymer foil thermoelectric power generator for wearable electronics", Sensors and Actutors A, 132, 325 – 33, 2006.

8. Francisco Suarez, Amin Nozariasbmarz, Daryoosh Vashaee and Mehmet C. Ozturk, "Designing thermoelectric generators for self-powered wearable electronics", Energy Environmental Science, 9, 2099 – 2113, 2016.

9. Vladimir Leonov and Ruud J. M. Vullers, "Wearable electronics self-powered by using human body heat: The state of the art and the precspective", Renewable and Sustainable Energy, 1, 062701, 2009.

10. P. Aranguren, D. Astrain, A. Rodriguez, A. Martinez, "Experiemental investigation of the applicability of a thermoelectric generator to recover waste heat from a combustion chamber", Applied Energy, 152, 121 – 130, 2015.

11. Sungmook Jung, Jongsu Lee, Taeghwan Hyeon, Minbaek Lee, and Dae-Hyeong Kim, "Fabric-based integrated energy devices for wearable activity monitors", Advance Materials, 26, 6329 – 6334, 2014.

12. Veena M, Omer O, Susasn T, David W, "Flexible technologies for self-powered wearable health and environmental sensing", Proceeding of the IEEE, 108, 665 – 681, 2015.

13. L. Francioso, C. De Pascali, I. Farella, C. Martucci, P. Creti, P. Siciliano, A. Perrone, "Flexible thermoelectric generator for ambient assisted living wearable biometric sensors", Power souces, 196, 3239 – 3243, 2011.

14. Wei W, Peining C, Sisi H, Xuemei S, and Huisheng P, "Smart Electronic Textiles", Angewandte Chemie, International Edition, 55, 6140 – 6169, 2016.

15. Tony V, Courtney H, Joseph R, Nicholas K, Chao H, Pasindu G, David E, Rutvik J, and Yanliang Z, "High-performance and flexible thermoelectric films by screen printing solution-processed nanoplate crystals", Scientific Reports, 6, 33135, 2016.

16. James D, Henry G, Steven M, Michael M, Shanshan Y, Feiyan L, Eric B, Brinnae B, Bongmook L, Veena M, Young Z, Omer O, Jason S, John M, David P and Alper B, "Low power wearable systems for continuous monitoring of environment and health for chronic

respiratory disease", IEEE Journal of Biomedical and Health Informatics, 20, 1251 – 1264, 2016.

17. Deepa M, Zuoqian W, Paul K. W, James W. E, "Printed flexible thermoelectric generators for use on low levels of waste heat", Applied Energy, 1556, 587 – 592, 2015.

18. Ziyang W, Vlandimir L, Paolo F, Chris V H, "Realization of a wearable miniaturized thermoelectric generator for human body applications", Sensors and Actuators A, 156, 95 – 102, 2009.

19. Wei H, Gan Z, Xingsing Z, Jie J, Guiqiang L, Xudong Z, "Recent development and applciations of thermoelectric generator and cooler", Applied Energy, 143, 1 – 25, 2015.

20. Zhisong L, Huihui Z, Cuiping M, Chang M L, "Silk fabric-based wearable thermoelectric generator for energy harvesting from the human body", Applied Energy, 164, 57 – 63, 2016.

21. Lymberis A, Paradiso R, "Smart fabrics and interactive textile enabling wearable personal applications: R & D state of the art and future challenges", IEEE EMBS Conference, 5270 – 5272, 2008.

22. Seiichi D, Norifumi I, Yusuke I, Shoichiro I, Keisuke S, Muneaki O, Kenji S, and Kentaro K, "Stack-type thermoelectric power generating module with flexible section and using phase changes of low-boiling-point medium", Energy Conversion and Management, 127, 103 – 111, 2016.

23. Robert J S, Steven J W, Karuna S. K, "Theoretical limits of thermoelectric power generation from exhaust gases", Applied Energy, 133, 80 – 88, 2014.

24. Andreas Patyk, "Thermoelectric generators for efficiency improvement of power generation by motor generators – Environmental and economic perspectives", Applied Energy, 102, 1448 – 1457, 2013.

25. Minijeong H, Jonghwa P, Youngoh L, and Hyunhyub K, "Triboelectric generators and sensors for self-powered wearable electronics", ACS Nano, 9, 3421 – 3427, 2015.

26. Tongcai W, Weiling L, Wei W, Shan-Tung T, "Waste heat recovery through plate heat exchanger based thermoelectric generator system", Applied Energy, 136, 860 – 865, 2014.

27. Chaoxing W, Tae Whan K, Fushan L, and Tailiang G, "Wearable electricity generators fabricated utilizing transparent electronic textiles based on polyester/ Ag Nanowires/ Graphene core-shell nanocomposites", ACS Nano, 10, 6449 – 6457, 2016.

28. Matteo S and Alessandro C, "Wearable electronics and smart textiles: A critical review", Sensors, 14, 11957 – 11992, 2014.

29. Franciso S P, Eduardo M, Manuel F M, and Eduardo P T, "Growth of vertically aligned ZnO nanorods using textured ZnO films", Nanoscale research letters, 6, 524, 2011.

30. Rasit A and Hayati M, "A review: Thermoelectric generators in renewable energy", International journal of renewable energy research, 4, 128 – 136, 2014.

CHAPTER 2

Experimental Methods and Characterization Techniques

2.1 Materials Fabrication

2.1.1 Scouring process

Scouring is an important treatment stage of cotton fibers for reducing the amount of impurities such as oils, wax, gums, fatty materials, natural coloring. The absence of impurities produce the fabric more hydrophilic for achieving uniform nanomaterials coating as shown in Fig. 2.1 before and after scouring process. The complete scouring process as shown below [1];
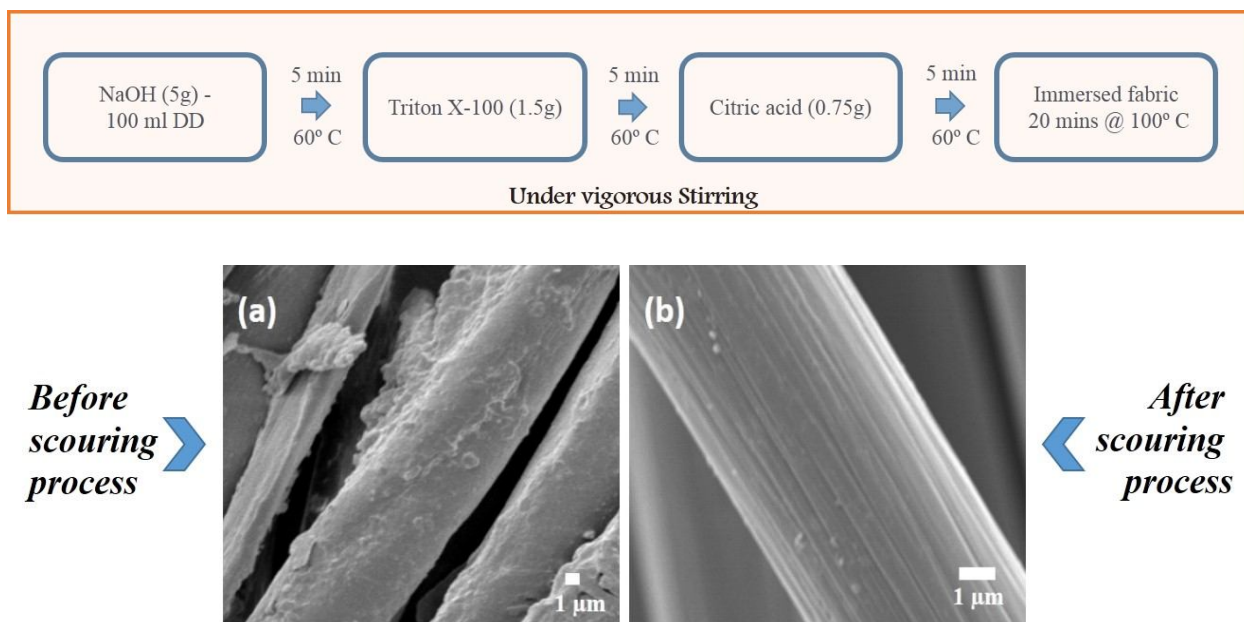
Fig. 2.1 SEM image of cotton fabric (a) before and (b) after of scouring process

The development of nanomaterials is closely linked to the following synthesis process.

2.1.2 Sol gel synthesis

Sol gel approach began with inorganic ceramic materials at early mid 1800's and especially fabrication of metal oxides. In a typical sol gel reaction process [2], the reactants involve conversion of monomers into a colloidal solution then it reacts as the precursor for an integrated network. The deposition of sol gel solution produces the coatings on the cotton fabric by dipping and followed by heat treatment to form an amorphous or crystalline coatings as shown in Fig. 2.2 (a – d).

2.1.3 Microwave approach

Since in 2000, the Microwave-assisted approach is known to transform electromagnetic energy into heat for the ultra-fast synthesis of chemical reactions using microwave irradiation [3]. It has homogeneous, rapid with deep internal heating as resultant produce high yield and lower quantities of side products, purifications of yield are easier, reactions are more reproducible, and the reaction temperature is accurate but it not reproducible with conventional heating. The cotton fibers microwave assisted synthesis has established with producing nanostructures to influence both side distribution of fibers effectively as shown in Fig. 2.2 (g – h).
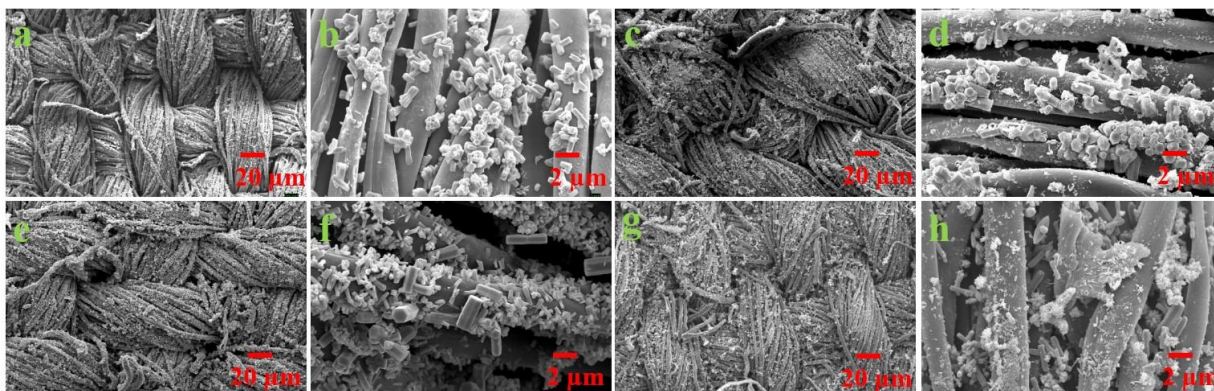
Fig. 2.2 Coating method for cotton fibers (a – d) Sol gel approach and (g – h) Microwave approach

2.1.4 Co-precipitation method

In this process, the desired component is precipitated under the aqueous region to synthesize high purity and crystallinity without significant defects. As the novel method performed at room temperature and suitable for quantifiable production because of its high yield, excellent repeatability, and low cost. Particularly, the metal hydroxides are precipitated from their precursor element because of low solubility, but the inclusion of alkaline solution can overcome it or raising the pH. For example, Fig. 2.3 (a – d) shows the coated cotton fabric nanostructures is done by the co-precipitation approach with the addition of amine groups and metal precursors [4].
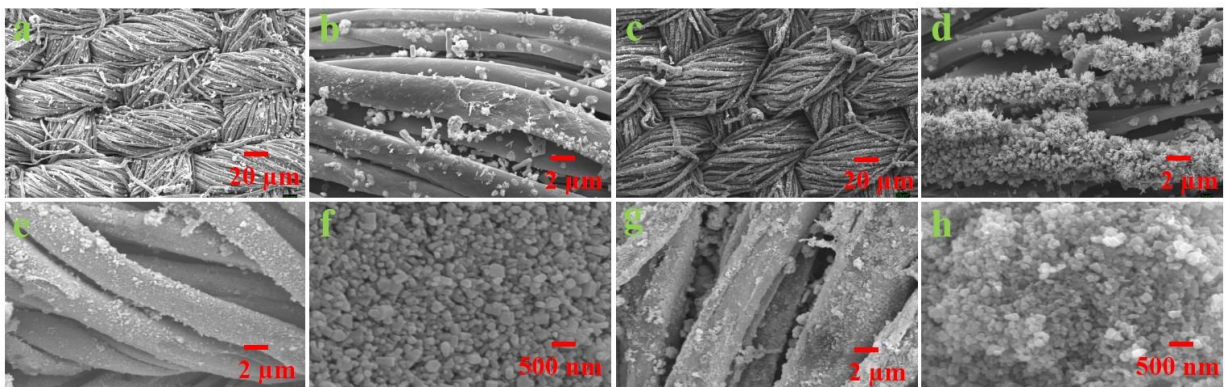
Fig. 2.3 Cotton fabric deposited with nanostructures via (a) co-precipitation method and (b) chemical bath method

2.1.5 Chemical bath deposition

Since from 1933, it was known that for solution growth method, and it adopts the simplest form of the concentrated solution which induces a solid phase to exsolve substrate mounting for thin films. Those yields are stable, adherent, uniform coatings with good reproducibility by a simple process [5]. To grow a denser nanostructure without seed layers are also possible but the precursor species tend to be very dilute within the solution during the deposition process and tailoring of chemical bath deposition is not possible without a clear understanding or control of mechanism. We could observe the coated nanostructures on cotton fiber as shown in Fig. 2.3 (e – h).

2.1.6 Sonochemical synthesis

It is the effect of sound wave propagating in forming acoustic cavitation in liquids, resulting high temperature and pressure in a microscopic region of the sonicated process. The most notable effects are consequences of primary and secondary radical reactions it increases chemical activity through the formation of new species [6, 7]. The effects in processes may modification of surface morphology and particle size ah high velocity interparticle collisions as shown in Fig. 2.4(a – d).
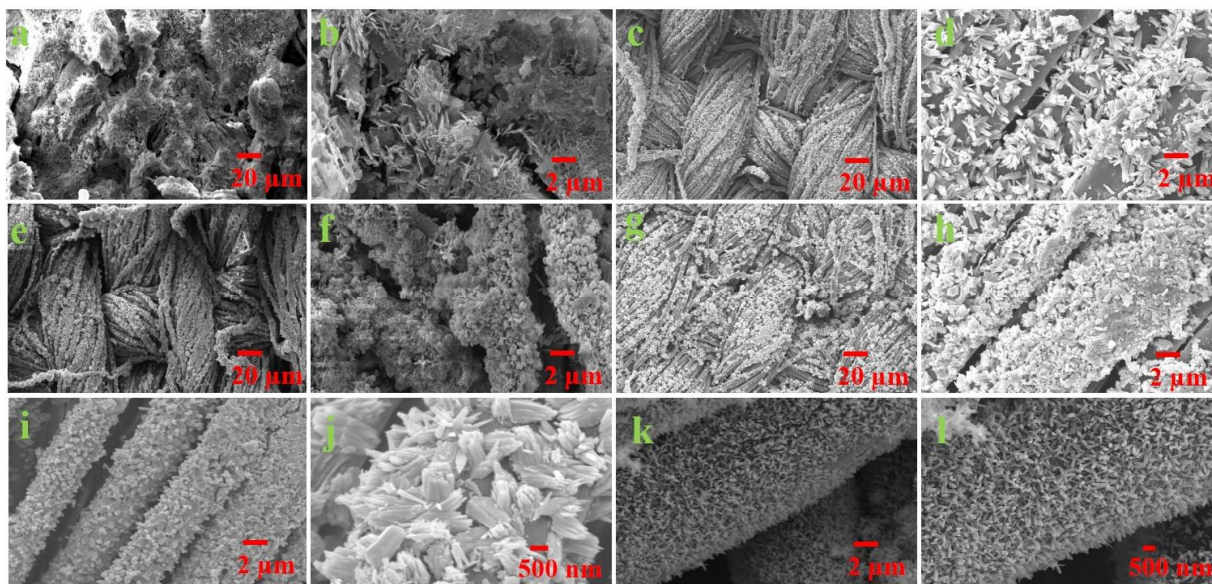
Fig. 2.4 Different techniques involved for coating on cotton fibers (a – d) sonochemical, (e – g) hydrothermal, and (I – l) solvothermal method.

2.1.7 Hydrothermal synthesis

In principle, Hydrothermal technique refers to heterogeneous reactions in aqueous media above 100° C temperature and 1 bar pressure, these resulting powder needs no more high-temperature calcination and thus can avoid the nanoparticles from re-clustering (Oswald repining). The growth of nanomaterials is performed in an apparatus consisting of a steel vessel with Teflon container innermost that sustained the pressure. The morphology and size of the nanoparticles could be tuned easily by operating temperature, pressure and time duration. Using hydrothermal synthesis for depositing metal oxide on the cotton fabric [8, 9] was shown in Fig. 2.4 (e – h).

2.1.8 Solvothermal synthesis

The phenomena of the solvothermal method are sol gel process followed by the hydrothermal approach, and they have involved two steps process for the crystallization process: crystal nucleation formation by sol gel process and subsequent growth rates by the hydrothermal approach. Particle size and morphology can by controlling by processing variables such as temperature, pH, precursor concentration and additives or surfactants. Thus, solvothermal

synthesis allows for precise control over the size, shape distribution and crystallinity of metal oxide nanostructures on cotton fabric [10 - 13] as shown in Fig. 2.4 (i – l).

2.2 Sample characterization technique

2.2.1 X-ray diffraction (XRD)

X-rays are considered waves of electromagnetic radiation with typical photon energies in the range of 100 eV – 100 keV. Impinging of X-rays used for diffraction applications in the range of few angstroms to 0.1 angstroms (1 keV – 120 keV). The phenomena could produce a diffraction pattern from the materials, which contains information about the atomic arrangement within the crystal. Braggs law (*nλ - 2d sin θ*) conditions satisfy when the interaction of incident rays with the samples produces constructive interference (in-phase) [14, 15]. In this work, the XRD measurements were performed in the step scanning mode θ - 2θ by using a Rigaku (Japan) X-ray diffractometer (RINT-2200) with a Cu kα radiation source (λ=0.154 nm) and in a step width of 0.02° and the instrument as shown in Fig. 2.5.

2.2.2 Scanning electron microscopy (SEM) with Energy-dispersive X-ray spectroscopy (EDS)

The sample is probed by a beam of electrons scanned across the surface. The images are generated from secondary electron, backscattered electrons, and diffracted backscattered electrons from the surface of solid specimens with the source of high-energy electrons. These signals reveal the information about the sample, including texture, elemental composition and orientation of materials. It owes its popularity to the versatility of its various modes of imaging and its resolution can approach 0.5 nm. The appearance of 3D micro-graph understands the surface structure of a sample. The solid-state detector is used to collect the distribution of X-ray emission from the sample during bombardment by an electron beam and to characterize the elemental composition

[16 - 18]. In this work, the morphology of the samples was recorded using a JEOL JSM 7001F and EDS Mapping by Apollo XV Silicon drift detector as shown in Fig. 2.6.

Fig. 2.5 Rigaku X-ray diffractometer

2.2.3 Transmission electron microscopy (TEM)

The microstructure of materials with atomic-scale resolution can be imaged and analyzed through high-energy beam transmitted through sample specimen. The crystallographic information can also be obtained from diffraction patterns. It can be used for various applications like cross-section analysis of layer thickness, defect analysis by dislocations and stacking faults, chemical composition and bonding from the single point or line scans. [19, 20] All the TEM analysis in this work was performed using JOEL JEM 2100F at an accelerating voltage of 200 kV as shown in Fig. 2.7.

Fig. 2.6 FESEM Image with EDS

Fig. 2.7 STEM Image with EDS

2.2.4 Thermogrametric analysis (TGA)

It is a technique in which, the mass of a substance is monitored as a function of temperature or time for the sample specimen in a controlled atmosphere. The sample pan that is supported by a precision balance, the pan resides in a furnace and is heated or cooled during the experiment. The mass of the sample is monitored during the operation [21]. In this work, TGA was performed using Shimadzu DTG 60 from 25° C to 800° C with the heating rate of 10° C min^{-1} in the presence of nitrogen gas atmosphere as shown in Fig. 2.8.

Fig. 2.8 TGA Instrument

2.2.5 X-ray photoelectron spectroscopy (XPS)

Electron spectroscopy for chemical analysis (ESCA) is also known as X-ray photoelectron spectroscopy (XPS). The average depth of analysis for an ESCA measurement is approximately 5 nm. An electron energy analyzer is used to measure the energy of the emitted photoelectrons from the sample surface, and in surface layer analysis technique can determine the information about board range of materials chemical state, elemental identity and quantitative of detected element

[22]. This work involves XPS analysis of all samples by Shimadzu ESCA 3100 as shown in Fig. 2.9.

Fig. 2.9 ESCA Instrument

2.2.6 Raman spectroscopy

When there is change in the dipole moment of a molecule due to an interaction with light, Raman band arises and it provides molecular vibrational, rotational, and other low frequency modes in the materials that can be used for sample identification and quantification. Raman effect is very weak to see with the naked eye, so we analyze the light with a highly sensitive spectrometer [23]. Generally, a diffraction grating or prism is used to detecting the scattered light from the excitation. In this work, Jasco NRS 5100 was used to analyses all the samples as shown in Fig. 2.10

Fig. 2.10 Raman Micro-Spectrometers

2.3 Wearable device measurements

2.3.1 Electrical measurements

A current-voltage (IV) characteristics is a relationship, exemplary representation of graph between the electric current through a material and the corresponding potential difference obtained. In the precise IV measurement, current/ voltage response can be measured while applying voltage/ current to obtain current versus voltage and resistance characteristics and power dissipated or generated can be determined from the IV curve by the resistive element [24 - 28]. Fig. 2.11 shows the JASCO, CEP-25BX with which IV_ characteristics were monitored in this study.

2.3.2 Thermopower measurements

In general, the thermoelectromotive force determined by using probes that are directly connected to the samples, and the temperature difference is measured through thermocouples. Consequently, for a good measurement of thermopower (Seebeck coefficient), it is necessary to measure the thermoelectromotive force and temperature difference instantaneously at the same place, to make sure the probes in excellent thermal and electrical connection with the samples, and to have a high precision measurement device. There are two primary methods used to measure thermopower which is the integral and differential methods. The integral method typically used for analysis with

large temperature difference, where one end of the sample is maintained at a constant temperature T_1 while the temperature of other end is varied in the temperature range of interest ($T_2 = T_1 + \Delta T$).

Fig. 2.11 JASCO, CEP-25X

The fitting technique is used to estimate the thermopower on complete measured data set of measured thermoelectromotive force V (T_1. T_2) as shown in Fig. 2.12 (a). The integral method succeeds in minimizing the influence of voltage offset. Since the applied temperature difference is large which will produce a large thermoelectromotive force. However, it is hard to maintain the temperature at one end of the sample due to the flow of heat from the high temperature applied at the other end. Moreover, it is also difficult to obtain the proper fit for evaluating the thermopower from the measured data. In additionally, the differential method can operate from a small temperature difference is applied across the sample and it is maintained at the average temperature ($T = (T_1 + T_2)/\Delta T$). Then the thermopower is evaluated from the linear fit of thermoelectromotive force and temperature difference for several sets of data as shown in Fig. 2. 12 (b).

(a) $S = \dfrac{dV}{dT}$ **(b)** $S = \dfrac{\Delta V}{\Delta T}$
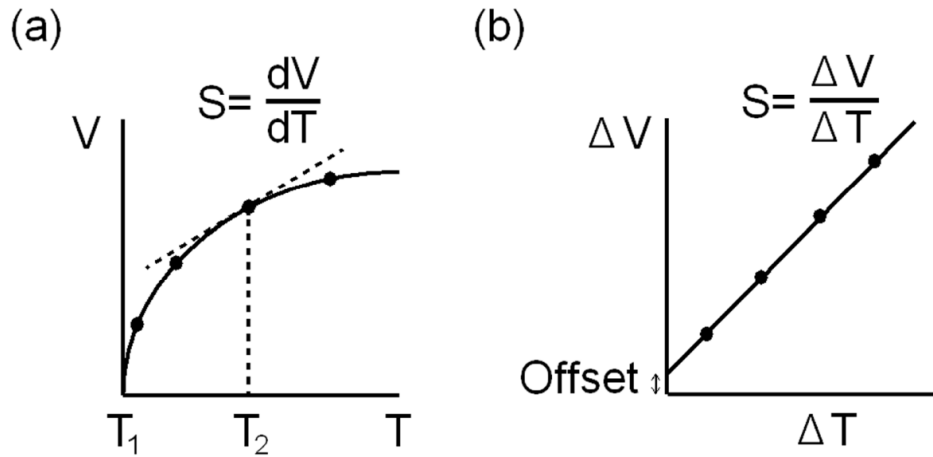
Fig. 2.12 Illustration of integral (a) and differential (b) technique for measuring thermopower (Seebeck coefficient)

Hence, this evaluation of thermopower is valid for constant thermopower at average temperature. This technique is also effectively eliminating the offset voltages that arise from thermocouples in similarities and no equilibrium contact interfaces. In this study, the thermopower of samples is measured to be constant in the average temperature range, and a schematic representation of experimental setup shown in Fig. 2. 13.
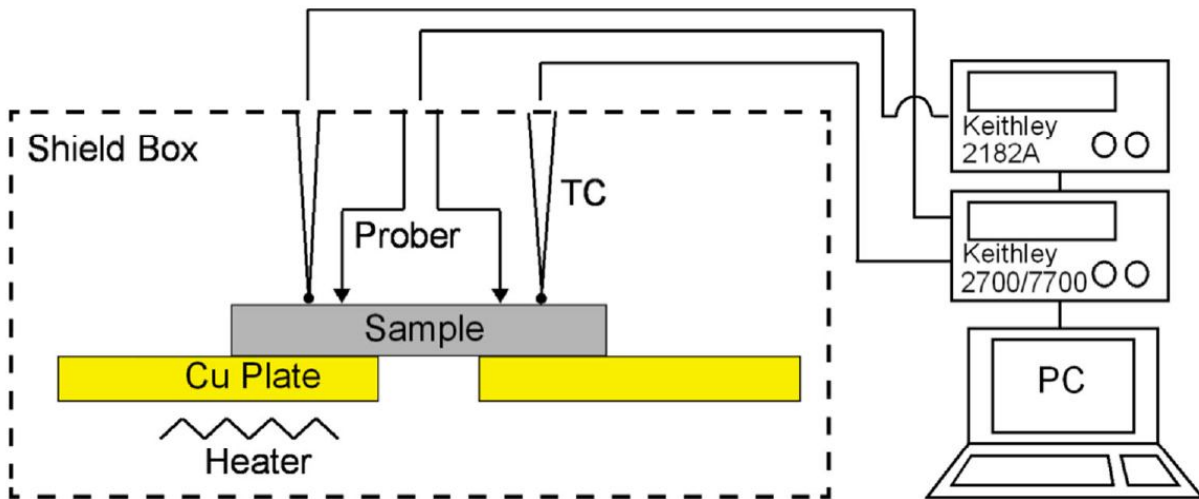
Fig. 2. 13 Schematic representation of system for measuring the thermopower

There are two Cu plates were positioned side by side with a gap of ~1 mm. The sample for measuring placed across the gap, associate with both plates. A resistive heater was placed underneath the plate, and by controlling the heater current, a temperature difference could be produced in a plane parallel to the sample surface. A couple of probes and two K-type thermocouples were directly connected to the sample surface. The time evolution of the thermoelectromotive force was measured by a nanovoltmeter (Keithley 2182A) and simultaneously with the temperatures at the high- and low-temperature regions by a digital meter (Keithley 2700) equipped with a switching module (Keithley 7700) [29 - 32].

2.3.3 Ultraviolet ray shielding measurements

The human body have largest organ is skin, since in the beginning people desired to use sunscreen products to get beautiful and to prevent the skin burns from sun tan, without the risk toward change to burns. Now, it is necessary for all people to use sunscreen products because for the protection against ultraviolet (UV) radiation. The UV radiation is broadly divided into three distinct bands in order of decreasing wavelength and increasing energy. UVA (320 – 400 nm) has a longer wavelength; it penetrates skin through both the epidermis and dermis, UVB (290 – 320 nm) has an intermediate wavelength; these rays can be blocked by sunscreen, automobile glass, and windows but UVA is not filtered. UVC (200 – 290 nm) has a shorter wavelength; it is effectively filtered by the atmosphere (Ozone layer) and is therefore not a forethought to be a considerable factor. Those imbalances can result in formation of wrinkles, hair loss, rashes, life-threatening cancers, and disorders in immune regulation.

UV protection factor (UPF) applications due to increasing global awareness on green/eco textile products and their market demand. Research has been intensified in the area of development of sustainable UV protective textile using plant extracts and other natural polymeric materials or

biocompatible. The Ultraviolet ray shielding measurement was analyzed by UV scattering and absorption spectroscopy by Lapsphere UV1000F as shown in Fig. 2.14. In the Australia/New Zealand standard AC/NZS 439:1996 method, Eq. (1) is used to determine,

$$UPF = \frac{\int_{290}^{400} E_\lambda \times S_\lambda \times d\lambda}{\int_{290}^{400} E_\lambda \times S_\lambda \times T_\lambda \times d\lambda}$$ -- (1)

Where E_λ is the relative erythemal spectrum effectiveness, S_λ is the solar UV spectral irradiance, T_λ is the spectral transmittance of the specimen (incoming light that passes through the sample) and λ represents the wavelength (nm). Laundering durability of the treated fabric was measured in agreement with AATCC test method 61-2006 [33 - 35].

Fig. 2. 14 UPF Measurement system

References

1. Awais K, Mazhar H P, Muhammad M, Max W, "A review on developments in dyeing cotton fabrics with reactive dyes for reducing effluent pollution", Journal of Cleaner Production, 87, 50 – 57, 2015.

2. Lamia Znaidi, "Sol-gel deposited ZnO thin films: A review", Materials Science and Engineering: B, 174, 18 – 30, 2010.

3. Ying J and Feng C, "Microwave-assisted preparation of inorganic nanostructures in liquid phase", ACS Chemical Reviews, 114, 6462 – 6555, 2014.

4. I. M. Kolthoff, "Theory of Coprecipitation. The formation and properties of crystalline precipitates", Journal of Physical Chemistry, 36, 860 – 881, 1932.

5. Dhananjay M and Ghanshyam J, "Short review on chemical bath deposition of thin film and characterization", AIP Conference Proceeding, 1728, 020597, 2016.

6. Tina H, Majid M, "A review on textile sonoprocessing: A special focus on sonosynthesis of nanomaterials on textile substrates", Ultrasonic Sonochemistry, 23, 1 – 10, 2015.

7. Hangxun X, Brad W Z, Kenneth S S, "Sonochemical synthesis of nanomaterials", RSC Chemical Society Reviews, 42, 2555 – 2567, 2013.

8. Weidong S, Shuyan S, and Hongiie Z, "Hydrothermal synthetic strategies of inorganic semiconducting nanostructures", RSC Chemical society reviews, 42, 5714 – 5743, 2013.

9. Oliver S H, Karen J E, Daniel T B, Laura T M, "Deep eutectic-solvothermal synthesis of nanostructures ceria" Nature Communications, 14150, 2017.

10. Kirsten M J, Chirstoffer T, Martin B, Bo B I, "In situ studies of solvothermal synthesis of energy materials", Journal of Chemistry and sustainability chemistry energy and materials, 7, 1594 – 1611, 2014.

11. Drik E, Hideto S, Yuji K, Hiroki S, Akira Y, Tsuguo F, "Solvothermal growth of znO", Progress in crystal growth and characterization of materials, 52, 280 – 335, 2006.

12. Prabhakar R, Woon-Ki K, and Yeon-Tae Y, "Solvothermal synthesis of ZnO nanostructures and their morphology dependent gas sensing properties", ACS Applied materials and interfaces, 5 (8), 3026 – 3032, 2013.

13. Pimente A, Rodrigues J, Duarte P, Nunes D, Costa F M, Monterio T, Martins R, Fortunato E, "Effect of solvents on ZnO nanostructures synthesized by solvothermal method assisted by microwave radiation: a photocatalytic study", 50, 5777 – 5787, 2015.

14. Ada L Ryland, "X-ray diffraction", ACS Journal of Chemical Education, 35, 80, 1958.

15. Solookinejad Gh, Rozatian A S H, Habibi M H, "Zinc oxide thin films characterization AFM< XRD and X-ray reflectivity", Experimental Techniques, 40, 1297 – 1306, 2016.

16. Amizam S, Abdullah N, Rafaie H A, and Rusop M, "SEM and XRD characterization of ZnO nanostructured thin films prepared by Sol-Gel method with various annealing temperatures", 37, 1217, 2010.

17. Havrdova M, Polakova K, Skopalik J, Vujteck M, Mokdad A, Homolkova M, Tucek J, Nebesarova, Zboril R, "Field emission scanning electron microscopy as an approach for nanoparticle detection inside cells", Micro, 67, 149 – 154, 2014.

18. Matthew T J, Barry C C, Joseph M, "SEM analysis of oxide thin films and reactions", Journal American Ceramic Society, 82, 1644 – 1646, 1999.

19. Abolhassani S and Philippe G, "Preparation of TEM samples of metal-oxide interface by the focused ion beam technique", Journal of Microscopy, 223, 73 – 82, 2006.

20. Notz K J, Jaffe H H, "Correlation of TGA and DTA temperatures in Decomposition reactions", Journal of American Ceramic Society, 43, 53 – 54, 1960.

21. Kerkhof F P J M and Moulijn J A, "Quantitative analysis of XPS intensities for supported catalysts", Journal of Physical chemistry, 83, 1612 -1619, 1979.

22. Gaashani R Al, Radiman S, Daud A R, Tabet N, Doun-Al Y, "XPS and optical studies of different morphologies of ZnO nanostructures prepared by microwave methods", Ceramics International, 39, 2283 – 2292, 2013.

23. Thoman H, Caterina S W, Naresh K, Albert Van DB, and Bert M W, "Surface- and Tip-enhanced raman spectroscopy in catalysis", Journal of physical chemistry letters7(8), 1570 – 1584, 2016.

24. Hassan Ei-Kashef, "Optical and electrical properties of materials", Review of Scientific Instruments, 65, 2056 – 2061, 1994.

25. Hannah J J, Jessica L B, Chirstopher L D, Sarwat A B, and Michael B J, "A review of the electrical properties of semiconductor nanowires: insights gained from terahertz conductivity spectroscopy", IOP Semiconductor Science and Technology, 31, 103003, 2016.

26. Donald Long, "Effects of pressure on the electrical properties of semiconductors", APS Physical review letters, 101, 1256, 1956.

27. P H Miller, "The electrical conductivity of Zinc Oxide", APS Physical Review Letters, 60, 890, 1941.

28. E E Hahn, "Some electrical properties of Zinc Oxide Semiconductor", AIP Journal of Applied Physics, 22, 855, 1951.

29. J De Boor and E Muller, "Data analysis for Seebeck coefficient measurements", Review of Scientific Instruments, 84, 065102, 2013.

30. Andres S, Maria A, Shahed R, Gabriel C, Miguel A T, Torres J C, Diez, "A thermoelectric by any other name…", Materials today, 15, 415, 2012.

31. Zhi-Gang C, Guang H, Lei Y, Lina C, Jia Z, "Nanostructured thermoelectric materials: Current research and future challenge", Progress in Natural Science: Materials International, 22, 535 – 549, 2012.

32. Faiz S, Asai K, Ishida A, and Ikeda H, "Seebeck coefficient of ultrathin silicon-on-insulator laters", IOP Applied physics express, 2, 071203, 2009.

33. Xue, Yin W, Jia ST, Ma JZ, "UV-durable superhydrobhobic textiles with UV-shielding properties by coating fibers with ZnO/ SiO2 core/ shell particles", IOP Nanotechnology, 41, 415603, 2011.

34. Omer K A and Tao Z, "Review on : Developing UV protection for cotton fabric", The Journal of the Textile Institute, 11, 1 – 13, 2015.

35. Wang L, Zhang X, Li B, Sub P, Yang J, Xu H, Liu Y, "superhydrophobic and ultraviolet-blocking cotton textiles", ACS Applied Materials and Interfaces, 3(4), 1277 – 81, 2011.

CHAPTER 3

Fabrication of hierarchical ZnO nanostructures on cotton fabric

3.1 Introduction

The body heat from human is one of the source of energy harvestings which produces electricity from tiny energies in the environment, called thermoelectric (TE) power generator. In this application, the power generator has formed in the textile, so-called wearable power generator. It is also available for the curtain, tent, and umbrellas and therefore, it is useful not only for a daily life but also for a natural disaster. For realizing the wearable power generator, it is essential to develop high-efficient flexible TE materials. Theoretically, the efficiency in TE power generator rises monotonously with increasing dimensionless figure-of-merit, ZT [1 - 5], where T is the absolute temperature. Z is the figure-of-merit defined by $(S^2\sigma)/\kappa$, where S is the Seebeck coefficient, σ is the electrical conductivity, and κ is the thermal conductivity. Henceforth, with the aim of improving the efficiency, an increase in Seebeck coefficient and a decrease in thermal conductivity are required. As a resolution of this purpose, the nanostructured materials are expected to enhance the Seebeck coefficient because of a carrier confinement effect and to lower the thermal conductivity because of an increase in the boundary scattering in phonon transport [6, 7].

For high-efficient wearable power generator, we have investigated the ZnO nanostructures grown on cotton fabric (CF) as a novel flexible TE material. ZnO is inexpensive, easy fabrication, and available for textile due to non-toxicity for skin [8 - 10]. Various growth techniques of ZnO have been developed for tuning its size and morphology, such as sol-gel method, solvothermal synthesis, chemical precipitation, microwave method, sonochemical route, chemical vapor deposition, and vapor-phase method [11, 12]. Among these techniques, the solvothermal method is a promising method to synthesize ZnO nanostructures with high purity and isometric ZnO crystallization. Furthermore, a variety of nanostructures such as nanorods, nanoneedles, nanotube,

nanosheets, nanoflakes, nanodiscs, and nanoflowers [13 - 16] can be obtained by solvothermal method. In applying the power generator to the textile, curtain, and so forth, the flexible TE material is required to have three principal functions of the superhydrophobic surface, ultraviolet (UV) shielding and high TE efficiency. Consequently, in this paper, we fabricated ZnO nanostructures on CF by the solvothermal method and characterized their hydrophobicity, UV transmittance, and TE properties.

3.2 Experimental procedure

Sodium hydroxide, Triton X-100, citric acid, zinc nitrate hexahydrate, and hexamethylenetetra- mine (hexamine) were purchased from Wako chemicals, Japan. All the chemicals were of analytical grade and used without further purification. The CF was cut into ~ 6.5 cm × 4.5 cm and scoured by treating the cotton cellulose material with a scouring solution containing an anionic and/or nonionic detergent (NaOH, trition, critic acid and water) to remove the wax, fatty materials or other impurities [17].

ZnO nanostructure has formed on the scoured CF by a two-step growth method consisting of a seed creation process followed by a nanostructure growth process. A typical solvothermal seeding process was as follows; 1 M of zinc nitrate hexahydrate was dissolved in 40 mL of deionized water under stirring. 2 M of hexamethylenetetramine was dissolved in 40 mL of deionized water, and this solution is added to the zinc nitrate hexahydrate solution to form ZnO. The similar experimental conditions were adopted for the molar ratio of zinc nitrate hexahydrate and hexamethylenetetramine from 1:1 to 2:1. The CF was immersed into ZnO solution for 1 h, and then it was ultrasonicated for 30 min. The mixture solution was transferred to the autoclave with the inner volume of 100 mL (TEFLON, F-1029-06) and the solvothermal seeding was carried out

at 120 °C for 3 h. ZnO-seed-coated CF was collected and washed with distilled water to remove the excess reactants. Finally, the ZnO-seed-coated CF was placed in hot air oven at 50 °C for 1 h.

At the second step or solvothermal growth of ZnO nanostructure, 80 mL of deionized water contained 1 M of zinc nitrate hexahydrate and 2 M of hexamethylenetetramine. The mixed solution was transferred into the autoclave, and the solvothermal growth was carried out at 120 °C for 9 h. The autoclave could cool to the room temperature; then the fabric was taken out from the solution and rinsed with deionized water three times. Then, it was rinsed with ethanol thrice. Finally, the product was dried at 50 °C for 1 h. The similar growth process was adopted for the series of experiments with molar ratio of zinc nitrate hexahydrate and hexamethylenetetramine 1:2, 1:1, 2:1 and after this, they are termed as Z1CF (1:2), Z2CF (1:1) and Z3CF (2:1), respectively.

Figure 3.1 shows a summary of the fabrication process of ZnO-nanostructure-coated CF by solvothermal method. Figure 3.1(a) shows the process photographs, where the glass frame designed and manufactured for the small-scale screening of ZnO seed and growth conditions. The CF is revealed to be fitted to the glass frame and placed inside of Teflon container, which helps to maintain the uniformity and denser formation of ZnO on both sides of the fiber surface. After scoured, as shown in Fig. 3.1(b), the cotton fibers are off-white in color [18]. The surface of fibers is smooth, and the striations are not visible after scoured. After the seed creation process, the nano-crystalline seed is observed the coat on the cotton fiber surface uniformly. After the growth process, ZnO nanostructures with high density and high aspect ratios are apparently found on CF.

(a)

1. Glass frame for cotton
2. Placed inside Teflon container

(b)

Bare Cotton fabric

2 mm / 1 µm

Scouring process

2 mm / 1 µm

ZnO seed layer

1 µm / 500 nm

ZnO growth layer

1 µm / 500 nm
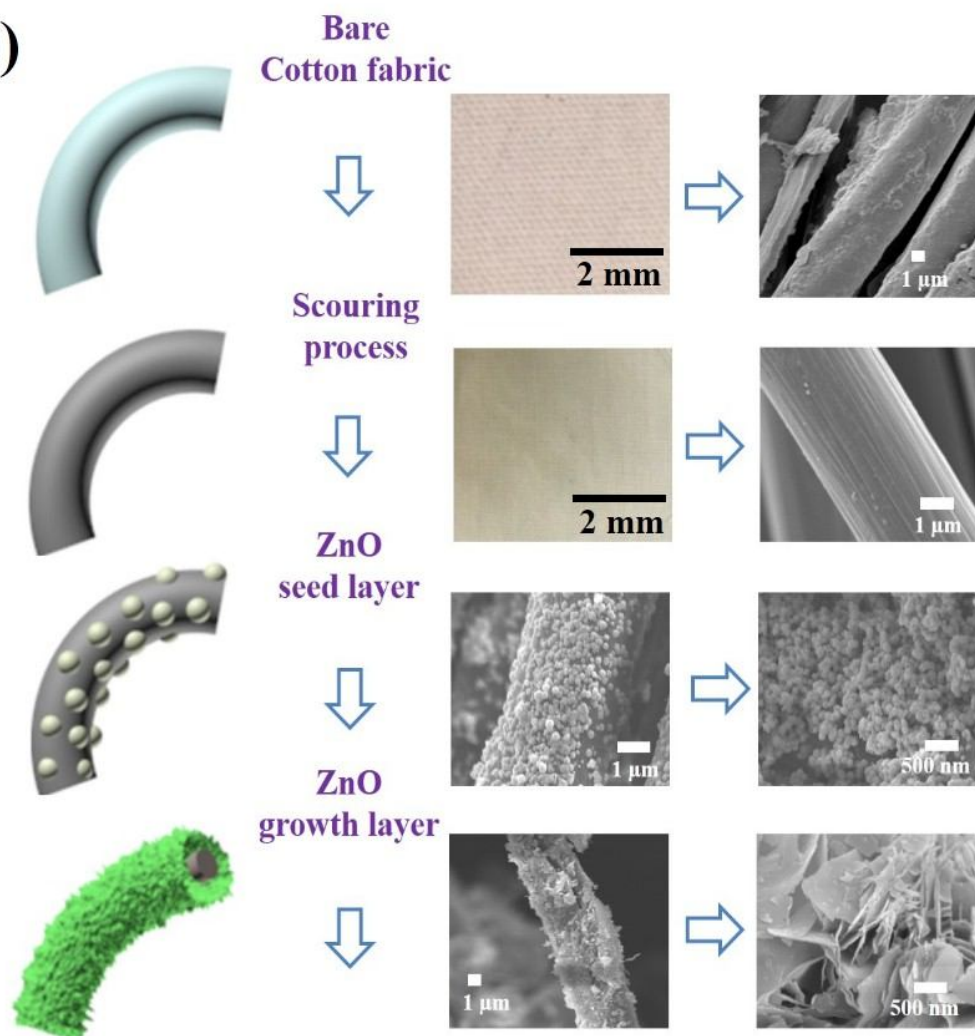
Fig. 3.1 (a) Method for solvothermal growth, (b) Fabrication process of ZnO nanostructures coated on cotton fibers

3.3 Results and discussion

3.3.1 Surface Morphology

Individual fibers of ZnO-seed-coated CFs are shown in Fig. 3.2 for Z1CF, Z2CF, and Z3CF after the first step, or the seed formation process. It is found from Figs. 3.2(a), 3.2(b), and 3.2(c) that ZnO nanostructures are formed on fiber surfaces with highly connected and dense, presenting round and hexagonal shapes. From the magnified image in Fig. 3.2(a), the average size of the particles was evaluated to be 20-150 nm in diameter. Figure 3.2(b) shows that smaller sheets are initiated along the vertically aligned sheets; nanosheets are hierarchically arrayed and combined. The width of the nanosheets gradually became narrower, which results from the simultaneous growth of the longitudinal and later growth of the nanosheets. The granular-like ZnO nanostructures are observed in Fig. 3.2 (c). Their diameter was evaluating to be in the range of 20-100 nm.

Figure 3.3 shows that the FESEM and TEM images of ZnO-nanostructures on CF for Z1CF, Z2CF, and Z3CF after the second step, or the growth process. In the case of Z1CF, the SEM images of Figs. 3.3(a1) and 3.3(a2) show high density and randomly-aligned nanorods without any preferred orientation, indicating that the ZnO nanorod array grows preferably on the surface of single fibrous fiber in the direction of c-axis [002], as seen in Fig. 3.3(a2). Furthermore, it shows that each nanorod has a uniform diameter along its entire length, indicating that the growth anisotropy is constantly maintained. From their TEM images of Fig. 3.3(a3), the as-prepared ZnO nanorod is found to be single crystalline with a wurtzite structure. Consequently, in the case of the concentration 1:2 (zinc nitrate: hexamine), the ZnO nanostructure grows preferentially along [002] direction because of the lowest surface energy of (001) facet [19, 20] and the faster growth velocity to [002] than those along [101] and [100] directions. Thus, the nanorods expected grew along the

[002] direction, and the diameter of 100 nm with various lengths was grow, as shown in Fig. 3.3(a3 & a4).
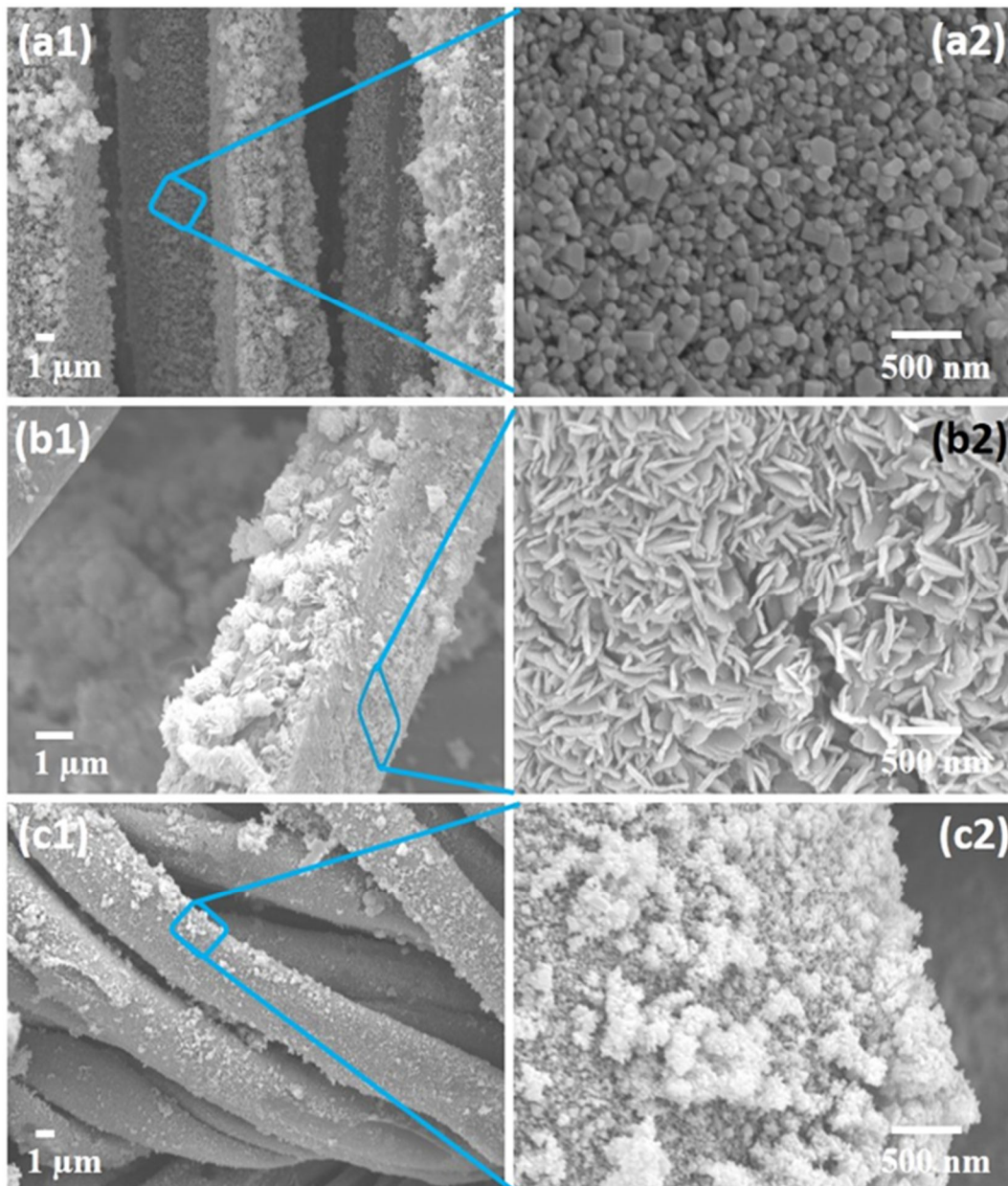
Fig. 3.2 FESEM images of ZnO seed layer coated fibers. (a) Z1CF, (b) Z2CF, (c) Z3CF
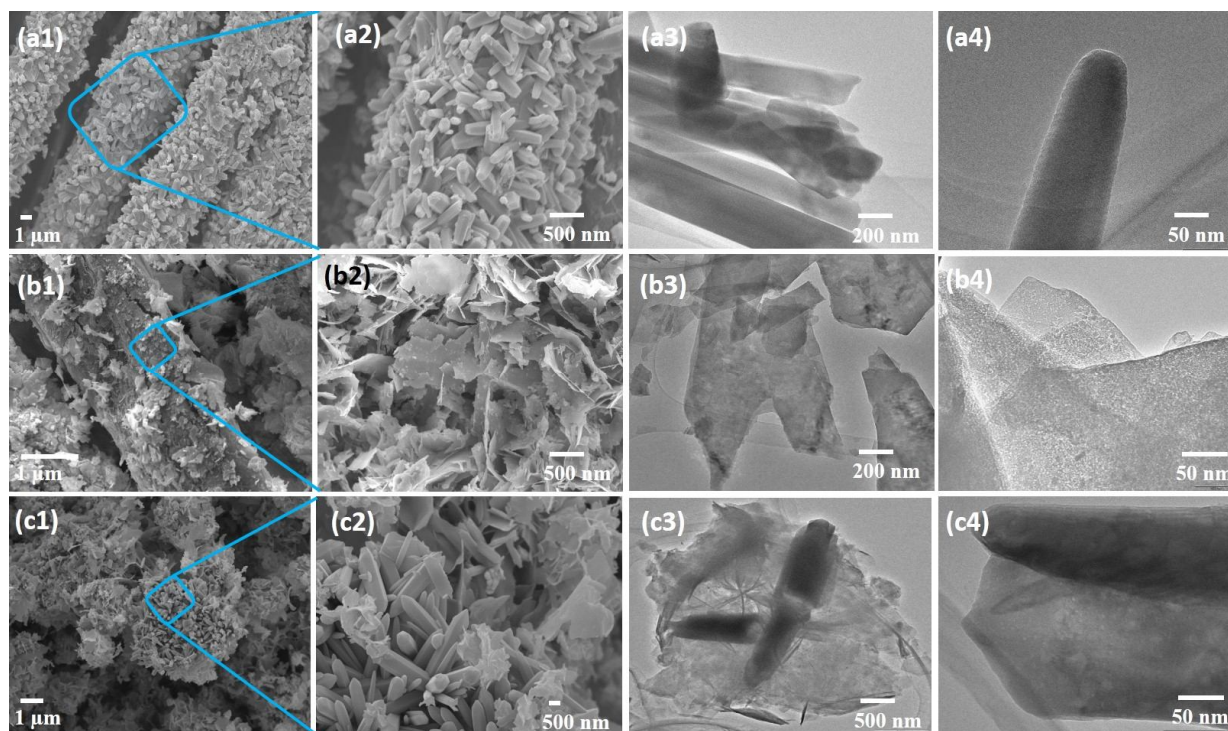
Fig. 3.3 FESEM and TEM images of ZnO growth layer coated fibers (a) Z1CF, (b) Z2CF,

(c) Z3CF

On the other hand, the nanosheets-like structures are obtained as shown in the Z2CF SEM images of Figs. 3.3(b1) and 3.3(b2). The thickness of nanosheets is estimated to be 4 nm and partly overlapped layer by layer, as seen in their TEM images of Figs. 3.3(b3) and 3.3(b4). Moreover, in the case of Z3CF, it is found from Figs. 3.3(c1) and 3.3(c2) that ZnO composite of nanosheets and nanorods is formed, where ZnO nanorods are surrounded by crumbled nanosheets with shrunken edges. The size of the ZnO nanorods is about 200 to 400 nm in diameter with nanosheets and it can be clearly seen that ZnO nanorods are uniformly anchored by the ZnO nanosheets, as observed in the TEM images of Figs. 3.3(c3) and 3.3(c4).

The TEM image Fig. 3.3 (a3) indicates that the as-prepared ZnO nanorods are single crystalline ZnO with a wurtzite structure. When the concentration was 1:2 (zinc nitrate: hexamine), the ZnO nanostructure grows preferentially along [002] direction because of the lowest surface energy of (001) facet [21]. The growth velocity along [101] and [100] directions is slower than that along [100] direction so that the pillar morphology was obtained. Consequently, the nanorods expected grew along the [002] direction and the diameter of 100 nm with various lengths were grown, as shown in Fig. 3.3 (a4). The nanosheets-like structure was obtained for the concentration was 1:1 (zinc nitrate: hexamine) shown in Fig. 3.3 (b1, b2). From the Fig. 3.3 (b3) TEM results, it is evidence that sheet morphology of ZnO is formed. Fig. 3.3 (b4) elucidate regions of relatively uniform intensity bounded layer by layer distinct lines, as opposed to a more continuous grey-scale image; the discrete nature of these flat contrast regions suggests a sheet structure of ZnO of relatively uniform thickness. When the concentration was 2:1 (zinc nitrate: hexamine), the Fig. 3.3 (c1) shows the transformation from rod to interlaced tattered nanosheets in the case of a high concentration of zinc source compared to hexamine. ZnO composite of nanosheets and nanorods was formed; ZnO nanorods were surrounded by crumbled nanosheets with shrunken edges as seen in Fig. 3.3 (c2). The size of the ZnO nanorods was about 200 to 400 nm in diameter with nanosheets, and it can be evidently seen that the ZnO nanosheets uniformly anchor the ZnO nanorods as observed TEM image in Fig. 3.3 (c3, c4).

3.3.2 Phase and structure of ZnO nanostructures

Figure 3.4(a) shows the XRD patterns of bare and ZnO coated cotton fabric. XRD profile exhibited typical diffraction peaks of a cotton fabric at 14.85°, 16.8° and 22.57° in all four samples and the typical diffraction peaks which would be an index to that of cotton fabric (CF; JCPDS card no. 03-0226) [22, 23]. Whereas, the ZnO coated fabric showed the three strong diffraction peaks

are in good agreement with standard powder diffraction peaks of ZnO (JCPDS card no. 75-0576), and the peaks can be indexed to wurtzite crystal lattice of ZnO. ZnO nanostructures are synthesized by the reaction of zinc nitrate and hexamine when the hexamine increased higher concentration compared with zinc nitrate; then hexamine plays an active part in providing a controlled supply of OH- anions by reacting with water [24]. ZnO coated diffraction peaks can be indexed to the wurtzite phase of ZnO. Besides, the predominant peak of the (002) reveals a texture effect of the arrays consistent with c-axis orientation due to the lowest surface energy and the growth velocity along the c-axis direction is the fastest leading to the formation of nanorods on the cotton fabric surface. Considering the growth direction of the ZnO nanorods, XRD result was somewhat consistent with the inordinate alignment of ZnO nanorods array on the surface of cotton fabric observed in the FESEM image. Concerning the growth mechanism of nanosheets, which is reasonable to presume that cellulose should be responsible for the suppression effect along c-axis direction when the hexamine, zinc nitrate was equal concentration and then slows down the c-axis growth [25]. ZnO c-axis oriented (002) reflection was weaker than the (100) and (101) reflections. This fact demonstrates two-dimensional nanosheets formation of ZnO (Z2CF) [26]. The co-occurrence of ZnO diffraction peaks (002) and (101) indicates that the nanorods and nanosheets (Z3CF) exhibit c-axis orientation. The diffraction peak (002) was from the polar plane of wurtzite ZnO, and the diffraction peak (101) was from the nonpolar crystallographic plan [27]. There are no impurity peaks observed for both the ZnO nanostructure coated cotton fabric and bare cotton fabric.

Figure 3.4(b) shows Raman spectra of the cotton and ZnO nanostructure coated cotton. There were no significant peaks observed in the bare cotton fabric, whereas ZnO coated fabric showed the

peaks at 332, 378, 409, 438, and 583 cm^{-1}. In order to group theory analysis, the $A_1+E_1+2E_2$ modes are Raman active [28].
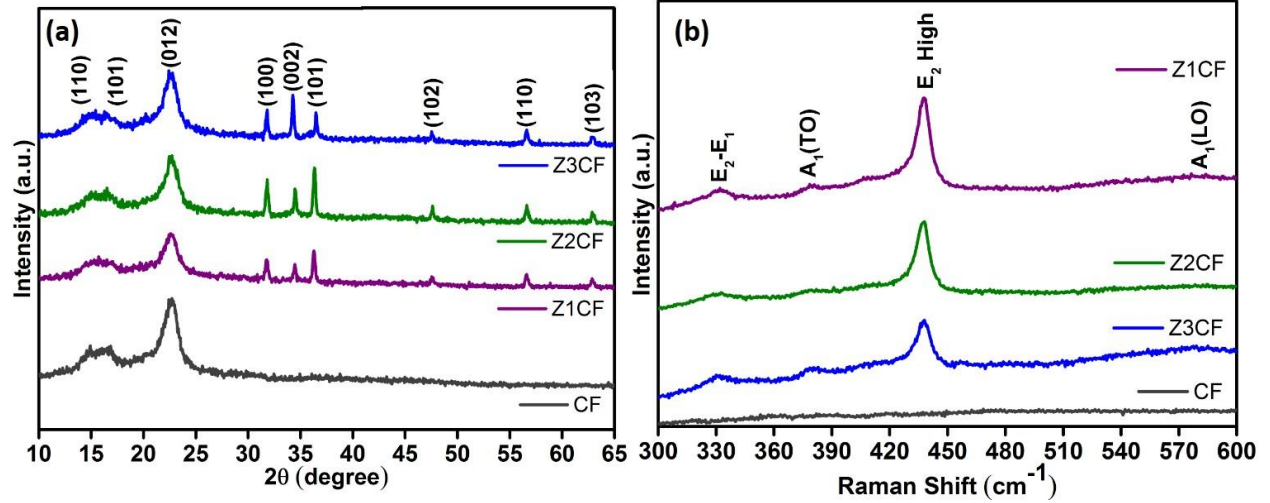
Fig. 3.4 (a) XRD pattern, and (b) Raman spectrum of ZnO coated cotton fabric

A strong characteristic peak 438 cm^{-1} of ZnO is a non-polar optical phonons E_2 (high) mode affirmed that the prepared nanostructures are crystalline and possess a wurtzite phase structure [29]. This also confirms that the composite nanostructures formed are of good crystal quality. Another peak at 332 cm^{-1} was due to secondary Raman scattering from zero-boundary phonons $2E_2$ mode. The other two weaker peaks at 378 and 409 cm^{-1} were due to A_1 (TO) and E_1 (TO) modes. They gave atomic displacements along the c-axis. The peak 583 cm^{-1} was due to E_1 (LO) mode, it was reported to be related to the oxygen deficiency [30].

3.3.3 Chemical composition

The chemical composition of the samples was obtained by an energy dispersive X-ray (EDX) spectroscope attached to FESEM. Figure 3.5(a) shows the EDX spectra of coated ZnO cotton fabric. The EDS results are consistent that the atomic percentage confirms the presence of Zn and O peaks attributed to the zinc and oxygen signal of the ZnO, and C arose from carbon tape

substrate used for holding the sample during measurement. Z1CF contained 61.13 wt% Zn, 21.12 wt% O, 17.76 wt%, Z2CF contained 75.71 wt% Zn, 13.26 wt% O, 11.03 wt%, and Z3CF contained 91.04 wt% Zn, 7.56 wt% O, 1.40 wt%. These differences in the contents of coated cotton fabric samples are indicating that the ZnO nanostructures are Zn rich with many oxygen vacancies [31]. No peak related to any impurity, which further confirmed the purity of the prepared samples.
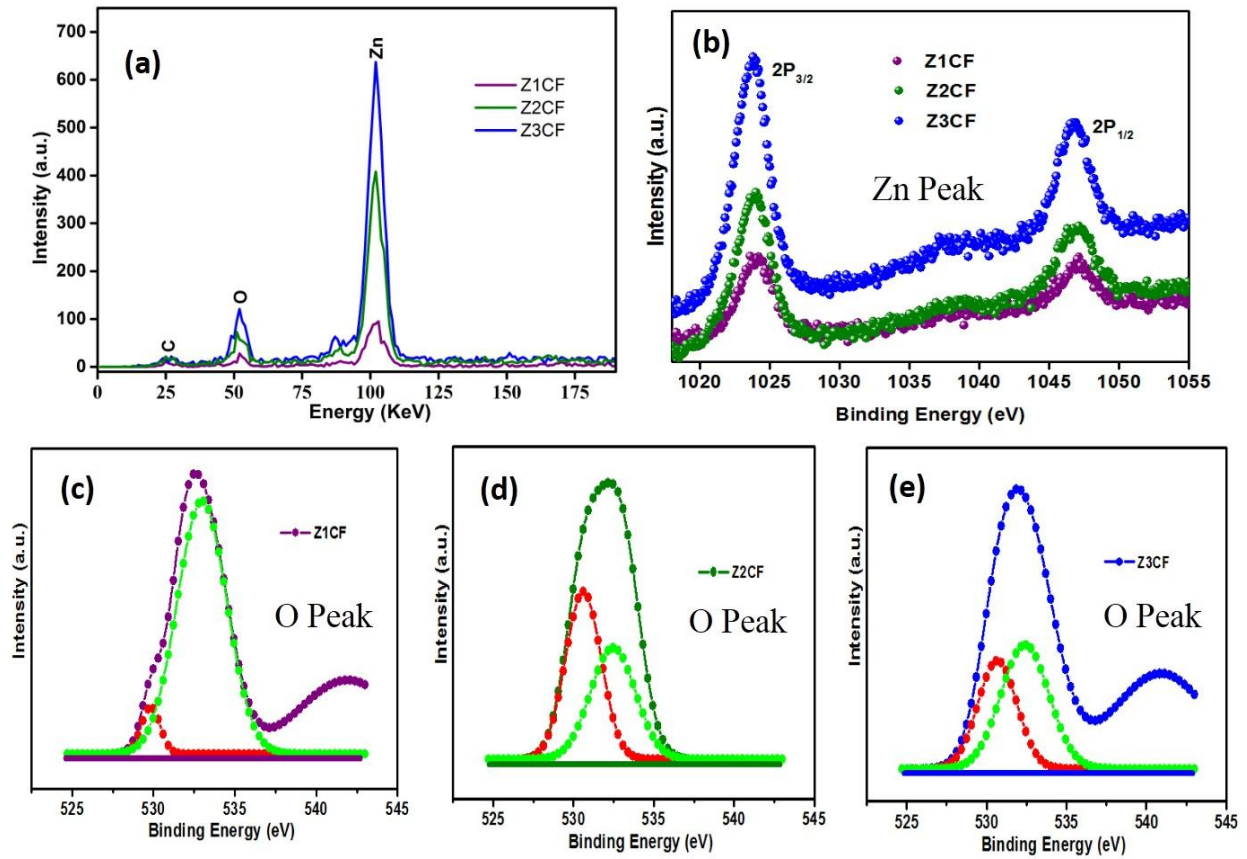
Fig. 3.5 ZnO nanostructure coated cotton fabric (a)EDX spectrum, (b) XPS spectra of Zn, and (c-e) XPS spectra of O

Figures 3.5 (b – e), shows the XPS spectra of samples of core level XPS spectra of Zn 2p and O 1s. The XPS spectra of pure ZnO at 1022.93 and 1045.81 eV, corresponds to Zn 2p3/2 and Zn 2p1/2, respectively [32]. Fig. 3.5 (b) shows the core level spectra of Zn had doublet peaks at

~1023.8 (Zn 2p3/2) and ~1046.9 eV (Zn 2p1/2), respectively, which indicating the presence of ZnO at the outermost layer [33]. Figures 3.5(c – e) shows O 1s peak which indicated an asymmetric in shape, therefore the peaks are deconvoluted into two peaks using the Gaussian fitting curve. The peak located at 530 eV was produced by the signature of the lattice oxygen O 1s in the Zn-O-Zn bonding originating from the surface-adsorbed molecules. Whereas, the peak at 532 eV correspond to the defect level oxygen in the ZnO nanostructures [34].

3.3.4 Wettability

Surface wettability of a solid surface is closely related to the chemical composition and the surface geometric structure. The hydrophobic property could be increased when the surfaces possess low surface energy in consonance with Zisman rule [35]. Moreover, the Wenzel model predicts that the hydrophobic property could be increased when the surface is roughened [36]. In cases of Z1CF and Z3CF, both the low surface energy and the high roughness enhance the hydrophobicity of surface. Figure 3.6(a) shows that the bare cotton fabric can be immediately wetted by the water droplet and the WCA close to 0°.
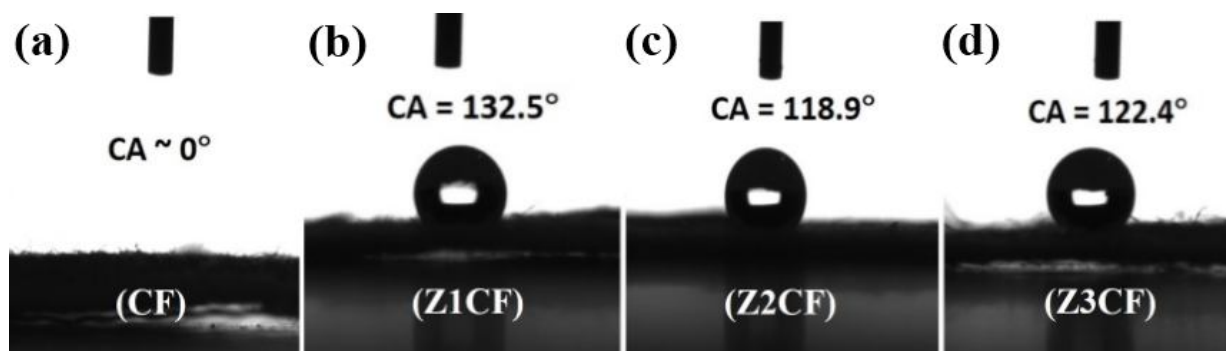
Fig. 3.6 Photography of water drops on the surface of (a) cotton fabric, (b) ZnO coated cotton fabric Z1CF, (c) ZnO coated cotton fabric Z2CF, and (d) ZnO coated cotton fabric Z3CF

The outstanding hydrophilicity was attributed to the abundant hydroxyl groups. High hydrophobic nature was obtained when the cotton fabric coated with ZnO nanostructures. The droplet kept spherical shape on the surface with the maximum WCA of 132.5°, 118.9°, 122.4° for the nanorods (Z1CF), nanosheets (Z2CF), ZnO nanorods and nanosheets (Z3CF), respectively as shown in Fig. 3.6(b), 6(c), and 6(d).

3.3.5 Evaluation of UV protection factor (UPF)

The Ultraviolet (UV) ray protection property of textiles is related to various factors, such as fiber chemistry, weave, finishing processes, fabric color, and the existence of additives and laundering. In this regards, many researchers have been investigated the UV shielding properties of the cotton fabric. Typically, a fabric with an UPF > 40 is considered as an excellent fabric against UV radiation [37, 38]. When the nanoscale particles have ability to retaining good UV absorption properties and realize a uniform distribution of the particles in host matrices which results in a significant increase in the effectiveness of blocking UV radiation. The transmittance and UV shielding properties of cotton fabric and ZnO nanostructures-coated cotton fabric are shown in Fig. 3.7(a). The UPF value of the bare fabric was 6.66. The bare fabric showed that the fabric afforded poor protection against UV radiation. An UPF values less than 15 indicates no protection against transmittance of UV radiation through fabric and on to skin. The black color represents the UV transmittance curve of the bare fabric, indicating that a high percentage of UVA and UVB light can penetrate the cotton. The other colors represented the UV transmittance curve of the ZnO nanostructure coated fabric, indicating that it can block almost all the UVB and a high percentage of UVA radiation. UV transmittance was increased at the longer wavelength of 370 nm. Since the actual damage to human skin from UV radiation is a function of the wavelength of the incident

radiation and the most damage is done by radiation in the 300 – 320 nm range, textiles must demonstrate effectiveness in this range [39, 40].

The transmittance of ZnO nanorods (Z1CF), nanosheets (Z2CF) and nanorods with nanosheets (Z3CF) greatly improved the UV protection property of the cotton fabric compared with bare cotton fabric. UV transmittance was decreased significantly.
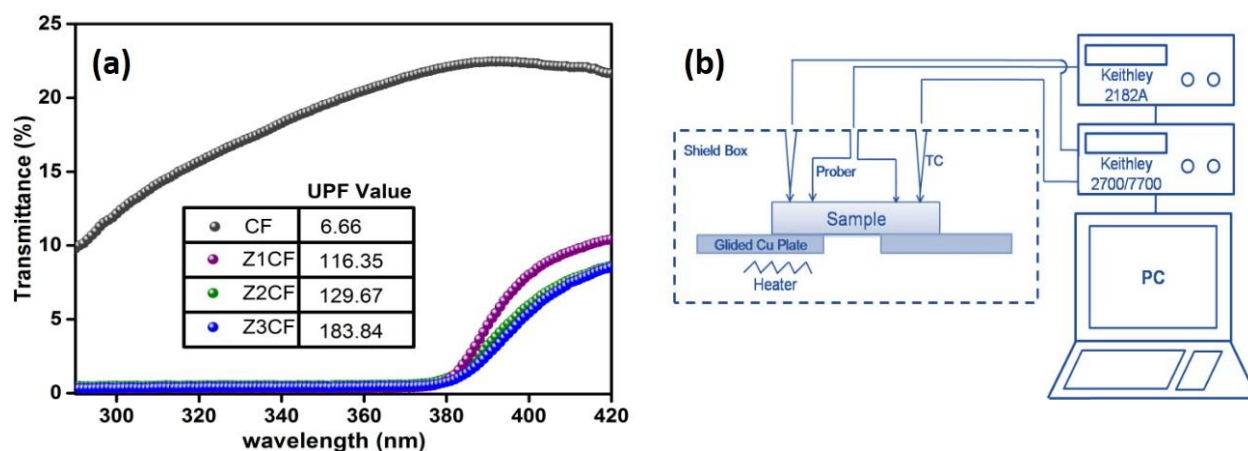
Fig. 3.7 (a) UV transmittance spectra of the bare fabric and the ZnO nanostructures coated fabric, (b) Schematic diagram of system for measuring the Seebeck coefficient

ZnO has a bandgap energy of ~3.3 eV that corresponds to the wavelength of ~375 nm. Light below these wavelengths has sufficient energy to excite electrons, and hence, it absorbed light does not destroy the inorganic semiconductors. It is evident that nanoparticles give higher transparency in the visible light region while the UV shielding property remains the same [41]. The percentage of transmittance in the UVB was lower than UVA and the UPF values of 1:2, 1:1, and 2:1 of the zinc nitrate hexahydrate: hexamethylenetetramine ratios were calculated as 116.35, 129.67, and 183.84, respectively. The UPF values of as-prepared fabric was compared with that of other reported ZnO coated UV blocking fabric as shown in Table 3.1. The UV shielding efficiency of ZnO composite (Z3CF) coated cotton fabric possessed the highest UPF value (183.84) among all

the UV protection fabrics excepting the ZnO copolymer (UPF 271). However, the preparation process of ZnO nanostructures coated cotton fabric was a solvothermal method that was more facile and green than the reverse PS-b-PAA micellar templates applied for the ZnO copolymer fabric. Furthermore, we have used the two-step solvothermal method without polymer, therefore, it is important to explore the new economical approach for the synthesis of ZnO composite nanostructures.

Table 3.1: Summarizes some of the UPF values for various ZnO coated cotton fabric

No	UV blocker	Treatment method	UPF	Ref.
1.	ZnO nanoparticles	Dip-dry-cure	15.87	45
2.	ZnO nanoparticles	Sol-gel-dry	21.78	46
3.	ZnO nanoparticles	In situ synthesis	22.8	47
4.	ZnO nanoparticles	In situ coating	33.8	48
5.	ppy-ZnO-CNT nanocomposites	Pad-dry-cure	40	49
6.	ZnO and polycarboxylic acids	Sol-gel and Pad-dry-cure	60	50
7.	ZnO-Starch nanocomposites	Pad-dry-cure	68	51
8.	Spherical shaped ZnO	Electrospinning	50	52
9.	Flower like ZnO	In situ synthesis	105.61	53
10.	ZnO (2 step process)	Microwave assisted hydrothermal	49	54
11.	ZnO nanoparticles	RF plasma	98.47	55
12.	ZnO-polymer	In situ	136	56
13.	Cu_2O/ZnO	In situ	87.31	57
14.	Nano-ZnO	Sol-dyed	125.76	58
15.	ZnO-copolymer (PS-b-PAA)	Micellar templates	271	59
16.	Needle-shaped ZnO nanorod	In situ growth	105.1	60
17.	ZnO nanorods (Z1CF)	Two-step solvothermal approach	116.35	This study
	ZnO nanosheets (Z2CF)		129.67	
	ZnO nanorods with nanosheets (Z3CF)		183.84	

3.3.6 Thermoelectric properties

Figure 3.7 (b) depicts a schematic diagram of the experimental setup. The Seebeck coefficient was measured by the same method as that used in our previous studies [42]. Transport and

thermoelectric properties of ZnO coated cotton fabric is shown in Fig. 3.8 and summarized in Table 3.2. The values of carrier concentration, mobility, and resistivity, were determined by Hall measurements at room temperature. The ZnO coated fabric show a negative Seebeck coefficient, which indicates n-type conduction due to oxygen vacancies. The resistivity and mobility of nanorods were higher than those of nanosheets and composite nanostructures. In contrast, carrier concentration of the nanosheets and the composite nanostructures was much larger than the nanorods. The trend of electrical resistivity cannot be simply related to the microstructure of the ZnO coated fabric. Additionally, it is possible to observe that the connection between grains appears poorer in the case of Z1CF, which resultant high resistivity. In Z2CF, boundary scattering of charge carrier is reduced in the thin film and hence, its electrical resistivity is decreased. Z3CF shows that the intergranular electron transport is expected to be easier than Z1CF, which explains qualitatively the lower value of the electrical resistivity. Overall, to explain the transport behavior of the ZnO coated fabric it is possible to invoke the correlation between carrier concentration, mobility, electrical resistivity; for example, the sample with the highest carrier concentration and lowest mobility this may ascribed to low electrical resistivity. Thermoelectromotive force was measured between two Cu electrodes. It is shown as a function of temperature difference in Fig. 3.9 (a). Seebeck coefficient was obtained from the slope of the curve. The result of the estimated Seebeck coefficient is drawn in Fig. 3.9 (b) as a function of average temperature. The absolute value of the Seebeck coefficient was calculated by the slope of linear fit of the plots was about 45, 6 and 28 µV/K, for the samples Z1CF, Z2CF and Z3CF, respectively. The negative Seebeck coefficient indicates that the major carriers are electrons. It is possible to appeal the anisotropy of crystallographic orientation; fully c-axis oriented samples (Z1CF) possess the highest Seebeck coefficient, followed by sample (Z3CF) with c- and a- or b- axis orientation and eventually by

composite nanostructures. The interplane parallel to the a–c or b–c plane provided a good path to electron transport. The presence of fully a- or b- axis possesses very small Seebeck coefficient (Z2CF).
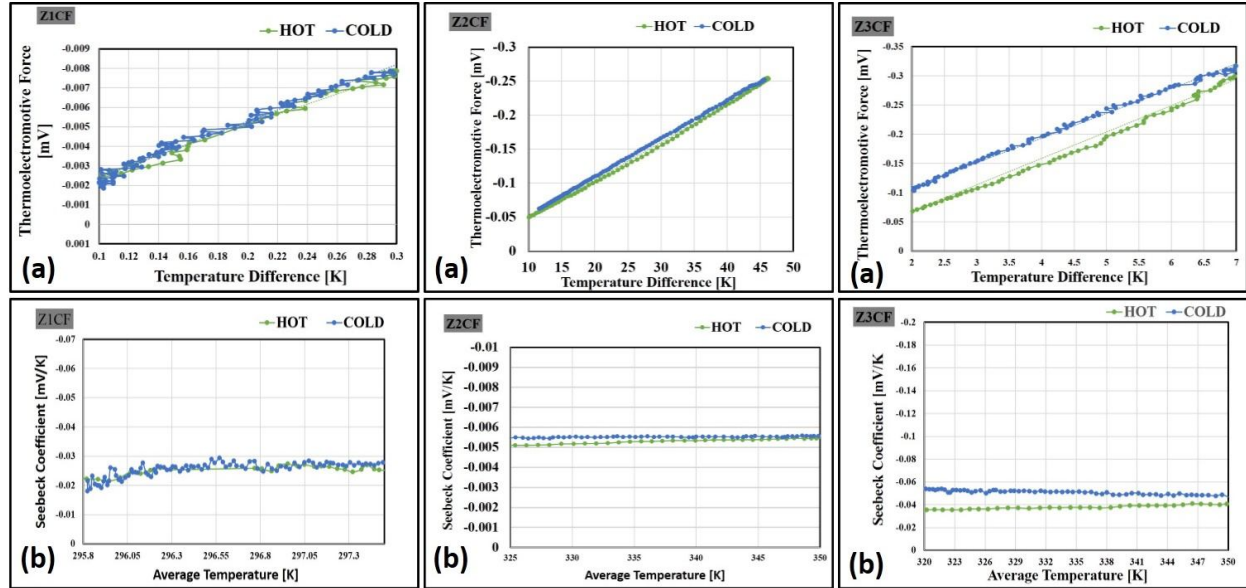
Fig. 3.8 (a) TEMF of ZnO nanostructure fabric as a function of temperature difference,

(b) Seebeck coefficient of ZnO nanostructure fabric as a function of average temperature.

Table 3.2: Room temperature thermoelectric properties

Sample	Conduction Type	Carrier Concentration n $(10^{19}\ cm^{-3})$	Resistivity ρ $(\Omega\text{-}cm)$	Mobility μ $(cm^{-2}/V\text{-}s)$	Seebeck coefficient S $(\mu V/K)$	Power factor PF $(\mu W/m.K^2)$
Z1CF	n	0.05	0.15	81.1	45	13
Z2CF	n	2.1	0.02	13.7	6	1.4
Z3CF	n	1.5	0.04	11.5	28	22

The power efficiency of thermoelectric material can be determined by the value of PF. From the values of Seebeck coefficient and electrical conductivity, we have calculated the PF of ZnO coated cotton fabric was calculated as PF = $\sigma.S^2$ as shown in Table. 3.2. A maximum power factor of 22

μW/m.k^2 was obtained for a Z3CF with 2 M of zinc nitrate and 1 M of hexamine. Z3CF showed much larger PF than those of the Z1CF or Z2CF because of its lower resistivity and higher Seebeck coefficient. It demonstrated that ZnO with composite nanorods and nanosheets structure could greatly improve its thermoelectric power factor.

3.4. Possible growth mechanism of ZnO nanostructures

Based on above results, we deliberated some plausible reasons for the morphology evolution of the ZnO nanostructures. Hexamine acted as both a capping agent and a stabilizer [29]. In the growth solution, hexamine act as a building block for the self-assembling of nanoparticles. Initially, in the growth solution the OH$^-$ anions and Zn^{2+} cations were released, which leads to the immediate precipitation of $Zn(OH)_2$ units. Subsequently ZnO nanostructures were formed by the solvothermal of $Zn(OH)_2$ units at prolonged reaction temperature and time. Besides the inherent fast growth, the electron pair N atoms of hexamine can selectively bind or be absorbed on certain Zn faces. This influences the growth of these faces, and results in the reduced agglomeration of nanoparticles. The affinity and coordination ability of the amine molecules towards the Zn ions metal complex were apparently more important in determining the nanostructure morphology [43 – 45].

Since the existence of ZnO seed layer can reduce the nucleation energy barrier and the lattice mismatch effectively, pre-coating the fabric with seeds of ZnO reflected in the impact on heterogeneous nucleation and crystal growth. In order to better understand the influence of the growth rate depends on the amount of reacting particles available, while nucleation will take place after supersaturation is achieved. The three distinct routes were employed as shown in Fig. 9, as for the concentration of starting solution resulting of the ZnO nanorods, nanosheets, and composite (nanorods and nanosheets). In first sample (Z1CF), seed and growth solution contains the

concentration of zinc nitrate and hexamine was 1: 2. The presence of high concentration of hexamine, a non-ionic ligand, encourages the oriented growth along the c-axis. Whereas, in the second sample (Z2CF), the concentration will be 1:1 and this process may slow down the growth in c-axis direction which leads to simultaneous growth on longitudinal and lateral direction. However, in the third sample (Z3CF), the concentration will be 2:1 where the zinc solutions led to the initial formation of $Zn(OH)_2$ as the major intermediate which would coalescence of ZnO nanorods and nanosheets. The secondary growth of ZnO resulted in subsequent formation of crumpled nanosheets with shrinkage edges surrounded on nanorods.
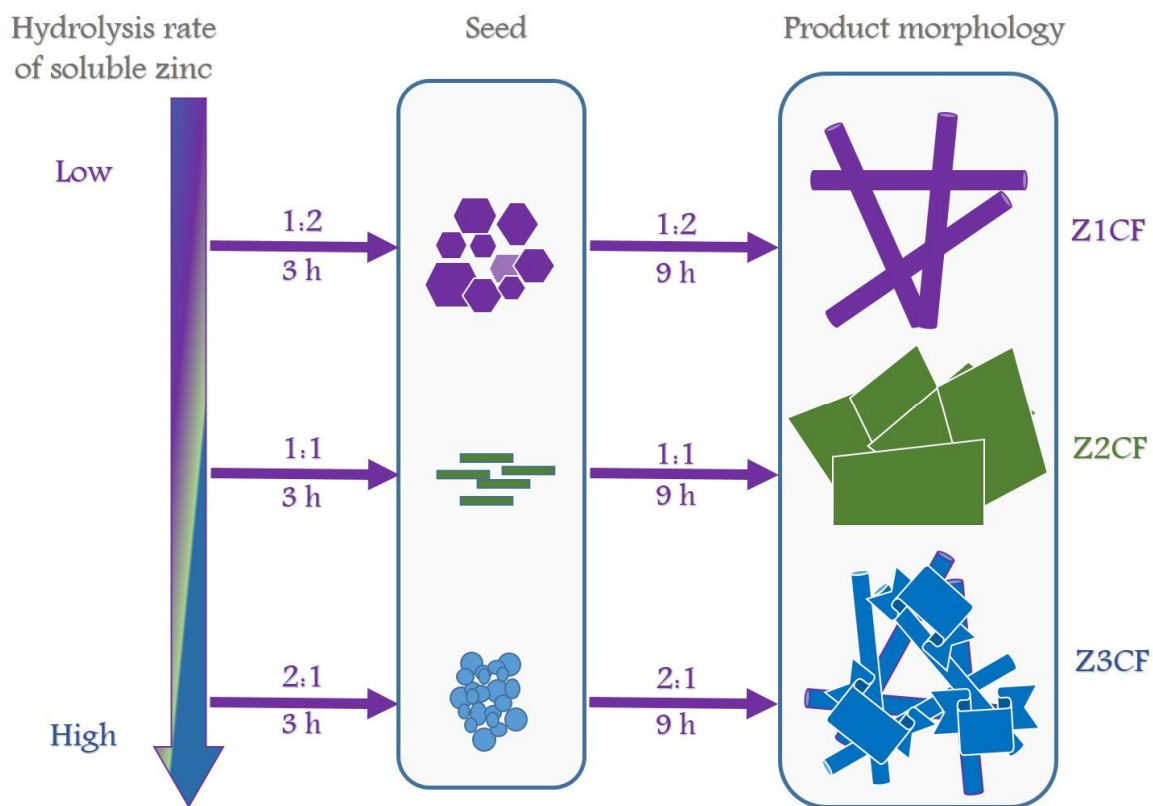
Fig. 3.9 Schematic illustration of the relationship among initial hydrolysis rate of soluble zinc, seed phase, and product morphology

3.5. Conclusion

The solvothermal method was employed to grow ZnO nanostructures on the surface of cotton fabric. The extraordinary enhancement of UV shielding efficiency of the modified fabric was obtained. The UPF value of the fabric with ZnO composite nanostructure was 183.84 which was 25 times higher than that of bare cotton fabric. The reasonable well dispersion condition of ZnO denser contributed to exceptional UV blocking. The PF of the coated fabric made by the ZnO composite nanostructure (nanorods and nanosheets) was 22 μW/m.k^2, which was much larger than that of the nanosheets or nanorods. Considering that, the enhanced performance of ZnO composite nanostructure is due to the excellent grain connectivity and superior crystallinity of the sample.

References

[1] T. M. Tritt and M. A. Subramanian, Thermoelectric materials, phenomena, and applications: A bird's eye view, Materials Research Bulletin, 31, 188-194, 2006.

[2] Y. Yang, X. H. Lin, T. Hou, F. Zhang and Z. L. Wang, Nanowire-composite based flexible thermoelectric nanogenerators and self-powered temperature sensors, Nano Research, 0124, 01-08, 1998.

[3] L. E. Bell, Cooling, heating, generating power, and recovering waste heat with thermoelectric systems, Science, 321, 1457-1461, 2008.

[4] S. J. Kim, J. H. We and B. J. Cho, Wearable thermoelectric generator fabricated on glass fabric, Energy Environmental Science, 7, 1959 – 1965, 2014.

[5] H. Im, H. G. Moon, J. S. Lee, I. Y. Chung, T. J. Kang, and Y. H. Kim, Flexible thermocell and utilization of body heat, Nano Research, 7, 443 – 452, 2014.

[6] C. Han, Z. Li and S. Dou, Recent progress in thermoelectric materials, Chinese Science Bulletin, 59, 2073 -2091, 2014.

[7] J. R. Szczech, J. M. Higgins and S. Jin, Enhancement of the thermoelectric properties in nanoscale nanostructured materials, Journal of Materials Chemistry, 21, 4037 – 4055, 2011.

[8] M. Zebarjadi, G. Joshi, G. Zhu, B. Yu, A. Minnich, Y. Lan, X. Wang, M. Dresselhaus, Z. Ren, and G. Chen, Power factor enhancement by modulation doping in bulk nanocomposites, Nano Letter, 11, 2225-2230, 2011.

[9] P. Veluswamy, S. Sathiyamoorthy, F. Khan, A. Ghosh, M. Abijit, Y. Hayakawa, and H. Ikeda, Incorporation of ZnO and their composite nanostructured material into a cotton fabric platform for wearable device applications, Carbohydrate Polymers, 157, 1801-1808, 2017.

[10] G. Ren, J. Lan, C. Zeng, Y. Liu, B. Zhan, S. Butt, Y-H. Lin, C-W. Nan, High performance oxides – based thermoelectric materials, JOM- Journal of Minerals Metal Materials, 67, 211 – 221, 2015.

[11] C. Jagadish, and S. J. Pearton, Zinc oxide bulk, thin films and nanostructures: processing, properties, and applications, Elsevier edition, 2006.

[12] C. F. Klingshirn, B. K. Meyer, A. Waag, A. Hoffmann, J. Geurts, Zinc oxide from fundamental properties towards novel applications, Springer edition, 2010.

[13] P. Rai, W-K. Kwak, and Y-T. Yu, Solvothermal synthesis of ZnO nanostructures and their morphology-dependent gas-sensing properties, ACS Applied Materials Interfaces, 5, 3026 – 3032, 2013.

[14] S. K. N. Ayudhya, P. Tonto, M. Okorn, V. Pavarajam, and P. Praserthdam, Solvothermal synthesis of ZnO with various aspect ratios using organic solvents, Crystal Growth. Designs, 6, 2446 – 2450, 2006.

[15] M. Navaneethan, J. Archana, and Y. Hayakawa, Morphological evolution of monodispersed ZnO nanorods to 3 dimensional hierarchical flowers by hydrothermal growth, RSC Crystal Engineering Communication, 15, 8246 – 8249, 2013.

[16] M. Navaneethan, J. Archana, M. Arivanandhan, and Y. Hayakawa, Chemical synthesis of ZnO hexagonal thin nanodiscs and dye-sensitized solar cell performance, Physica Status Solidi RRL, 6, 120 – 122, 2012.

[17] T. J. Athauda, W. S. Lepage, J. M. Chalker, and R. R. Ozer, High density growth of ZnO nanorods on cotton fabric enables access to a flame-resistant composite, RSC Advances, 4, 14582 – 14585, 2014.

[18] N. Abidi, L. Cabrales, and E. Hequet, Functionalization of a cotton fabric surface with titania nanosols: applications for self-cleaning and UV-protection properties, ACS Applied Materials Interfaces 1, 2141 – 2146, 2009.

[19] S. Saini, P. Mele, H. Honda, T. Suzuki, K. Matsumoto, K. Miyazaki, A. Ichinose, L. Molina Luna, R. Carilni, A. Tiwari, Effect of self-grown seed layer on the thermoelectric properties of ZnO thin films, Thin Solid Films, 605, 289 – 294, 2016.

[20] H. Li, S. Jiao, and L. Hongtao, Growth and characterization of ZnO nanoflakes by hydrothermal method: effect of hexamine concentration, Journal of Materials Science: Materials Electron, 25, 2569 – 2573, 2014.

[21] N. Rajamanickam, S. Rajashabala, and K. Ramachandran, On the structural and optical properties of nano-ZnO and its morphologies, Journal of Luminesces 146, 226 – 233, 2014.

[22] G. N. Narayanan and K. Annamalai, Role of hexamethylenetetramine concentration on structural, morphological, optical and electrical properties of hydrothermally grown zinc oxide nanorods, Journal of Materials Science: Material Electron, DOI 10.1007/s10854-016-5376-6.

[23] B. D. Boruah and A. Misra, Energy-efficient hydrogenated zinc oxide nanoflakes for high-performance self-powered ultraviolet photodetector, ACS Applied Materials Interfaces, 8, 18182 – 18188, 2016.

[24] X. Li, P. Liang, L. Wang, F. Yu, Preparation and characterization of high uniformity zinc oxide nanosheets, Frontiers of Optoelectronics, 7, 509 – 512, 2014.

[25] W. K. Tan, K. A. Razak, Z. Lockman, G. Kawamura, H. Muto, A. Matsuda, Synthesis of ZnO nanorods-nanosheet composite via facile hydrothermal method and their photocatalytic activities under visible-light irradiation, Journal of Solid State Chemistry, 211, 146 – 153, 2014.

[26] T. C. Damen, S. P. S. porto, and B. Tell, Raman effect in zinc oxide, Journal of Physical Review, 142, 570 – 574, 1966.

[27] S. Bera, H. Khan, I. Biswas, S. Jana, Polyaniline hybridized surface defective ZnO nanorods with long-term stable photoelectrochemical activity, Applied Surface Science, 383, 165 – 176, 2016.

[28] V. Russo, M. Ghidelli, P. Gondoni, C. S. Casari, and A. L. Bassi, Multi-wavelength Raman scattering of nanostructured Al-doped Zinc oxide, Journal of Applied Physics, 115, 073508 (1-10), 2014.

[29] P. Sehgal and A. K. Narula, Influence of amines as surfactant on the optical, thermal, and structural properties of nanostructured ZnO, Applied Physics A, 119, 1405 – 1412, 2015.

[30] P. K. Samanta and A. K. Bandyopadhyay, Chemical growth of hexagonal zinc oxide nanorods and their optical properties, Applied Nanoscience, 2, 111 – 117, 2012.

[31] S. B. Amor, M. Jacquet, P. Fioux, M. Nardin, XPS characterization of plasma treated and zinc oxide coated PET, Applied Surface Science, 255, 5052 – 5061, 2009.

[32] M. Gancheva, M. M. Velichkova, G. Atanasova, D. Kovacheva, I. Uzunov, R. Cukeva, Design and photocatalytic activity of nanosized zinc oxides, Applied Surface Science, 368, 258 – 266, 2016.

[33] R. Al-Gaashani, S. Radiman, A. R. Daud, N. Tabet, Y. Al-Douri, XPS and optical studies of different morphologies of ZnO nanostructures prepared by microwave methods, Ceramics International 39, 2283 – 2292, 2013.

[34] M. D. McCluskey and S. J. Jokela, Defects in ZnO, Applied physics, 106, 071101, 1 – 13, 2009.

[35] W. A. Zisman, Relation of the equilibrium contact angle to liquid and solid constitution, Advance Chemistry Series, 43, 1 – 51, 1964.

[36] R. N. Wenzel, Surface roughness and contact angle, Journal of Physical Chemistry, 53, 1466 – 1467, 1949.

[37] A. Becheri, M. Durr, P. L. Nostro, P. Baglioni, Synthesis and characterization of zinc oxide nanoparticles: application to textiles as UV-absorbers, Journal of Nanoparticles Research 10, 679 – 689, 2008.

[38] Th. I. Shaheen, M. E. El-Naggar, A. M. Abdelgawad, A. Hebeish, Durable antibacterial and UV protections of in situ synthesized zinc oxide nanoparticles onto cotton fabrics, International Journal of Biology Macromolecules, 83, 426 – 432, 2016.

[39] M. S-Khalilabad and M. E. Yazdanshenas, Bifunctionalization of cotton textiles by ZnO nanostructures: antimicrobial activity and ultraviolet protection, Textile Research Journal, 83, 993 – 1004, 2013.

[40] E. S. Ates and H. E. Unalan, Zinc oxide nanowire enhanced multifunctional coatings for cotton fabrics, Thin solid films, 520, 4658 – 4661, 2012.

[41] S. Kathirvelu, L D Souza and B Dhurai, UV protection finishing of textiles using ZnO nanoparticles, Indian Journal of Fibers and Textile Research, 34, 267 – 273, 2009.

[42] F. Salleh, K. Asai, A. Ishida, and H. Ikeda, Seebeck coefficient of ultrathin silicon-on-insulator layers, Applied Physics Express 2, 071203 (1-3), 2009.

[43] Lori E G, Benjamin D, Yuhas M L, David Z and Peidong Y, Solution-Grown Zinc oxide nanowires, Journal of Thin films, 45,7535 – 7543, 2005.

[44] Innocent U, Manoj K R, Elias K S, Aloysius F H, Yogi D G, One dimensional-ZnO nanostructures: Synthesis, properties and environmental applications, Materials Science Semiconductor Proceeding, 13, 2070 – 2083, 2013.

[45] N S Ridhuan, K A Razak, Z Lockman, A A Aziz, Structural and morphology of ZnO nanorods synthesized using ZnO seeded growth hydrothermal method and its properties as UV sensing, PLOS one, 7, 50405, 2012.

Incorporation of ZnO and their composite nanostructured

material into a cotton fabric platform

4.1. Introduction

With the growing concerns of the energy crisis and environmental protection, the development of Wearable Power Generator (WPG) devices has taken an accelerated pace. Wearable Power Generator devices could be used to tap the temperature gradient between a hot object (human body) and cold (ambient) one and convert this into solid-state thermal energy scavenging employing thermoelectric (TE) generators. The performance of TE material is closely related to the dimensionless figure-of-merit (zT), which is given by $zT = [(S^2 \sigma)/\kappa]\,T$, where S, σ, κ, and T denote the thermopower (Seebeck), electrical conductivity, thermal conductivity, and temperature, respectively [1 – 3]. TE materials have prominent aspects like reliability, environmental benignity, and easy incorporation into existing technologies. They can be used as long-life power sources and provide a long-lasting solution to the ever-growing demand for implantable medical devices. This increasing demands for lightweight, high flexible, stretchable, and washable presents critical challenges for the progress of WPG [4 – 7].

The selection of the material has a significant role in the fabrication of high performing TE materials. Owing to its flexible nature, conducting polymers (CPs) are favorable materials for the practical TE applications. Because of their high flexibility, environmental stability, and facile synthesis, they have potential for use on human skin [8 – 10]. However, most of the CPs such as polyaniline, polypyrrole, and poly (3,4-ethylenedioxythiophene) polystyrene sulfonate (PEDOT: PSS) are expensive and require complex treatments to achieve good electrical conductivity [11 – 13]. Hence, efforts have been made to find an alternative for fabricating flexible TE materials and composite materials have recently been attracting more and more attention since they possess many advantages including high thermopower, easy process-ability and cost-effectiveness [14 – 16].

The encapsulation of MoS2 with polymers by precipitation process and the variations in thermopower efficiency at room temperature, 0.1 to 0.2 µV/K. Polychlorotrifluorethene was used as a binder and graphite was added as a conductive component to the copper (I) oxide composites, to adjust the thermopower and the electrical conductivity [17]. The polymer/carbon nanotube composites synthesized by vacuum filtration method and the thermopower was found to be around 22.2 µV/K at room temperature [18]. The Ag/PEDOT: PSS/ ZnO composite prepared structures by Ink-jet-printing technology and thermopower were reported to be around -35 µV/K at room temperature. PEDOT: PSS is a conductive polymer and was used to form the matrix of the composite containing ZnO nanoparticles, and Ag-ink was used for the interconnects between PEDOT: PSS and ZnO nanoparticles [19]. The highly flexible copper oxide-graphite-polymer composites prepared by sol-gel method and the device exhibited thermopower values between 10 - 600 µV/K at room temperature [20]. The reported Thermopower value was of about 285 µV/K near room temperature for Te nanowire/P3HT polymer composite by TeO_2 reduction process, using hydrazine as a solvent [21].

Therefore, nanocomposites consisting of homogeneous and uniform dispersion of nanoparticles in the polymer matrix lead to higher TE properties. Moreover, polymers having crystalline with amorphous structure or polymers with nanoparticle interfaces create boundaries that scatter phonons, thus ensuring low thermal conductivity [22 – 24]. The selection criteria of antimony (Sb) based on the following properties; it is electrical and thermal conductivity are lower than most metals conductivities, N type dopant for semiconductor industry, best thermoelectric materials at room temperature, due to existence of minimum in lattice thermal conductivity [25]. Similarly, for silver it has semiconductor intermetallic compounds which will have unexpectedly low thermal conductivity which leads to improved thermoelectric properties, P type dopant for

semiconductor industry, it is stable in air with highest electrical conductivity. There are no available reports, which describe the influence of Sb-/Ag- ZnO-composite on cotton fabric using the solvothermal method for application on WPG [26]. The interaction of Sb-/Ag- ZnO with textile material would make major difference in thermopower. In this study, we modified cotton fabric with Sb-/Ag- ZnO-composite by in situ solvothermal growth technique at low temperature to develop flexible n-type and p-type TE material. In the present work, ZnO and its composites were prepared by solvothermal methods and its structural, morphological, electrical and thermoelectric properties were studied.

4.2. Experimental Procedure

4.2.1 Preparation of ZnO/ ZnO composites fabric via solvothermal method

Zinc nitrate hexahydrate, hexamethylenetetramine (hexamine), silver nitrate, and antimony trichloride taken were analytic grade from Wako chemicals, Japan and used without further purification. Plain weave cotton fabric (density of 125.45 g/m^2 and thickness of 0.15 mm) was used as substrate and the fabric was ultra-sonicated in ethanol and water for 5 min, then dried at 60 °C overnight and cooled to room temperature. 0.1 M of zinc nitrate hexahydrate and 0.02 M X (silver nitrate/ antimony trichloride) were dissolved in 40 mL of deionized water under magnetic stirring. 0.2 M of hexamine was dissolved in 40 mL of deionized water and added slowly to the Zinc nitrate hexahydrate -X solution. After a few minutes, the cotton fabric was immersed in the solution. Similar procedure was adopted for 0.2 M of zinc nitrate hexahydrate, 0.02 M X (silver nitrate/ antimony trichloride) and 0.1 M of hexamine. The above processes were performed at a temperature of 50 °C and the solution was stirred magnetically for 2 hours (Stage 1). The prepared fabric solution was placed in a 100 mL Teflon-lined stainless steel autoclave, which was sealed and heated at 120 °C for 1 hour, then cooled down to room temperature. The fabric with the

resultant seed creation was collected and washed three times thoroughly with absolute ethanol and distilled water. Finally, the product was dried in an oven for 2 hours at 60 ℃ (Stage 2). The same process was performed as the second step, with the growth period maintained as 5 hours, which led to the formation of ZnO-composite nanostructures (Stage 3) and the series of efforts for the various stages were tabulated as shown in Table 4.1. The diagrammatic representation of deposition of ZnO composites over cotton fabrics is shown in Fig. 4.1.

Table 4.1. Description of sample code and their chemical concentrations

| S. No	Zinc nitrate hexahydrate (M)	Hexamine (M)	Silver nitrate (M)	Antimony Trichloride (M)	Sample code
1.	0.1	0.2	-	-	Z1
2.	0.2	0.1	-	-	Z2
3.	0.1	0.2	0.02	-	SZ1
4.	0.2	0.1	0.02	-	SZ2
5.	0.1	0.2	-	0.02	AZ1
6.	0.2	0.1	-	0.02	AZ2
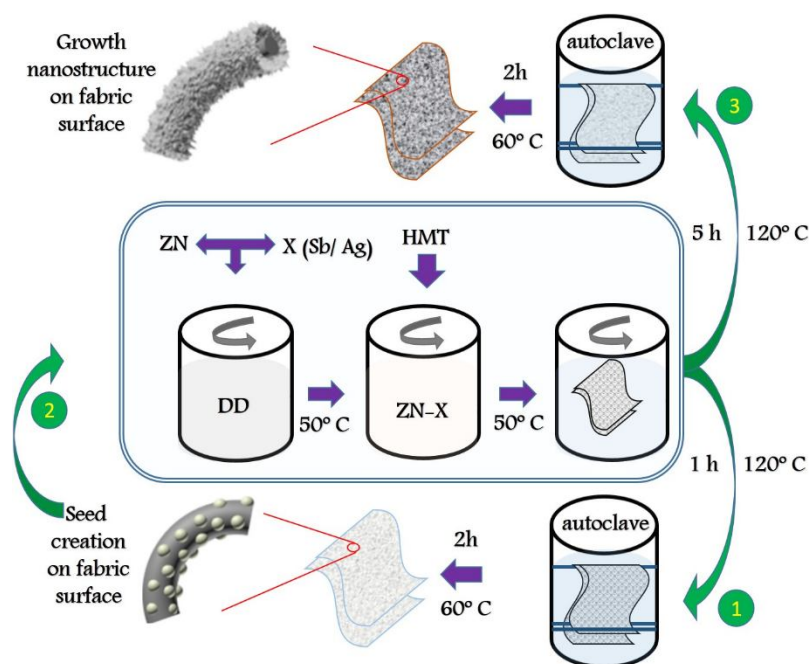
ZN- Zinc nitrate hexahydrate, Sb- Antimony trichloride, Ag- Silver nitrate, HMT – Hexamine
Fig. 4.1 Fabrication process of the nanostructured coated cotton fabric

4.3 Result and discussion

4.3.1 Structural analysis

In this study, we have prepared samples with six different concentrations: ZnO, Sb-ZnO, and Ag-ZnO with ratios 1:2 M, 2:1 M of Zinc nitrate hexahydrate and hexamine and they were labelled as Z1, Z2, SZ1, SZ2, AZ1, and AZ2 respectively, yielding nominal compositions. Fig. 4.2 (a) and (b) represent the XRD analysis that was employed to investigate the crystalline phase constitution of the as-synthesized sample. The XRD pattern shows the typical diffraction peaks which could be indexed to that of cellulose (CF; JCPDS card no. 03-0226) and ZnO cotton fabric showed the strong diffraction peaks that are in good agreement with the known hexagonal wurtzite phase of ZnO (Z1, Z2; JCPDS card no. 89-1397). However, a relatively stronger intensity was observed for the ZnO (1 0 0) and (1 0 1) diffraction peaks, which indicates that the preferred growth direction is along the c-axis, almost perpendicular to the individual cotton fiber and surface. Moreover, the intensities of the Z1 and Z2 (see Fig. 4.2 (a) and Fig. 4.2 (b)) peaks enhance observably with increasing precursor concentration from 1:2 to 2:1, which is consistent with the variation in the quantity of zinc nitrate hexahydrate and hexamine. The ZnO diffraction peaks appear in all patterns, but they become less intense as the Sb-/ Ag- ZnO composites are formed indicating less crystallinity. New peaks begin to appear in SZ1, SZ2 peaks (see; Fig. 4.2 (a) and Fig. 4.2 (b)) which belong to the Sb impurity phase, which are in good agreement with the tetragonal phase of metallic Sb (JCPDS card no. 89-1610). The effect of Sb in ZnO rich condition is such that due to the low-pressure oxygen (PO_2) which suppresses the incorporation of Sb in the Zn sites and the formation of Sb_{Zn} donors, low electron concentrations are resulted.
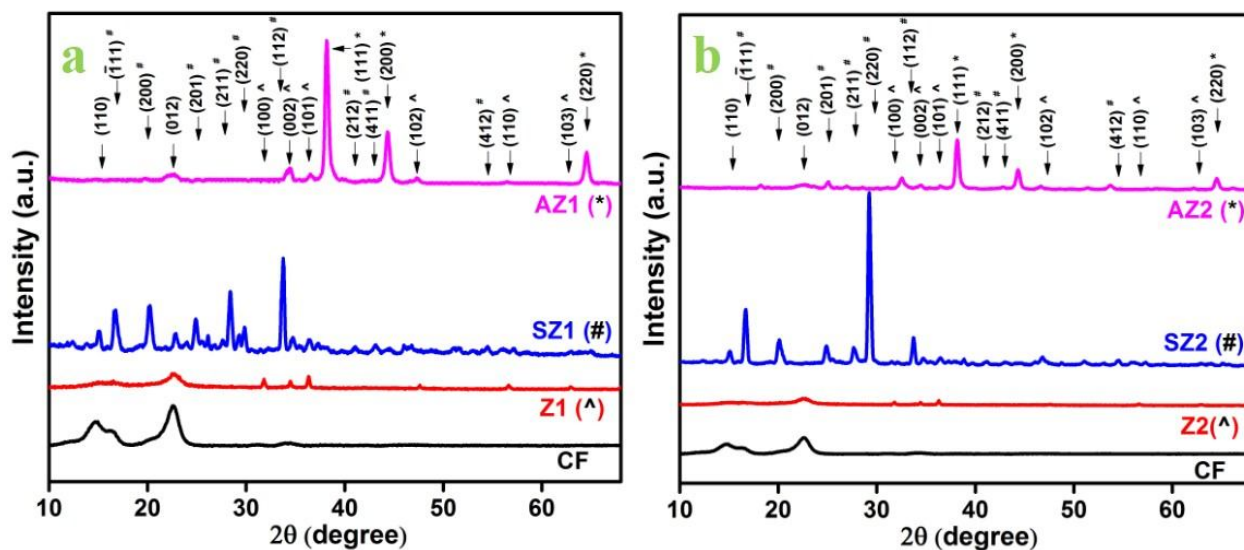
Fig. 4.2 XRD analysis for the obtained fabric before and after the solvothermal treatment

On the other hand, high PO_2 favors incorporation of Sb in the Zn sites and instead suppresses the incorporation of Sb in the O sites, both factors leading to higher electron concentration and mobility. Due to this, secondary peaks are generated and a decrease in the peak position value is generally observed when a composite element with a longer ionic radius replaces Zn^{2+} at the substitution sites of the ZnO crystal lattice. There are additional peaks which appear in AZ1, AZ2 (see; Fig. 2 (a) and Fig. 2 (b)) and they revealed the diffraction patterns of metallic Ag (JCPDS card no. 04-0783), which can be indexed to the (1 1 1) and (2 0 0) crystal planes of the face-centered-cubic (FCC) phase. Moreover, the Ag^+ ion has a higher ionic size than a Zn^{2+} ion, probably substituting Zn^{2+} ions, and the appearance of Ag peaks in the diffraction patterns clearly indicates the formation of crystalline silver clusters in the nanoparticles [27]. Therefore, the increment in the XRD peak positions in this case suggests that the Ag ions have occupied the interstitial sites of ZnO, which is consistent with the reported results [28].

4.3.2 Morphological study

The FE-SEM images revealed the ZnO nanorods array grown on the surface of a single fiber and preferred axis of growth of nanorods is perpendicular to the fiber as shown in Fig. 4.3 (a-d). Figure 4.3 (a, b) shows that for 1:2 ratio of zinc nitrate hexahydrate: hexamine, due to the higher concentration of hexamine longer nanorods are obtained. Fig. 4.3 (c, d) shows that for 2:1 ratio of zinc nitrate hexahydrate: hexamine however, the size of the ZnO nanorods dramatically decreases with the increase in zinc nitrate hexahydrate concentration and decrease in hexamine concentration. This indicates that the type of capping molecules has an influence on the formation of ZnO nanorods. It can be clearly seen that the concentration of hexamine is an important factor that influences the length and dimension of the nanorods (Fig. 4.3a, 4.3c). In fact, the hexamine can step into the nucleation process of ZnO and inhibit the formation of nanorods (Fig. 4.3b, 4.3d). In Figure 4.3 (e-h), a uniform layer of high-density Sb-ZnO, composite nanorods are formed on the fiber surface and the product is highly compact, intertwining into a cluster. As can be seen from this figure, when Sb is composited with ZnO grain size decreases and grain number increases due to the increase in metal nucleation centers, which confirm the enhancement in crystallinity. Figure 4.3 (i-l) exhibits a typical image of the Ag-ZnO composite. The absence of nanorods, and the reasonable presence of silver have been shown to initiate the growth of nanosheets assembled into 3D network architectures, with lots of interspaces and intermesh with each other to form voids simultaneously between the adjacent sheets.
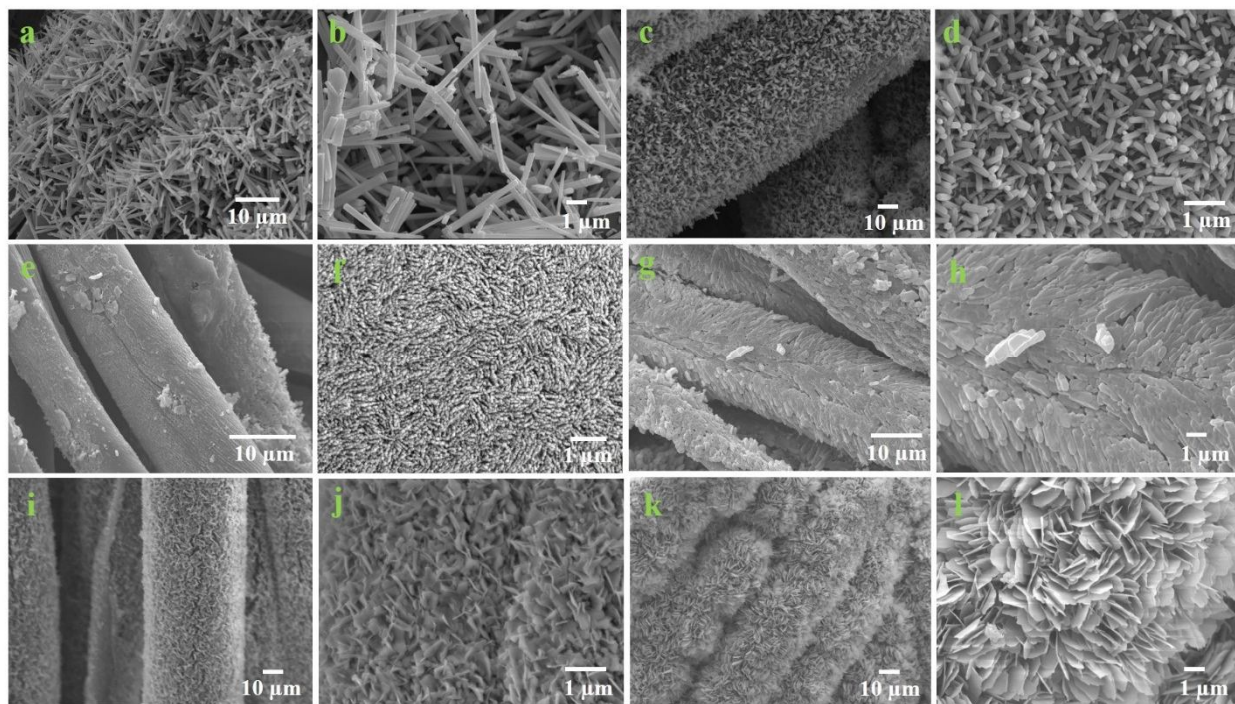
***Fig. 4.3 FESEM images of solvothermally treated fabrics obtained from (a - d) ZnO,
(e - h) Sb-ZnO, and (i - l) Ag-ZnO composite***

4.3.3 Binding between ZnO/ ZnO-composite fabric

With the XRD analysis, it was confirmed that a Sb-/ Ag- ZnO Composite is deposited on the surface of the cotton fabric. To further clarify the chemical states of ZnO, Sb-/ Ag- ZnO-composite, XPS spectral analysis was carried out with the binding energies calibrated using C 1s (284.8 eV). Figure 4 shows the scan survey spectra of the samples, in which all the peaks are attributed to ZnO, Sb, and Ag, confirming the formation of the composite with the fabric. The Zn $2p_{3/2}$ and Zn $2p_{1/2}$ peaks are also shifted to a higher binding energy with a value of 0.35 – 0.5 eV (Fig. 4.4a) because of the heat treatment, which can be explained by the difference in electronegativity (χ) of Zn (χ=1.65), Sb (χ=2.05) and Ag (χ=1.93).
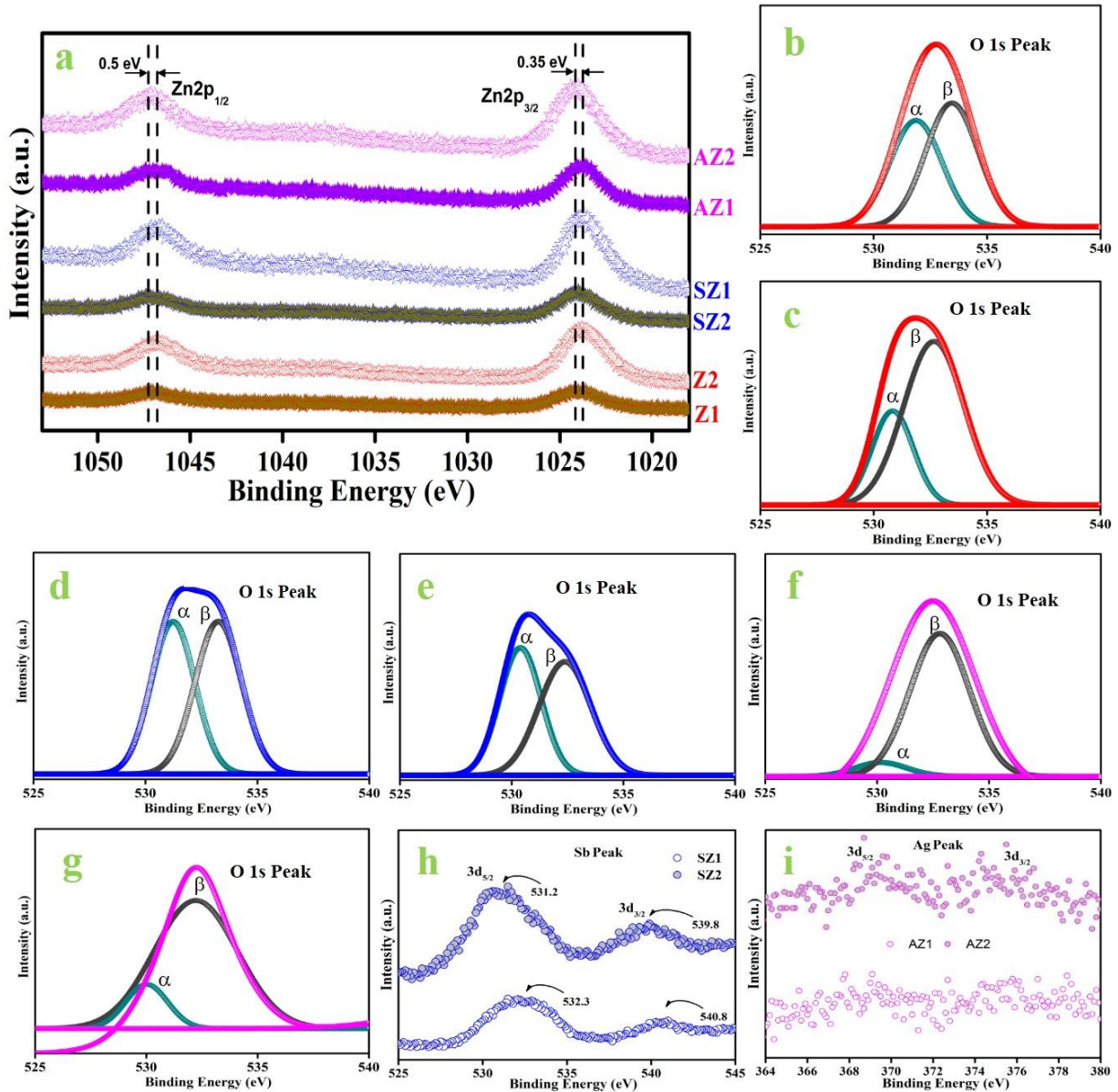
Fig. 4.4 XPS spectra of (a) Zn 2p corresponding to the Zn core, (b-g) oxygen 1s peak, (h) Sb core, and (i) Ag core

This comparably higher electronegativity of Sb and Ag attracts electrons from Zn, resulting in a decrease in its electron screening effect [29]. Fig 4.4 (b-g) shows the O 1s peaks for ZnO, Sb-ZO, Ag-ZO composite samples. All the O 1s peaks are nearly asymmetric, suggesting that there are at least two kinds of oxygen species on the sample surfaces. The O 1s peak which can be consistently deconvoluted into a Gaussian peak marked with 'α' is closely associated with the lattice oxygen of ZnO.

The observed a similar component in their O 1s spectra and associated this to the O^{2-} ion in the wurtzite structure which is surrounded by the Zn atoms. Then the 'β' is attributed to the oxygen deficiencies or vacancies within the ZnO matrix whereas the higher binding energy component is probably due to some surface hydroxyl species [30]. The reported similar components in their O 1s spectra and ascribed to the high binding energy state on Zn-OH species. In addition, the two sets of peaks are associated with Sb $3d_{5/2}$ and Sb $3d_{3/2}$ peaks were assigned to binding energies 531 ± 0.9 eV and 540 ± 0.9 eV; O1s and Sb $3d_{5/2}$ are superposed around 531 ± 0.9 eV as shown in Fig. 4.4(h). The existence of the Sb $3d_{3/2}$ represents antimony oxide, indicating that the antimony has probably incorporated into the Zn sites [31]. Hence, the reported that similar Sb 3d peaks are characterized by a doublet which arises due to the spin-orbit coupling of $3d_{3/2}$ and $3d_{5/2}$. The binding energies of Ag $3d_{5/2}$ and Ag $3d_{3/2}$ are 368 ± 0.5 eV and 374 ± 0.8 eV, which confirms the formation of metallic Ag^+ as shown in Fig. 4.4(i). The Ag-ZnO ratio may be ascribed to the increased number of Ag atoms occupying O sites, while the Sb atoms seem most likely to occupy the Zn sites [32]. Thus, suggested that the electron density of Ag in Ag-ZnO-composite is decreased. This reduction of electron density of Ag might be owing to the transfer of electron from Ag to ZnO [33, 34].

4.3.4 UV shielding analysis

To investigate the UV shielding effect, ZnO and ZnO-composite coated on cotton fabric, were measured in the wavelength region 200 nm to 800 nm using the bare cotton fabric as the reference. The measurements were performed in at least three different spots and the results were averaged together. The calculated ultraviolet protection factor (UPF) values are shown in Fig. 4.5 (a). The UV transmittance values of the ZnO/ ZnO-composite coated fabrics are found to be much higher than thereference (CF; 6.664), which indicates that the coated fabrics show

improved blocking of UV radiation. The UPF values of ZnO, Sb- ZnO, and Ag- ZnO fabrics are 64.34 (Z1), 64.5 (Z2), 67.36 (SZ1), 69.34 (SZ2), 83.85 (AZ1), and 83.96 (AZ2). These UPF values can be classified as excellent, and very good UV shielding respectively, according to ASTM D 6603 for UV radiation protection categories of fabrics [35]. These results show clearly that the coating of cotton fabric with ZnO-composite can greatly enhance the UV-shielding properties of fabrics.
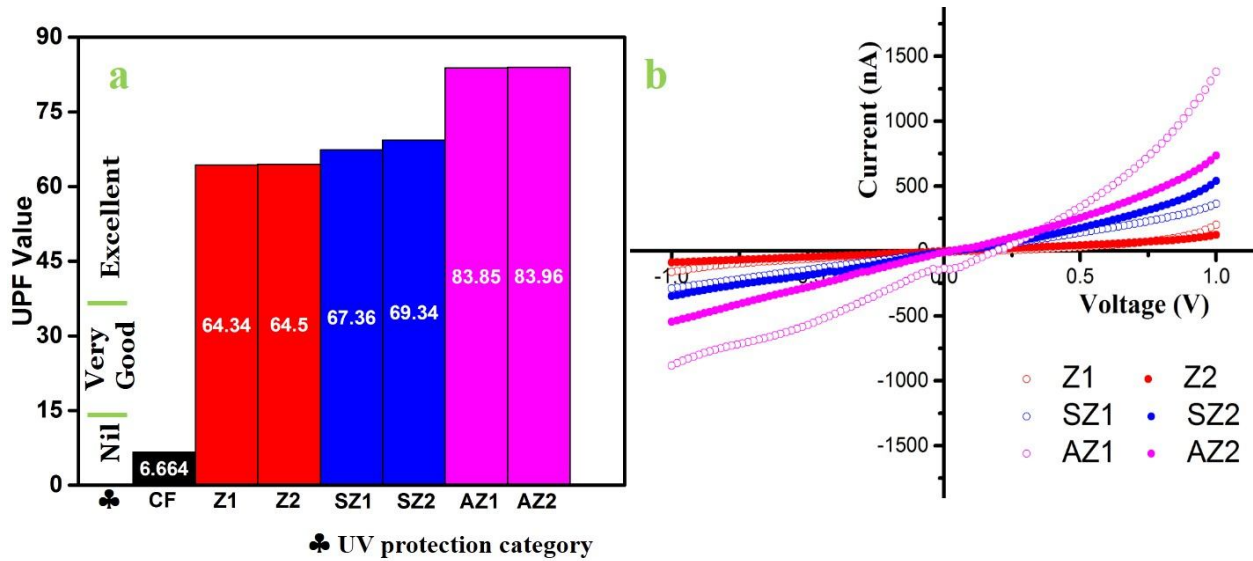
Fig. 4.5 (a) UV shielding properties, and (b) I – V characteristics of the ZnO/ ZnO-composites coated fabric

4.3.5 Electrical conductivity

The current-voltage (I-V) characteristics of ZnO/ ZnO-composite fabrics are shown in Fig. 4.5 (b) and is found to be linear, indicating the ohmic conduction mechanism. It is found that the conductivity of the as-grown n-type (ZnO and Sb-ZnO-composite) and p-type (Ag-ZnO-composite) fabric varies. The I-V measurements were carried out between two points on the fabric surface, and the experiment was conducted 3 times at different places to ensure that the obtained conductivity represented the whole of the coated fiber layer. It is noteworthy that the I-V plot representing Sb-/ Ag- ZnO composite nanoparticles resembles that of metallic conductors with

considerably low ohm resistance. This approves that composites of antimony and silver with metal oxides increases the conductivity as well as supports the physiochemical characterizations and that the pure ZnO I-V plot follow semiconductor behavior at lower and higher concentrations. This may be due to the replacement of Zn^{2+} by Sb^{3+} or Ag^{3+}, thus contributing additional charge carriers to the electrical conduction. Thus, the increase in the electrical conductivity may be associated with the presence of large number of charge carriers introduced by the additive [36].

4.3.6 Thermopower

Semiconductors are known to have many carriers like metals, which gives raise to low thermal conductivity, thus subsequently resulting in enormous thermopower. Thermopower is a thermoelectromotive force induced by the Seebeck effect in response to a temperature difference across the coated cotton fabric. It is well known that cotton fabric acts as an insulator, so we cannot measure the thermopower, the results of all other samples are shown in Fig. 4.6. The slope of the graph represents the thermopower of the ZnO/ ZnO-composites. If the difference in temperature is less than 5 degrees, the relationship between the thermoelectromotive force and the difference in temperature should be almost linear. If the slope is negative, it means the material is n-type, otherwise it is p-type. For n-type material, the majority charge carriers are electrons; and for p-type, holes. Fig. 4.3 (a) and (c) show ZnO nanorods based on 1:2 and 2:1 ratio of zinc nitrate hexahydrate and hexamine and depict longer nanorods at higher hexamine concentration (1:2) and shorter nanorods on other (2:1). At the same time, the absolute value of the thermopower decreases from 36.311 µV/K (see graph: Z1) to 10.534 µV/K (see graph: Z2). Thus, it is possible to observe that the longer nanorods have connections with each other that contribute to the electron transport being easier than in the other case, which explains the quantitatively higher value of thermopower with the longer nanorods [37].
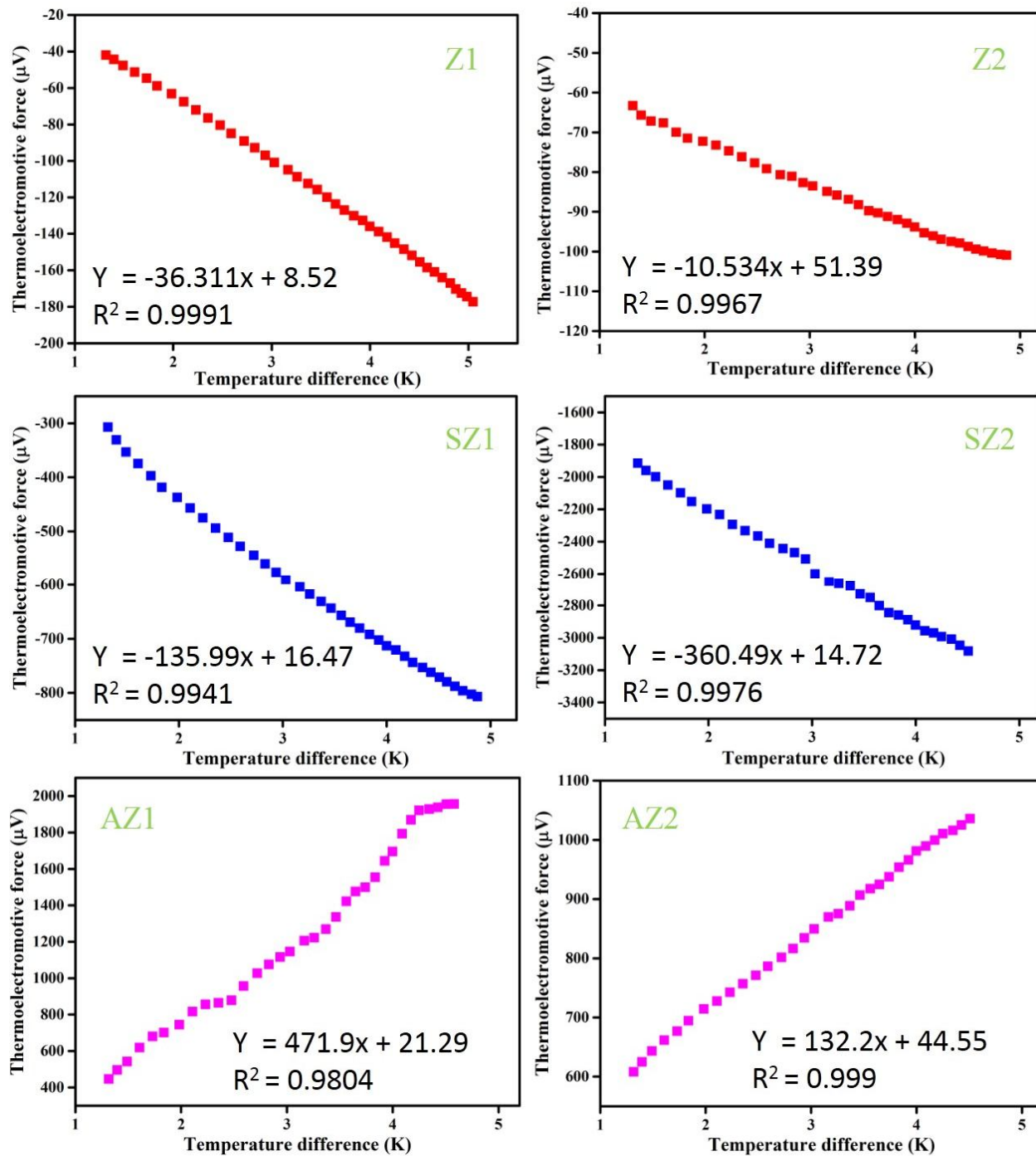
Fig. 4.6 Measured thermoelectromotive as a function of the temperature difference

Although, the thermopower increases for Sb-ZnO composite from 135.99 µV/K (see graph: SZ1) to 360.49 µV/K (see graph: SZ2). It is worth noting that the Sb/ZnO network on the surface

of the fiber is formed as a freestanding composite, which should be attributed to the Sb incorporation into the Zn sites and oxygen vacancies, which leads to n-type behavior [38 – 40]. It is possible to observe that the laterally continual nanorods on the surface of each individual fiber can explain the higher value of thermopower (SZ2). The Ag-composite with ZnO is shown as positive, which means that the material is p-type, and it seen with a thermopower value of 471.9 µV/K (see graph: AZ1), 132.2 µV/K (see graph: AZ2 respectively. Therefore, the growth process of ZnO is disrupted, when the Ag composites are introduced, and the growth process is again favored when enough Ag have recombined with the Zn material that may cause the positive effect on the charge separation efficiency [41, 42]. It is of great importance to note here that both the compounds (AZ1 and AZ2) possess the p type thermopower but AZ1 exhibit the higher value due to the intergranular crystal structure, which plays an important role in charge transport.

4.4. Conclusion

In this study, a simple, versatile, and effective approach for the development of ZnO/ Sb-/ Ag-/ ZnO-composite on cotton fabric prepared by solvothermal method was described. It was demonstrated that the coating of ZnO/ Sb-/ Ag-/ ZnO-composite can convert an insulator, a cotton fabric into a conductive fabric. The existence of nanostructures on the fabric surface caused an excellent UV shielding property in the Ag- ZnO-Composite fabric, as was demonstrated by an UPF value of 83.96. Additionally, the coated fabric showed good I – V characteristics with rectifying behavior of conductivity. Furthermore, we have investigated the thermopower of the coated fabric, which attributes to the intergranular crystal structure of Ag-ZnO composite, possessing the highest value of 471.9 µ/K. It is concluded that the nanocomposites, having a higher thermopower and UV shielding, is a better candidate for wearable device applications.

References

1. Vladimir Leonov, and Ruud J. M. Vullers, Journal of Renewable and Sustainable Energy, 1, 062701, 1-10, 2009.

2. Ziyang Wang, Vladimir Leonov, Paolo Fiorini, Chris Van Hoof, Sensors and Actuators A: Physical, 56, 95-102, 2009.

3. Pandiyarasan Veluswamy, Suhasini Sathiyamoorthy, Kalari Hanuman Chowdary, Omprakash Muthusamy, Karthikeyan krishnamoorthy, Tsunehiro Takeuchi, Hiroya Ikeda (2016), Journal of Alloys and Compounds, 695, 888-894, 2017.

4. Sun Jin Kim, Ju Hyung We and Byung Jin Cho, Energy & Environmental Science, 1(3), 1-8, 2013.

5. Yong Du, Kefeng Cai, Song chen, Hongxia Wang, Shirley Z Shen, Richard Donelson & Tong Lin, Scientific Reports, 5, 6411, 1-6, 2015.

6. Andrea Cadei, Alessandro Dionisi, Emilio Sardini and Mauro Serpelloni, Measurement Science and Technology, 25, 012003, 1-14, 2014.

7. Sami Boufi, Israel Gonzalez, Marc Delgado-Aguilar, Quim Tarres, M. Angels Pelach, and Pere Mutje, Carbohydrate Polymers, 154, 151-166, 2016.

8. Ming He, Feng Qiu, and Zhiqun Lin, Energy & Environmental Science, 6, 1352-1361, 2013.

9. Mario Culebras, Clara M. Gomez and Andres Cantarero, Materials, 7, 6701-6732, 2014.

10. Mariappan Premanathan, Krishnamoorthy Karthikeyan, Kadarkaraithangam Jeyasubramanian, Govindasamy Manivannan, Nanomedicine: Nanotechnology, Biology, and Medicine, 7, 184-192, 2011.

11. Junjie Li, Xinfeng Tang, Han Li, Yonggao Yan, Qingjie Zhang, Synthetic Metals, 160, 1153-1158, 2010.

12. Jiansheng Wu, Yimeng Sun, Wen-Bo Pei, Ling Huang, Wei Xu, Qichun Zhang, 196, 173-177, 2014.

13. Olga Bubnova, Zia Ullah Khan, Abdellah Malti, Slawomir Braun, Mats Fahlman, Magnus Berggren and Xavier Crispin, 10, 429-433, 2011.

14. Brendan T. McGrail, Alp Sehirlioglu, and Emily Pentzer, Angewandte Minireviews, 54, 1710-1723, 2015.

15. Maria Ibanez, Zhishan Luo, Aziz Genc, Laura Piveteau, Silivia Ortega, Doris Cadavid, Oleksandr Dobrozhan, Yu Liu, Maarten Nachtegaal, Mona Zebarjadi, Jordi Arbiol, Maksym V. Kovalenko & Andreu Cabot, Nature Communications, 7, 10766, 1-7, 2016.

16. Naveed Mengal, Iftikhar Ali Sahito, Alvira Ayoub Arbab, Kyung Chul Sun, Muhammad Bilal Qadir, Anam Ali Memon, and Sung Hoon Jeong, Carbohydrate Polymers, 152, 19-25, 2016.

17. Rabin Bissessur, Mercouri G. Kanatzidis, J. L. Schindler and C. R. Kannewurf, Chemical Society, Chemical Communications, 1582-1585, 1993.

18. Lirong Liang, Caiyan Gao, Guangming Chen, and Cun-Yue Guo, Materials Chemistry C, 4, 526-532, 2016.

19. Angelina Besganz, Volker Zollmer, Robert Kun, Edit Pal, Lorenz Walder, Matthias Busse, Procedia Technology, 15, 99-106, 2014.

20. Virgil Andrej, Kevin Bethke, and Klaus Randemann, Physical Chemistry Chemical Physics, 18, 10700-10707, 2016.

21. Ya Yang, Zong-hong Lin, Techien Hou, Fang Zhang, and Zhong Lin Wang, Nano Research, 5(12), 888-895, 2012.

22. Y. Agari, A. Ueda, Y. Omura, and S. Nagai, Polymer, 38(4), 801-807, 1997.

23. Olga Bubnova, Zia Ullah Khan, Hui Wang, Slawomir Braun, Drew R. Evans, Manrico Fabretto, Pejman Hojati-Talemi, Daniel Dagnelund, Jean-Baptiste Arlin, Yves H. Geerts, Simon Desbief, Dag W. Breiby, Jens W. Andreasen, Roberto Lazzaroni, Weimin M. Chen, Igor Zozoulenko, Mats Fahlman, Peter J. Murphy, Magnus Berggren & Xavier Crispin, Nature Materials, 13, 190-194, 2013.

24. Roch Chan Yu King, Frederick Roussel, Jean-Francois Brun, Carole Gors, Synthetic Metals, 162, 1348-1356, 2012.

25. J. Navratil, Z. Stary and T. Plechacek, Materials Research Bulletin, 31 (12), 1559 – 1566, 1996.

26. R. Carlini, D. Marre, I. Pallecchi, R. Ricciardi, G. Zanicchi, Intermetallics, 45, 60 – 64, 2014.

27. R. S. Zeferino, M. B. Flores and U. Pal, Journal of Applied Physics, 109, 014308 (1-6), 2011.

28. Sara Khosravi-Gandomani, Ramin Yousefi, Farid Jamali-Sheini, Nay Ming Huang, Ceramics International, 40, 7957-7963, 2014.

29. Hyung-Sik Woo, Chang-Hoon Kwak, ll-Doo Kim, and Jong-Heun Lee, Materials Chemistry A, 2, 6412-6418, 2014.

30. L. L. Yang, Q. X. Zhao, M. Willander, X. J. Liu, M. Fahlman, J. H. Yang, Applied Surface Science, 256, 3592-3597, 2010.

31. Niranjan S. Ramgir, Imtiaz S. Mulla, and Vijayamohanan K. Pillai, Physical Chemistry B, 110, 3995-4001, 2006.

32. U. Nithiyanantham, Sivasankara Rao Ede, M. Fevzi Ozaydin, Hong Liang, A. Rathishkumar and Subrata Kundu, RSC Advance, 5, 89621-89634, 2015.

33. Wan-Gyu Kwak, Man Hwan Oh, Myoung-Seon Gong, 115, 317-324, 2015.

34. Weiwei Lu, Guosheng Liu, Shuyan Gao, Shantao Xing, and Jianji Wang, 19, 445711 (1-10), 2008.

35. Polona Dobnik Dubrovski and Darko Golob, Textile Research Journal, 79 (4), 351-359, 2009.

36. B. L. Zhu, C. S. Xie, J. Wu, D. W. Zeng, A. H. Wang, X. Z. Zhao, Materials Chemistry and Physics, 96, 459-465, 2006.

37. Junghyeok Kwak, Chang-Eun Kim, Yuho Min, Ji-Hwan Lee, Aloysius Soon, and Unyong Jeong, Crystal Engineering Communication, 17, 5734-5743, 2015.

38. Yongliang Li, Liang Huang, Peixin Zhang, Xiangzhong Ren and Libo Deng, Nanoscale Research Letters, 10 (414), 1-7, 2015.

39. X Song, P H M Bottger, O B Karlsen, T G Finstand and J Tafto, Physica Scripta, 014001, 1-6, 2012.

40. B. L. Zhu, S. J. Zhu, X. Z. Zhao, F. H. Su, G. H. Li, X. G. Wu, and J. Wu, Physica Status Solidi A, 208 (4), 843-850, 2011.

41. Hongi Li and Jean-Luc Bredas, Advanced Materials, 28, 3928-3936, 2016.

42. L. Zilberberg, S. Mitlin, H. Shankar, and M. Asscher, Physical Chemistry C, 119, 28979-28991, 2015.

CHAPTER 5

Hydrothermal growth of reduced graphene oxide on cotton fabric

5.1 Introduction

For the past several decades, cotton has been considered as the most promising material in various fields, such as protective clothing, medical textiles, sportswear and automotive textiles. It is more superior when comparing with other material, since it has the excellent comfort, softness and biodegradability [1]. Functionalization of cotton with nanosized material is used for stain resistance, antimicrobial, controlled hydrophilicity/hydrophobicity, antistatic, ultraviolet (UV) protective, wrinkle resistant and shrink-proof abilities [2].

UV-rays blocking property of a fabric is enhanced with a dye, pigment and UV absorber coating. It absorbs UV radiation and blocks the transmission through a fabric to the skin, which enhances the sun protection [3]. For the past two decades, metal oxides like TiO_2 [4], ZnO [5-7], SiO_2 [8] and Al_2O_3 [9] are known as UV blocking materials. Among the various semiconductor materials, graphene and graphene derivatives have attracted significant attention due to its unique properties, such as mechanical [10], electrical [11], thermal [12] and optical properties [13]. If the exfoliated sheets contain only one or few layers of carbon atoms like graphene with oxygen, these sheets are termed graphene oxide (GO) and subsequent reduction of GO is carried out using reducing agents. However, these approaches often involve highly toxic chemicals, longer duration for reduction process and high temperature treatments [14-18]. The development of effective and nontoxic alternative-reduction-process is necessary for the high quality of reduced GO (rGO) on cotton fabric. Recently, a variety of nanocomposites based on graphene and its derivatives have been scrutinized for UV protection factor (UPF) applications due to constantly increasing global awareness on green/eco textile products. Research has been intensified in the area of development of sustainable UV protective textile using plant extracts and other natural polymeric materials or biomolecules.

Lijun et al. [19] reported the best functionalization of cotton fabric coated with low graphene nanoplate by a pad-dry-cure method. According to Tang et al. [20], GO nanosheets and polyaniline for conductive and UV blocker are fabricated by a vacuum filtration deposition method. Tian et al. [21] suggested that the graphene can be nanocomposites by polymer such as chitosan. Although the pad-dry-cure method is simple and the most common method for preparing cotton fabric/nanocomposites, the yielded material gradually degenerates under the irradiation of UV. In addition, durability of protective action is limited, which devaluates their usefulness. Therefore, a new approach is required to enhance the UV protection of cotton fabric.
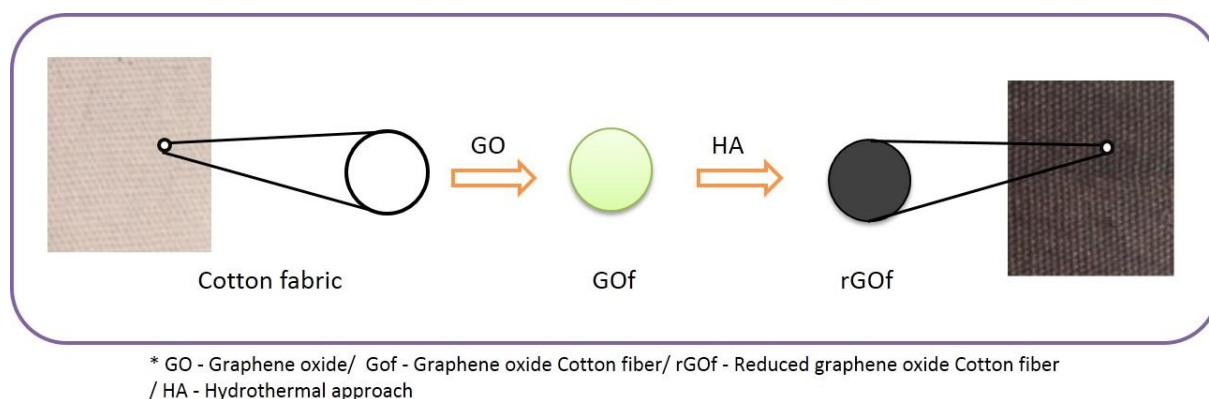
Among various energy harvesting techniques, the thermoelectric has been proven able to harvest energy from human body at a high efficiency and large output power density. Comparing with other energy harvesting approach, the thermoelectric energy is nearly independent to the weather and working environment. Moreover, it is facile to be designed into fabric due to its simple structure and huge materials choices [22 – 24]. In this work, rGO-deposited cotton fabric is synthesized by a new non-toxic method and the functional properties are studied.

5.2 Experimental procedure

All the chemicals were of analytical grade and used without further purification. Graphite (Merck), hydrochloric acid (HCl; 37%, Merck), sulfuric acid (H_2SO_4; 98%, Merck), potassium permanganate ($KMnO_4$; 99%, Merck) and hydrogen peroxide (H_2O_2; 35%, Merck). Scoured and bleached 100 % cotton fabric was used as a substrate. Hydrothermal method was adopted to reduce the GO to rGO directly on cotton fabric. The GO was prepared from graphite powder by modified Hummer's method [25]. The bare cotton fabric of 2x2 cm^2 was immersed in GO solution for 2 h and sonication was carried out for 24 h. Then GO deposited cotton fabric was washed three times with de-ionized water to remove the unexfoliated GO and it was dried at 45° C for 24 h. In order

to prepare the rGO, the GO-deposited cotton fabric was stirred with 2 M of hydrazine monohydrate solution for 5 mins. It was placed in a Teflon-lined autoclave and was kept in the furnace at 90° C for 48 h. Finally, the bare cotton fabric will pale white in color but rGO deposited cotton fabric shown as black in color as shown in Fig. 5.1

X-ray diffraction (XRD) analysis performed on X-ray diffractometer system (X'pert PRO PANalytical). Raman spectroscopy was measured using JASCO NRS -7100. Field-emission scanning electron microscope was obtained by JEOL JSM 7001F. The UV blocking efficiency was recorded by a UV spectrophotometer (LAPSPHERE UV1000F). In the Australia/New Zealand standard AC/NZS 4399:1996 [26].

* GO - Graphene oxide/ Gof - Graphene oxide Cotton fiber/ rGOf - Reduced graphene oxide Cotton fiber
/ HA - Hydrothermal approach

Fig. 5.1 Digital Photographic image of Cotton fabric before and after rGO deposited

5.3 Results and Discussion

5.3.1 Structural analysis

XRD patterns of the bare cotton fabric and rGO-deposited cotton fabric are shown in Fig. 5.2(a). The both samples have similar diffraction peaks at 16.52°, 22.82° and 34.58° that correspond to cellulose and are good agreement with JCPDS file no 3-0226. A small peak corresponding to graphite (002) at 25.5°, as clearly shown in inset and good agreement with the previous report [27]. The broadening and shift of the diffraction peak of graphite from 26° to 25.5° is considered to indicate the short-range order in stacked graphene layers [28].

Figure 5.2 (b) represents the Raman spectra of bare cotton fabric and rGO-deposited cotton fabric. The bare cotton fabric does not show any significant peak. Whereas, rGO-deposited cotton fabric exhibits two peaks at 1354 and 1596 cm^{-1} which correspond to the G and D bands of graphite, respectively. The G and D bands are related to the first order scattering of E_{2g} mode and disorder-induced mode, respectively [29]. Therefore, it is noted that the bands observed in our sample are shifted to higher wave numbers. The peak shift in the G band may be due to the recrystallization in sp^2 hybridization and that in the D band is due to the presence of defects, vacancies and distortion of the sp^3 domains during oxidation [30].
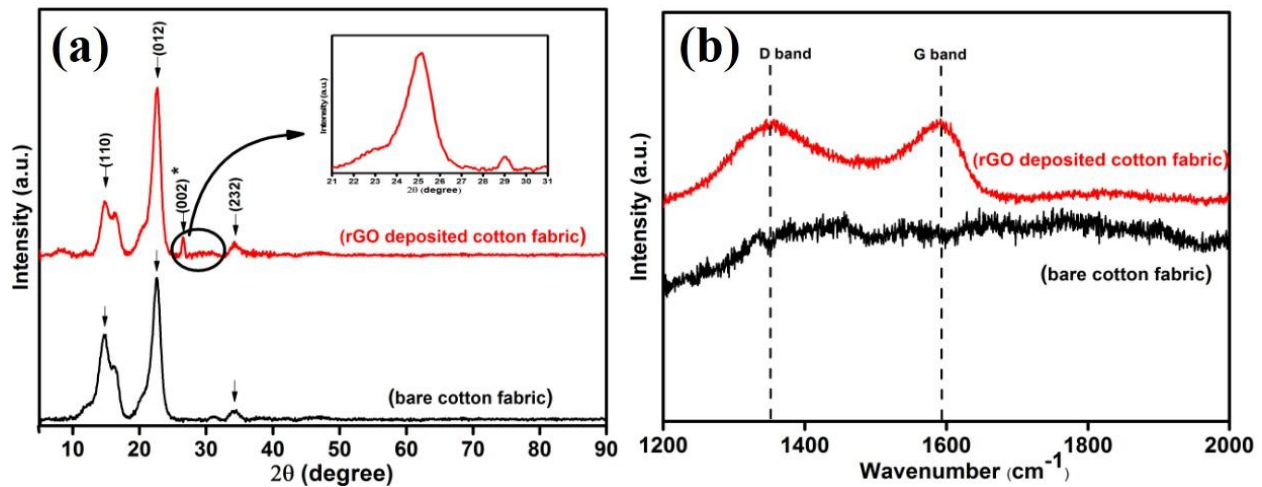
Figure 5.2 (a) XRD patterns, (b) Raman spectra of bare cotton fabric and rGO-deposited cotton fabric.

5.3.2 Morphology study

The photographic images of bare cotton fabric and rGO cotton fabric are shown in Fig. 5.2(a). The white color of the cotton fabric changed into blackish color after rGO deposition confirms that the rGO is uniformly deposited on the cotton fabric. Figures 5.2(b) and 2(c) represent the FE-SEM images of bare cotton fabric and rGO-deposited cotton fabric, respectively.
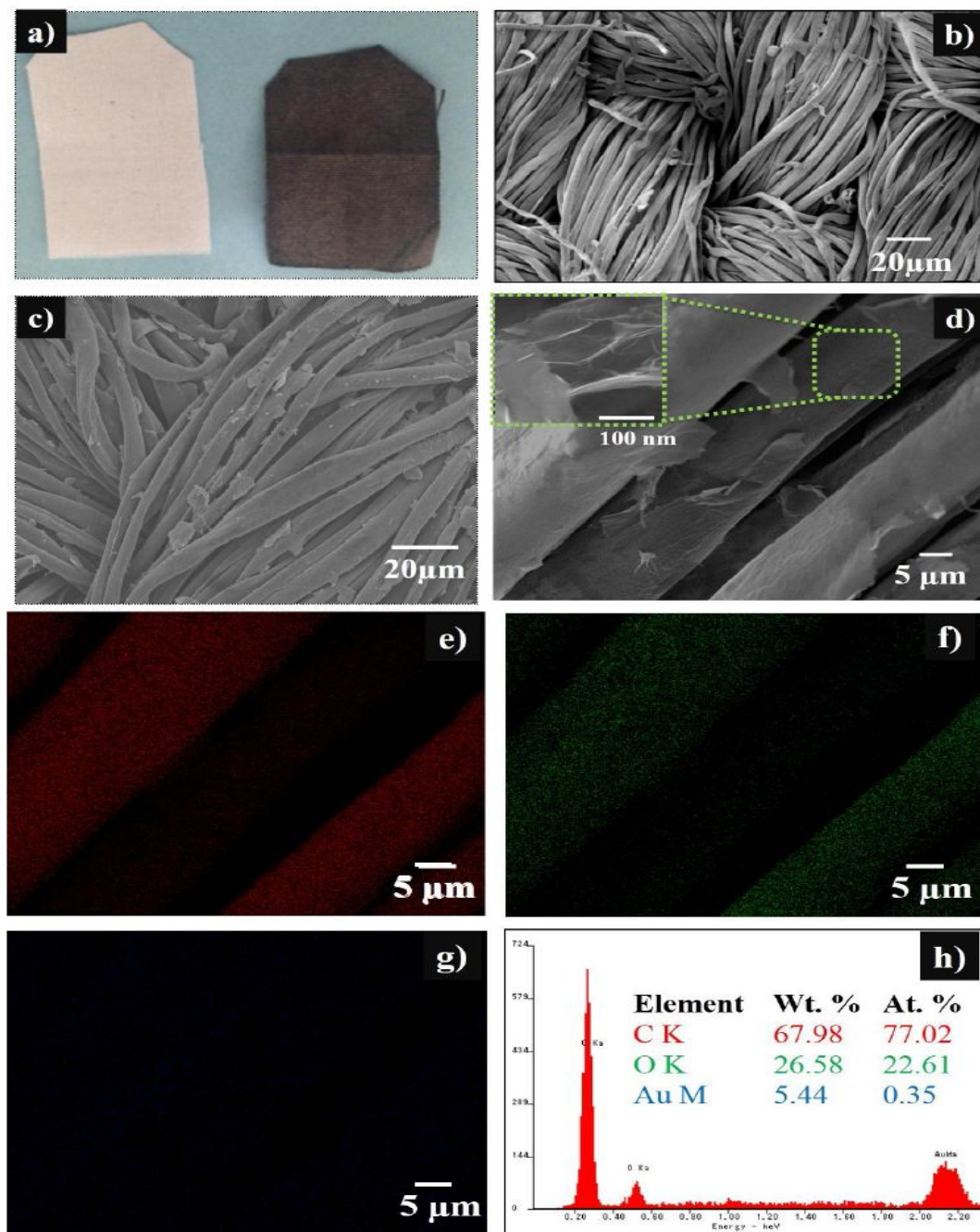
Figure 5.3 FESEM images of the surface of the cotton fabric: (a) photography of bare cotton fabric (left) and rGO/ cotton fabric (right); (b) bare cotton fabric; (c) rGO/Cotton fabric; (d) high magnification micrographs (inset shows single fabric surface); (e) carbon compostion; (f) Oxygen composition; (g) gold composition and (h) Elemental compostion with respect to histogram graph.

Figure 5.3(d) represents the higher magnified image of rGO cotton fabric and inset shows the single fabric surface. It was observed that the surface of the rGO-coated cotton fabric was not as smooth as the bare cotton fabric. It is noted from Fig.5.3(d) inset that wrinkled like wave structure was formed on the surface. This formation indicates the presence of reduced nature of GO on the cotton fabric. Furthermore, the amount of rGO incorporation is monitored by taking EDAX elemental mapping shown in Figs. 5.3(e), 5.3(f) and 5.3(g). From these results, the elements covering the cotton are C and O atoms with the composition of 77.02 and 22.61 %, respectively.

5.3.3 UV shielding analysis

UV transmittance of bare cotton fabric and rGO-deposited cotton fabric are shown Fig. 5.4 (a). It is noted that the UV transmittance is decreased significantly by the rGO deposition, comparing with the bare cotton fabric. The UV protection property was taken for rGO-deposited cotton before and after the laundering. It is clearly found that the UV protection is improved by rGO deposition. In addition, the spectrum does not change even after 10 times laundering, which indicates that rGO deposited on the cotton is very stable and hardly influenced by laundering. Based on the UV transmittance spectrum, UPF value is evaluated and shown in Fig. 5.4 (b). UPF values are calculated to be 442.69 and 422.32, for rGO cotton before and after laundering process respectively, while the UPF value for the bare cotton is 7.83. The rGO deposition is found to enhance the UV protection of cotton fabric. In addition, there is no significant difference in the rGO UPF values before and after the laundering process. Thus, it can be concluded that the synthesized rGO cotton has good durability condition.

5.3.4 Thermopower

To evaluate the Seebeck coefficient (thermopower), the temperature difference and thermoelectromotive force need to be measured and the measured time evolution of higher temperature region (T_H) and lower temperature region (T_L) are shown in Fig. 5.5 (a). Through Fig. 5.5 (a), it can be seen clearly that, the temperature is increased systematically after that it is decreased by controlling the heater current. Then, the temperature difference is determined by $\Delta T = T_H - T_L$. From the measured thermoelectromotive force and temperature difference, the Seebeck coefficient is obtained by $S = -\ TEMF/\Delta T$ as shown in Fig. 5.5 (b) of rGO coated cotton fabric. Therefore, Seebeck coefficient obtained during increase and decrease temperature of 340 – 346K are identical and it is indicated that the measured Seebeck coefficient is valid. Since, the Seebeck coefficients in this temperature region are also found to be nearly constant. Consequently, it is found that the measured Seebeck coefficient are higher.
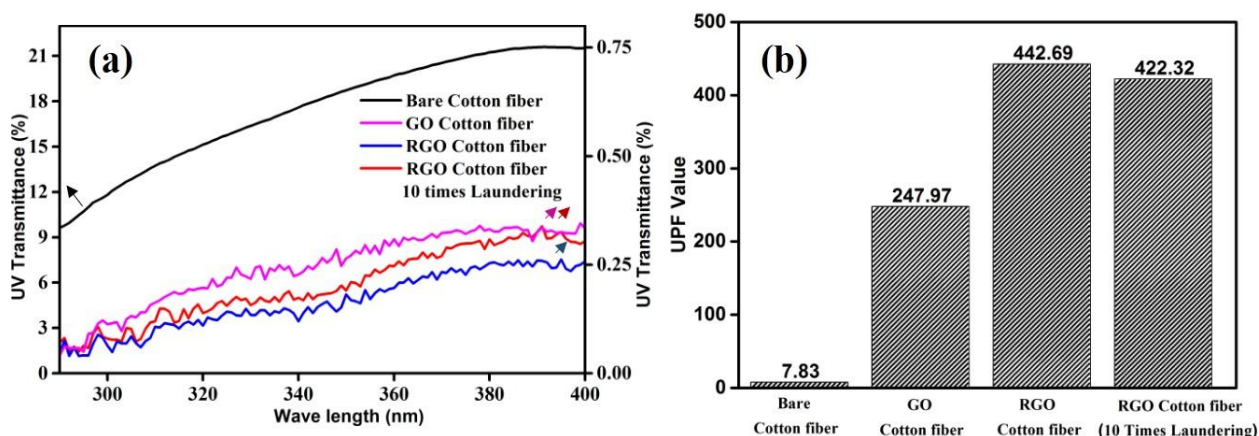
Figure 5.4 UV protection ability of fabric specimens (a) UV transmittance spectrum and (b) UPF values with laundering effect.
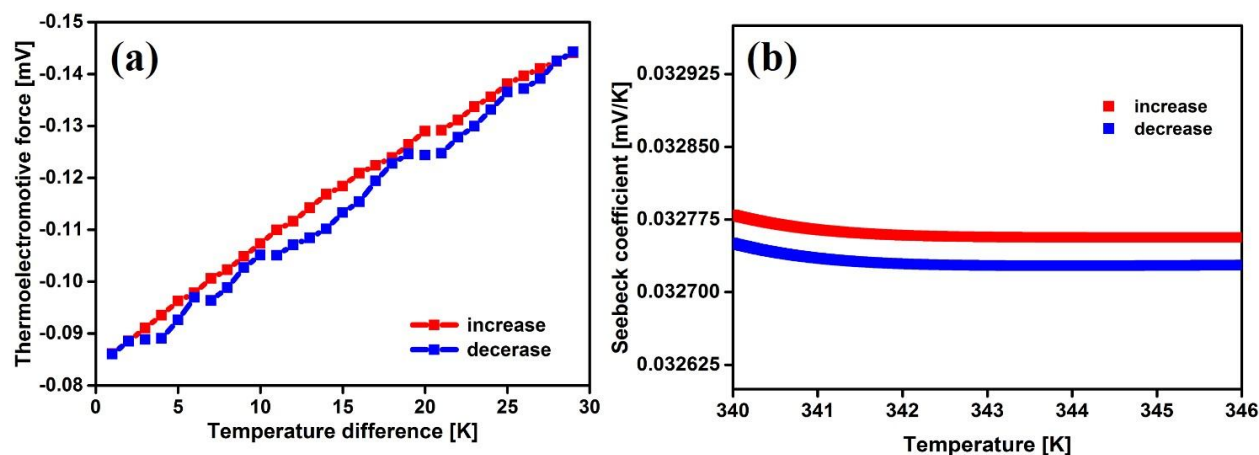
Figure 5.5 (a) Thermoelectromotive force as a function of temperature difference and

(b) Seebeck coefficient as a function of average temperature.

5.4 Conclusion

The rGO deposited cotton fabric was successfully prepared by hydrothermal method. XRD and Raman spectrum confirmed the presence of rGO on the surface of the cotton fabric. The FESEM images indicated that the rGO-deposited cotton fiber had wrinkle-like wave structure. The UPF values of bare cotton and rGO deposited cotton fabric before and after laundering process were calculated as 7.83, 442.69 and 442.32, respectively. It is confirmed that the prepared material showed the excellent UV shielding property and good durability. The calculated Seebeck coefficient obtained from the linear approximation and larger value obtained.

References

1. M. Abhijit, M. Samrat, Y. Ravindra, International Journal of Thermal Science, 49, 2042, 2010.

2. M. Joshi, Bhattacharyya, Textile Progress, 43 (3), 155, 2010.

3. H. Gwendolyn, C. Patricia, Journal of Cotton Science 9, 47, 2005.

4. N. A. Ibrahim, R. Rakia, F. A. Ahmed, Journal of Indian Textiles, 40, 65, 2010.

5. S. Kathirvelu, D. Louis, D. Bhaarathi, Indian Journal of Fibers & Textile Research 34, 267, 2009.

6. M. Zhiping, S. Qiuping, Z. Linping, C. Huantian, Thin Solid Films, 517, 2681, 2009.

7. V. Alexander, V. Arseniy, A. Igor, Y. Victor, Microelectronics Engineering, 90, 96, 2012.

8. R. H. Wang, J. H. Xin, X. M. Tao, Inorganic Chemistry, 44, 3926, 2005.

9. A. Nursen, F. Philippe, L. Johan, V. Henk, P. Dirk, Journal of Sol-Gel Technology, 59, 327, 2011.

10. L. Changgu, W. Xiaoding, W. Jeffrey, H. James, Science, 321, 385, 2008.

11. M. Orlita, C. Faugeras, P. Plochocka, P. Neugebauer, G. Martinez , D. Maude, Physics Review Letters, 101, 267601, 2008.

12. A. A. Balandin, S. Ghosh, W. Bao, I. Calizo, D. Teweldebrhan, F. Miao, C. N. Lau, Nano Letters, 8(3), 902, 2008.

13. F. Bonaccorso, Z. Sun, T. Hasan, A. C. Ferrai, Nature photonics, 4, 611, 2011.

14. P. Sungjin, A. Jinho, R. P. Jeffrey, V. Aruna, M. Shanthi, S. .R Rodney, Carbon, 49, 3019, 2011.

15. Chun KC, Martin P, Chemistry Society Reviews, 43, 291, 2014.

16. D. Yang, et al., Carbon 47, 145, 2009.

17. H. A. Becerril, J. Mao, Z. Liu, R. M. Stoltenberg, Z. Bao and Y. Chen, ACS Nano 2(3), 463, 2008.

18. G. Eda, G. Fanchini and M. Chhowalla, Nature Nanotechnology, 3, 270, 2008.

19. Q. Lijun, et al., Carbon 80, 565, 2014.

20. T. Xiaoning, et al., Synthetic Metals, 202, 82, 2015.

21. T. Mingwei, T. Xiaoning, Q. Lijun, Z. Shifeng, G. Xiaoqing, H. Guanting, Materials Letters 145, 340, 2015.

22. C. Wood, A. Chmielewski and D. Zoltan, Reviews Science Instruments, 59, 951, 1988.

23. W. H. Kettler, R. Wernhardt and M. Rosenberg, Review Science Instruments., 57, 3053, 1986.

24. F. Salleh, K. Asai, A. Ishida and H. Ikeda, Applied Physics Express, 2, 071203-1, 2009.

25. W. S. Hummers, RE. Offeman,. Journal of American Chemistry Society, 80(6), 1339, 1958.

26. Standards Australia/Standards New Zealand Sun Protective Clothing—Evaluation and Classification. Report No. AS/NZS 4399, Standards Australia, Sydney and Standards New Zealand, Wellington, 1996.

27. K. Karthikeyan, V. Murugan, K. Gui-Shik, JK. Sang, Current Nanoscience, 8, 934, 2014.

28. LM. Malard, MA. Pimenta, G. Dresselhaus, MS. Dresslhaus, Physics Rep, 473, 51, 2009.

29. S. Stankovich, et al., Carbon, 45, 1558, 2007.

30. W. Yajun, W. Fengmei and H. Jun, Nanoscale, 5, 11291, 2013.

CHAPTER 6

Functionalization of carbon fabric with ZnO nanostructures

6.1 Introduction

Improvement in quality of life is seen not only in healthcare but also in other areas such as wearable devices [1], power generation [2], sensors [3], and electromagnetic/ultraviolet interference shielding textiles [4, 5]. The power generator has attracted much attention due to their ability of direct conversion of heat to electricity. Especially, the wearable power generator (WPG) is one of the candidates for energy harvesting and is helpful even in the event of disaster since its flexibility can be used for the fabrication of curtains and tent. Therefore, the WPG materials require high efficiency and easy fabrication with low cost and large area [6]. The performance of WPG material is closely related to the dimensionless figure-of-merit (zT), which is given by $zT=(S^2\sigma)/\kappa$ T, where S, σ, κ, and T denote the thermopower (Seebeck coefficient), electrical conductivity, thermal conductivity, and temperature respectively [7]. Since the advent of nanostructured power generation materials exhibits high zT owing to maximization of power factor $(S^2\sigma)$ and reduction in κ [8]. Throughout the literatures, the nanometer-scaled crystalline structure can reduce κ by enhancing the boundary scattering of phonons, but it degrades the power factor, simultaneously. With the aim of bettering the power factor, an increment of thermopower is expected by tailoring the density of states through nano structuration such as nanocomposites [9] and super lattices [10], and doping modulation [11].

Traditional materials for thermoelectric such as bismuth telluride have been studied and utilized commercially for the last half century, but recent advancements for materials selection is one of the foremost function of effective thermoelectric device as it determines the reliability of fabrication in terms of industrial and economical aspects. Recently, many researcher's efforts have been made to utilize oxide nanomaterials for WPG applications [12 – 15] which may provide environmental stable, mechanical flexibility, and light weight with low cost of manufacturing. In

precise, fabric containing ZnO have shown great promise as N-type materials with improved transport and UV shielding properties [16, 17]. On the other hand, we have focused on ZnO nanostructures as a high-efficiency WPG material because they are non-toxic to skin, inexpensive and easy to obtain and possess attractive electronic properties, which means that they are available for clothing with low-cost fabrication. Up-to-date, several coating methods have been used to grow ZnO films including Sputtering [18], Electrochemical [19], Sol-Gel [20], and Hydrothermal [21] method. Most studies of ZnO coated fabric were focused on relationship of the coated technique and basic optical, electrical properties. To our observation, we publicizing about the thermoelectric properties of ZnO nanostructures coated carbon fabric for the first time.
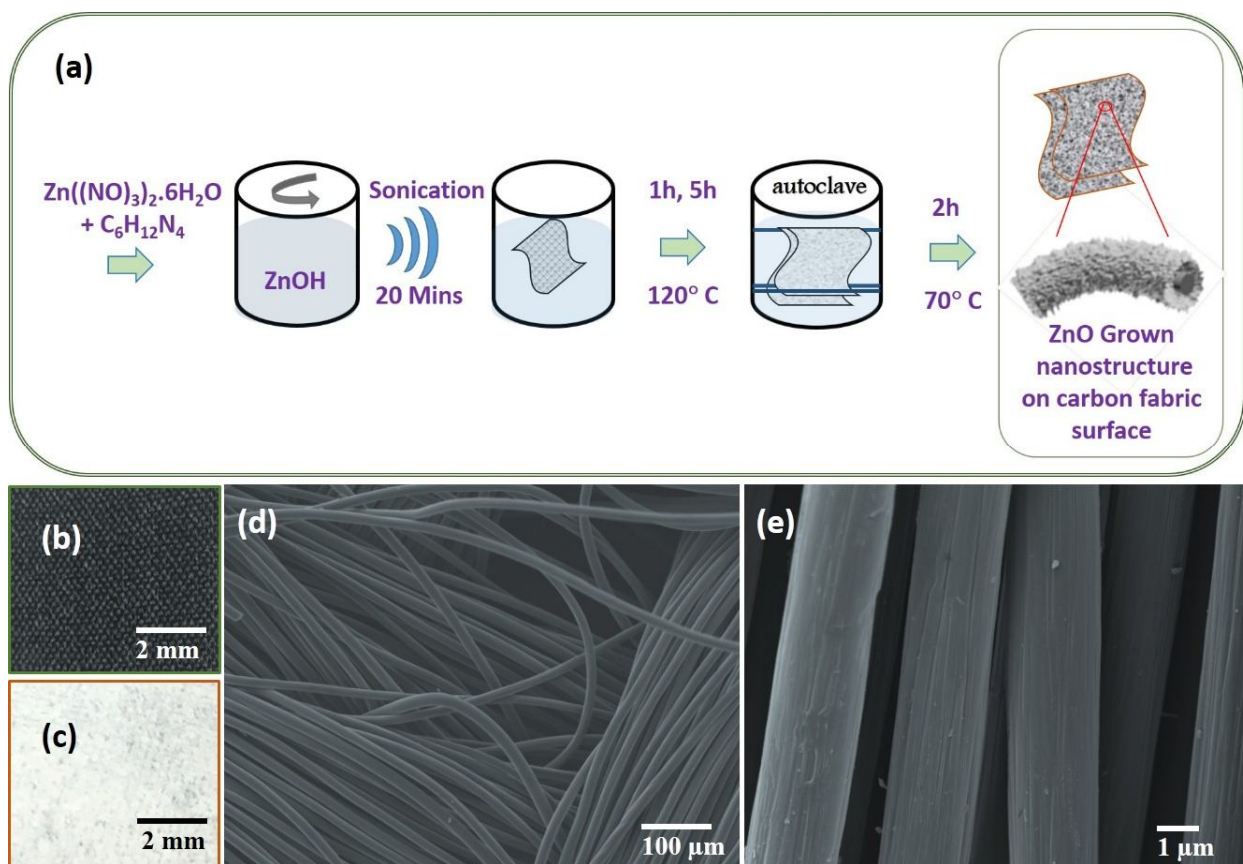
In this paper, a facile sonochemical assisted hydrothermal growth of hierarchical ZnO nanostructures on carbon fabric demonstrated. Zinc nitrate hexahydrate and hexamine (HMT) were used as zinc source and the alkali source respectively. In the momentous morphological changes were obtained by tuning the zinc precursor concentration. When the zinc concentration increased, the ZnO nanorods/sheets became denser, and growth period indicated the morphological changes from rods to sheets nanostructure arrays under same growth temperature. Therefore, it is imperative to explore the new approach for the synthesis of ZnO nanostructures; well it works out to be an easier and economical process.

6.2 Experimental procedure

Zinc nitrate hexahydrate ($Zn(NO_3)_2 \cdot 6H_2O$), and hexamine (($(CH_2)_6N_4$)) were of analytical grade purchased from Sigma-Aldrich and are used without further purification. Commercially available carbon coated fabric was treated with ultrasonic bath in ethanol and water for about 20 min, and then dried under a N_2 stream, which was used as a substrate for the growth of ZnO nanostructures during the sonochemical assisted hydrothermal process. 0.2 M of zinc nitrate was

dissolved in 40 mL of deionized water under continuous magnetic stirring. 0.1 M of hexamine was dissolved in 40 mL of deionized water and added slowly to the zinc nitrate solution. After a few minutes, the carbon fabric was immersed in the solution. The black colored fabric turned to pale white color, indicating the formation of ZnO nanoparticles. Similar solution procedure was adopted for 0.1 M of zinc nitrate and 0.2 M of hexamine. The above processes were performed at 50° C temperature. Both the reaction mixtures were stirred continuously until it became a transparent solution, followed by 20 mins of ultrasonication at room temperature. The prepared fabric solution was placed into a 100 mL Teflon-lined stainless steel autoclave, which was sealed and maintained at 120° C for 1 h and 5 h, then cooled down to room temperature. The resultant fabric was collected, washed three times individually with absolute ethanol and distilled water thoroughly. Finally, the product was dried in an oven for 2 h at 70° C and the entire process can be schematically represented as shown in Figure 6.1 (a).

Carbon fabric and ZnO nanostructure coated carbon fabric was characterized by field emission scanning electron microscopy images were obtained using a JEOL JSM 7001F microscope equipped with EDS mapping. X-ray diffraction pattern was obtained by a Rigaku X-ray diffractometer, with Cu-Kα radiation and a step interval of 0.02/sec. The analysis of X-ray photoelectron spectroscopy (XPS) was performed via a Shimadzu ESCA 3100. The thermogravimetric stabilities to heat were carried out under N_2 ambient, measured with DTG-60 (TG/DTA). The UV shielding property was performed by using Lapsphere UV1000F analyzer. The resistivity measurements were carried out in the room temperature using a conventional four-probe technique. The Seebeck coefficient was evaluated by our handmade system at around room temperature [22].

(a) Zn((NO)₃)₂·6H₂O + C₆H₁₂N₄ → ZnOH · Sonication 20 Mins · 1h, 5h 120° C · autoclave · 2h 70° C · ZnO Grown nanostructure on carbon fabric surface

(b) 2 mm
(c) 2 mm
(d) 100 μm
(e) 1 μm

Fig. 6.1 (a) Schematic representation of the ZnO seed creation and growth process on carbon fabric; (b) and (c) the photographic images of carbon cloth before and after ZnO nanostructures growth; (d) Typical FESEM images of bare carbon fabric substrate; (e) Magnified image showing the smooth carbon fabric.

6.3 Result and discussion

6.3.1 Morphology study

The photography of the pristine carbon fabric with ZnO before and after the growth of nanostructures is shown in Figure 6.1 (b) and (c). It can be observed that the pure carbon fabric is in deep black color while the ZnO nanostructure coated carbon fabric is in white. The morphology of the bare carbon fabric at low and high magnifications was shown in Figure 6.1 (d) and (e).

Figure 6.1 (d), exhibits the ordered texture structure and the magnified image in Figure 6.1 (e) illustrates that each carbon fiber with smooth surface has a uniform diameter of around 2 μm.

The Figure 6.2 elucidates the morphology of the grown ZnO nanostructures, to control the morphology we carried out a parametric study by changing the molar concentration of hexamine and zinc nitrate together with the synthesis time. Based on this study, achieving nanorods structures was feasible with 2:1 and 1:2 concentrations of both reactants for the synthesis time of 1 h at 120° C as shown in Figure 6.2 (a – d) and hereafter, they are termed as CFZ1 (a, b) and CFZ2 (d, e). Similarly, synthesis time of 5 h led to the formation of nanosheets like structure as shown in Figure 6.2 (e – h) and hereafter, they are termed as CFZ3 (e, f) and CFZ4 (g, h).

The obtained ZnO coating was partially covered on the fiber surface (Figure 6.2a, 6.2b, 6.2e, 6.2f) when small amount (1 M) of hexamine was used. Hexamine offers the OH^- ions to accelerate the reaction, initially less OH^- ions existed in the solution when 1 M of hexamine was employed. On the other hand, some hexamine molecules would decompose at the reaction temperature of 120°C, which would further decrease the number of OH^- ions present in the solution. All these factors would weaken the reducing ability of ZnOH and reduce the reaction rate, which lead to the decrease in density and incompleteness of the ZnO coatings. The surface of carbon fiber was almost completely covered by ZnO when the volume of hexamine was increased to 2 M (Figure 6.2c, 6.2d, 6.2g, 6.2h). Moreover, the volume of hexamine used herein would increase the pH value of the solution, and the chemical reaction was found to proceed more quickly. As the pH value increased, the formation of nuclei, the subsequent crystal growth was enhanced, and denser coatings were obtained. When the period of growth increased from 1h to 5h, a change of structure from nanorods to nanosheets was observed, which is the reason for the suppression effect observed along the c-axis direction at a prolonged time and growth was

observed to occur in the longitudinal direction due to many growth units around ZnO nuclei [23, 24].
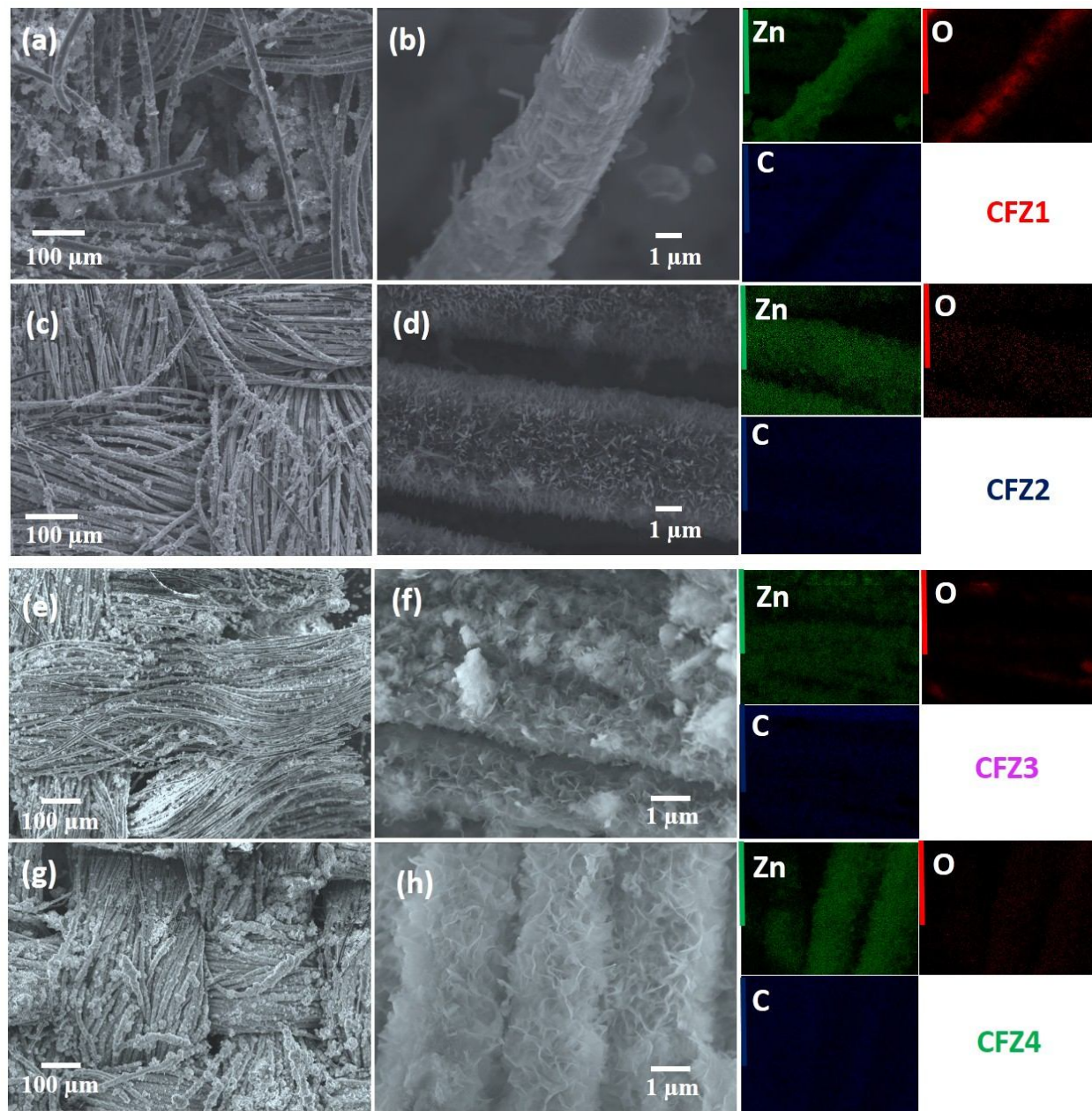
Fig. 6.2 FESEM micrograph and elemental mapping images of as-fabricated ZnO nanostructures growing on carbon fabric.

From the FESEM image, the ZnO nanorods and nanosheets were compact and continuous, and nanostructures coexisted on the surface of the fabric. The coating was found to be uniform and not

peeling off, signifying that the adherence between the carbon fabric and ZnO coating was very strong. The spatial distribution of Zn, O and C elements were evident that the ZnO was coated on the carbon fabric as expected. Moreover, the distribution of Zn, O and C elements was also found to be homogeneous.
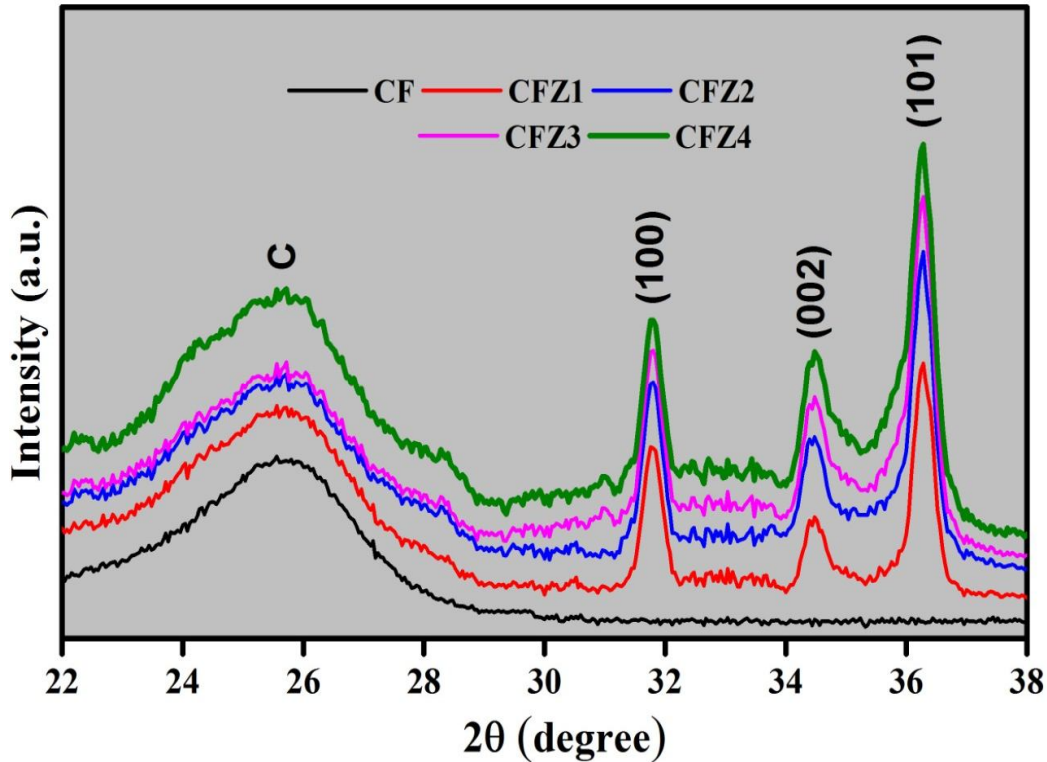
Fig. 6.3 XRD Pattern of Carbon fabric coated with/ without ZnO

6.3.2 Structural analysis

Figure 6.3 showed the XRD pattern of ZnO/ Carbon fabric. In all the samples, XRD pattern exhibited typical diffraction peaks of carbon fabric at 25.8°. Whereas, the ZnO coated fabric showed three strong diffraction peaks at 31.67°, 34.12°, and 36.20° corresponding to (100), (002) and (101) planes of wurtzite ZnO respectively, and the result was in good agreement with the

reported data (JCPDS No. 36-1451) [25]. No impurity peaks were detected, which confirms that the carbon fabrics were successfully deposited with ZnO nanostructures.

6.3.3 Chemical composition

The surface chemical analysis of the ZnO nanorods and nanosheets coated carbon fabric is shown in Figure 6.4. XPS spectra was carried out with the binding energies calibrated using C 1s (284.8 eV). The Zn 2p core level of pure ZnO has two fittings peaks located at about 1022.93 and 1045.81 eV attributed to Zn $2p_{1/2}$ and Zn $2p_{3/2}$ [26]. Similarly, Figure 6.4 (a) shows the Zn $2p_{3/2}$ and Zn $2p_{1/2}$ peaks at 1022.8 and 1045.7 eV of ZnO nanorods, and others at 1023.3 eV and 1046.2 eV are attribute to Zn $2p_{3/2}$ and Zn $2p_{1/2}$ peaks of ZnO nanosheets, respectively. This shift observed at a higher binding energy with a value of 0.11 to 0.37 eV because of heat treatment [27]. The Zn 2p binding energy of the nanosheets is greater than that of the nanorods, which indicates that the nanosheets is more oxidized than the nanorods. Figure 7.4 (b – f) shows the O 1s peaks, due to its asymmetric shape, the peaks were deconvoluted into two peaks (α and β) using Gaussian fitting curve. The 'α' peak was closely associated with the lattice oxygen of ZnO and 'β' peak should be the evidence of oxygen vacancies within the ZnO matrix and the higher binding energy component is probably due to the presence of some surface hydroxyl species [28]. Thus, changes in the intensity of this component may be about the variations in the concentration of the oxygen vacancies O bonding in the ZnO fabric. The related study indicated that as discussed for the XRD analysis, there is no impurity.
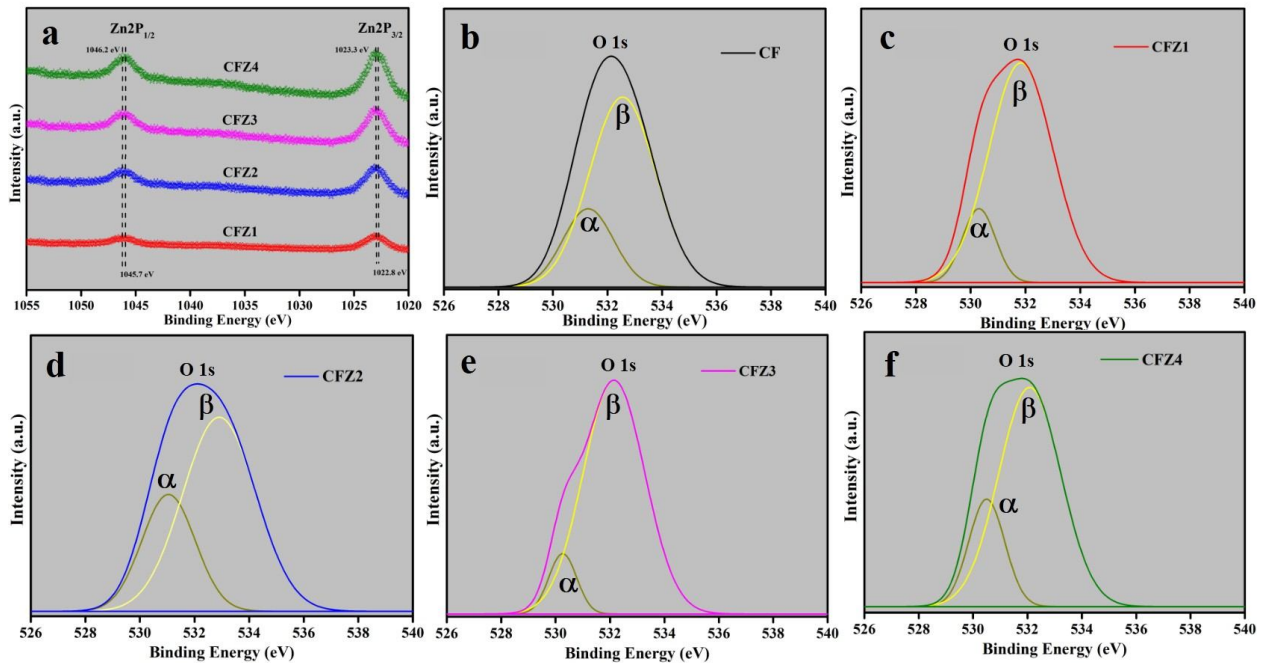
Fig. 6.4 XPS spectra of (a) Zn 2p corresponding to the Zn core and (b-f) oxygen 1s peak

The intensity of the β peak exceeds those of the α peaks, which indicating the strong Zn-

It is well known that the crystalline morphology and structure obtained during ZnO coating on carbon fabric processing plays an important role on the physio-mechanical behavior of the resulting coated fabric, conditioning its potential uses. In this way, the control of crystallization process is a successful approach for improving physio-mechanical properties of coated fabric. Therefore, it is of great interest to investigate the nucleation, crystallization, and structural development of the ZnO coated fabric [29].

6.3.4 Thermal degradation

This would help to optimize the manufacturing conditions to obtain high performance coated fabric and to exploit their potential in practical applications. In Figure 6.5 (a) shows, that there are two stages of weight loss. The initial mass loss occurred from100° C to 200° C, in which the small weight loss mainly due to release of either water or amines. The degradation of the carbon fabric became constant beyond 223° C and there is no further loss in weight suggests the presence of

only pure organic contents [30]. The second weight loss occurred at 430° C, could be attributed to the degradation of the zinc nitrate. Moreover, there is no further loss in weight, which indicates that there is no more zinc nitrate as well as no residual water molecules remained on the coated fabric.

6.3.5 UV shielding analysis

Figure 6.5 (b) shows the UPF value of ZnO coated carbon fabric; bare carbon fabric (CF) obtained a value of 28.62. When the carbon fabric treatment with 1 h period of growth time with hexamine is lesser than zinc nitrate, the UPF value were 38.45 and hexamine is higher than zinc nitrate, the UPF value were 73.82, respectively, which was considered very good and excellent UV-blocking property.
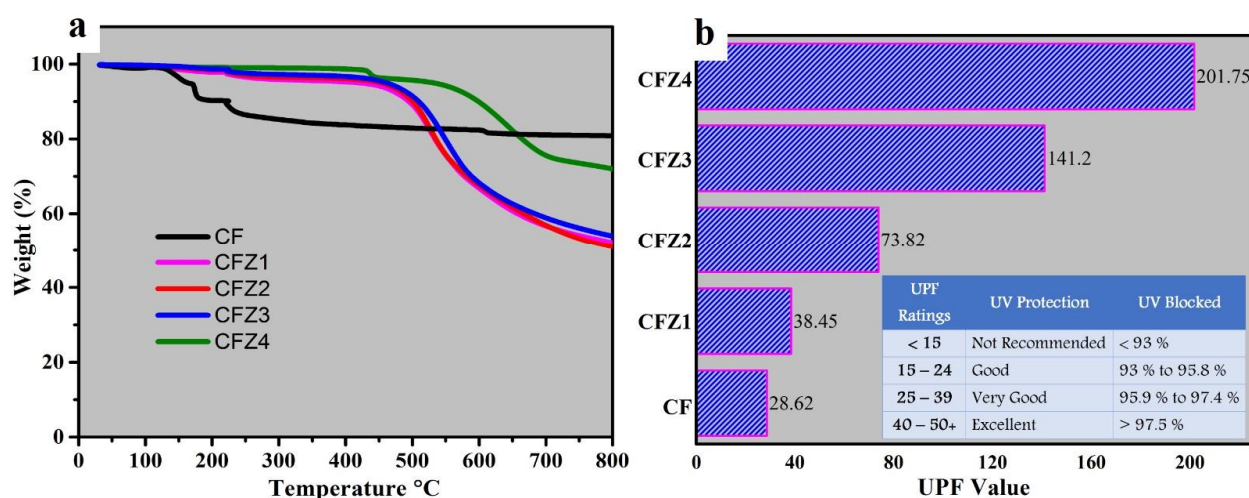
Fig. 6.5 (a) TGA and (b) UV shielding property

Similarly, when raising the carbon fabric treatment with 5 h period, the UPF values were 141.2 and 201.75 respectively, which is considered as excellent UV-blocking property. The UPF value obtained for bare carbon fabric was 28.62. The carbon fabric obtained after a treatment for 1 h was investigated in two different concentrations- When the hexamine (H) concentration was lesser than that of zinc nitrate (ZN), the UPF value was 38.45. However, when the concentration

of zinc nitrate was increased the UPF value was 73.82. This proves to be an excellent UV- blocking property. Now when the growth period was increased for a period of about 5 h, the UPF values were found to be 141.2 (H<ZN) and 201.75 (ZN>H). In higher molar ratio of hexamine concentration, the driving force is the maximization of the free energy of the entire reaction system. In this case, the nucleation rate is relatively high to create great amount of ZnO nuclei, which turns to denser coverage on carbon fibers. Therefore, the better performance of the ZnO nanosheets is attributed to its morphology and denser coverage [31].
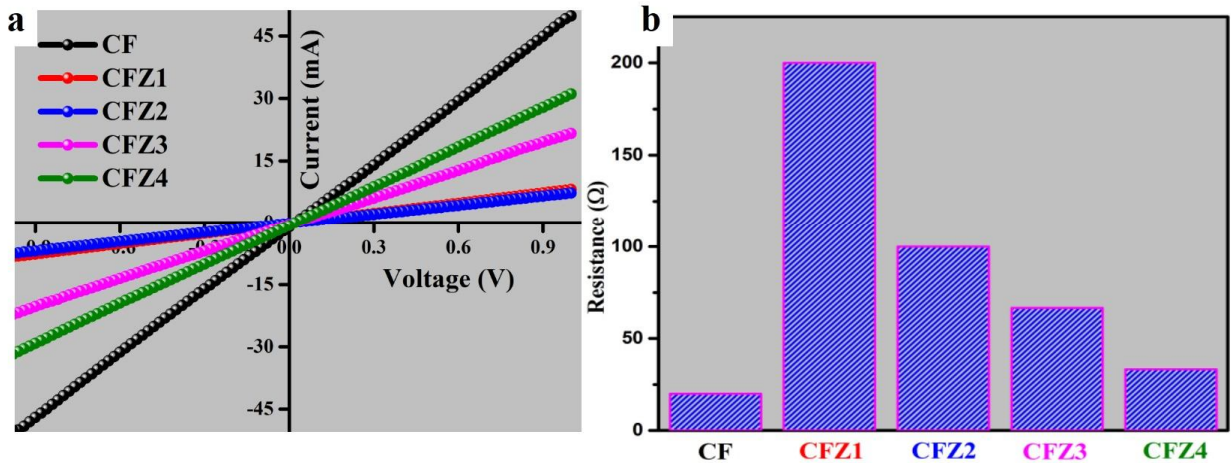
Fig. 6.6 (a) I – V characteristics and (b) Electrical Resistance

6.3.6 Electrical conductivity

To assess the quality of the electrical contact between the ZnO grown nanorods and nanosheets on carbon fabric I-V characteristics curves were obtained. I-V measurement was carried out between two points on the fabric surface, and the experiment was conducted 3 times at different places to ensure that the obtained conductivity represented the coated fiber layer as shown in Figure 6.6 (a). Significantly, the results were found to be linear, indicating that the ohmic contact is very stable. Figure 6.6 (b) image shows the resistance of ZnO/ Carbon fabric. With 1 h growth period, the ZnO nanorods (CFZ1) of 2:1 concentration showed the highest resistivity of 200 Ω and ZnO nanosheets

(CFZ4) of 1:2 concentrations with a growth time of 5 h had better conduction of the fabric about 33 Ω. However, the molar ratio of zinc nitrate and hexamine demonstrates the coated fabric did become higher when the denser nanosheets with high hexamine concentration, this is presumably due to smaller grain size resulted in closer spacing between sheets to sheets and more direct conduction pathway for generated electrons transfer [32].

6.3.7 Thermopower

Thermopower is a thermoelectromotive force (TEMF) induced by the Seebeck coefficient in response to a temperature difference across the fabric and the resultant thermopower was estimated as a function of average temperature. The results show that these techniques are a valuable tool and trend reported in the literature previously [33].
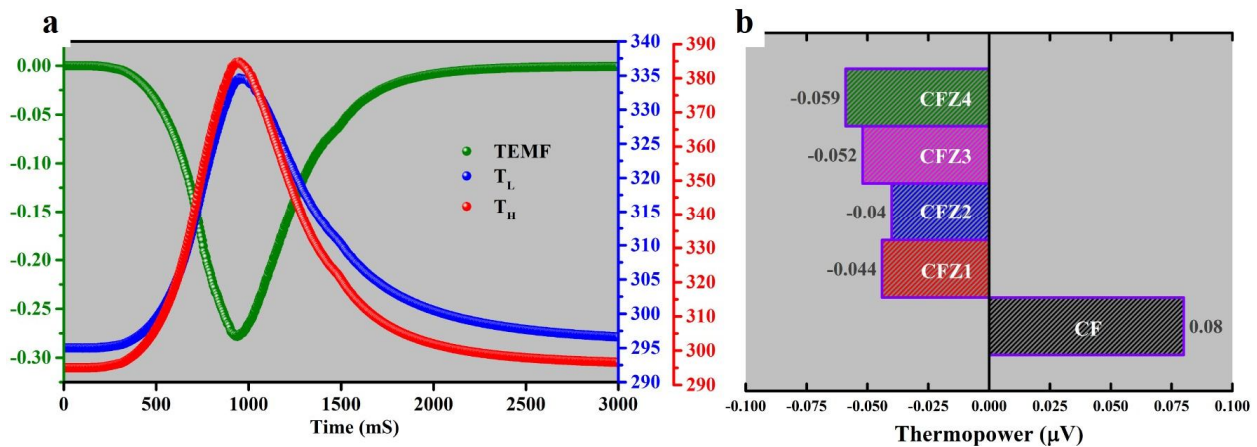
Fig. 6.7 (a) Time versus TEMF and Temperature difference of CFZ4 (b) Comparison TEMF of Carbon fabric and ZnO coated Carbon fabric

When the current is modified for increasing and decreasing the temperature, the generated TEMF with respect to the time evolved is demonstrated in Figure 6.7 (a) for the CFZ4 sample. The trend observed is a gradual decrease in the absolute value of thermopower from 100 mS to 800 mS as temperature rise. Following the decrease, there is an increase of TEMF after 900mS as the temperature becomes low. As expected for an N-type semiconductor, the TEMF values are

negative. The ZnO coated carbon fabric results agree with the thermopower values reported in the literature for ZnO thin films [34] and bulk [35]. In Figure 6.7 (b) shows the bar graph of thermopower value with and without ZnO coating. In general, the absolute value of the thermopower was calculated by the linear fit between voltage (ΔV) and temperature difference (ΔT). The thermopower of ZnO coated on fabric was about -0.04 ~ 0.054 µV/K and for bare carbon fabric it was found to be about 0.08 µV/K. In addition to the carrier concentration, it is important to note that there was change of carrier type from P-type to N-type resulting due to coating of ZnO on carbon fabric. Thus, thermopower of ZnO on fabric was successfully obtained.

7.4 Conclusion

In this work, we have designed unique binder-free array-type ZnO nanostructures grown directly on carbon fabric obtained by sonochemical assisted hydrothermal method. This approach allows ZnO nanostructures to grow effectively on carbon fabric in the absence of a template, catalyst or even a surfactant to inhibit growth and this method seems to be fast with reproducibility. With prolonged growth period, morphology changes from nanorods to nanosheets were observed. The FESEM images also confirm a significant difference in the morphology of the fabric before and after ZnO coating. EDX Mapping, XRD, XPS analyses were showed that there is a linear relationship between the coated layers of ZnO content and bare fabric. The UV protection value obtained by UV transmittance indicated excellent protective value for ZnO coated carbon fabric owing to their absorption. An enhancement of the thermopower was observed with ZnO coating due to the change in carrier concentration. This phenomenon is believed to be related with the formation of ZnO nanostructures on carbon fabric.

Reference

[1] W. Zeng, L. Shu, Q. Li, S. Chen, F. Wang, and X. Tao, Advanced Materials., 26, 5310-5336, 2014.

[2] J. Chen, Y. Huang, N. Zhang, H. Zou, R. Liu, C. Tao, X. Fan, and Z. L. Wang, Nature Energy, 1, 1-8, 2016.

[3] S. Choi, Z. Jiang, Sensors and Actuators A Physics, 128, 317-326, 2006.

[4] V. Pandiyarasan, J. Archana, A. Pavitra, V. Ashwin, M. Navaneethan, Y. Hayakawa, and H. Ikeda, Materials Letter, 188, 123-126, 2017.

[5] P. Saini, V. Choudhary, N. Vijayan, and R. K. Kotnala, The Journal of Physical Chemistry C, 116, 13403-13412, 2012.

[6] M. Stoppa and A. Chiolerio, Sensors, 14, 11957-11992, 2014.

[7] H. Alam, and S. Ramakrishna, Nano Energy, 2, 190-212, 2013.

[8] J. Li, W. Liu, L. Zhao, and M. Zhou, NPG Asia Materials., 2, 152-158, 2010.

[9] P. Veluswamy, S. Suhasini, F. Khan, A. Ghosh, M. Abhijit, Y. Hayakawa, and H. Ikeda (2017), Carbohydrate Polymers, 157, 1801-1808, 2017.

[10] M. Tan, Y. Deng, and Y. Hao, The Journal of Physical Chemistry C, 117, 20415-20420, 2013.

[11] G. Kim, L. Shao, K.Zhang, and K. P. Pipe, Engineered doping of organic semiconductors for enhanced thermoelectric efficiency, Nature Materials, 12, 719-723, 2013.

[12] G. Ren, J. Lan, C. Zeng, Y. Liu, B. Zhan, S. Butt, Y. Lin and C. Nan, Journal of Minerals Metals & Materials Society, 67, 211-221, 2015.

[13] A. Nag, and V. Shubha, Journal of Electronic Materials, 43, 962-977, 2014.

[14] G. Kieslich, G. Cerretti, I Veremchuk, R. P. Hermann, M. Panthofer, J. Grin, and W. Tremei, Physica Status Solidi A, 213, 808-823, 2016.

[15] H. Ohta, K. Sugiura and K. Koumoto, Inorganic Chemistry 47, 8429-8436, 2008.

[16] J. Kim. S.A. Hong, J.Yoo, Chemical Engineering Journal, 266, 179-188, 2015.

[17] Y. M. Im, T. H. Oh, J. A. Nathanael, and S. S. Jang, Journal of Materials Letter, 147, 20-24, 2015.

[18] I. Valenti, S. Benedetti, A. di Bona, V. Lollobrigida, A. Perucchi, P. Di Pietro, S. Valeri, and P. Torelli, Journal of Applied Physics, 118, 165304 (1-7), 2015.

[19] A. Henni, A. Merrouche, L. Telli and A. Karar, Journal of Electroanalytical Chemistry, 763, 149-154, 2016.

[20] S. Kim, G. Nam, H. Yoon, H. Park, H. Choi, J. S. Kim, J. S. Kim, D. Y. Kim, S. Kim, and J. Leem, Journal of Electrons Materials Letter, 10, 869-878, 2014.

[21] L.L. Wang, B. Z. Lin, M.P. Hung, L. Zhou, G. N. Panin, T. W. Kang, D. J. Fu, Solid State Electronics, 82, 99-102, 2013.

[22] V. Pandiyarasan, S. Suhasini, J. Archana, M. Navaneethan, M. Abhijit, Y. Hayakawa, H. Ikeda, Journal of Applied Surface Science, DOI: 10.1016/j.apsusc.2016.12.202, 2017.

[23] M. Mo, J. C. Yu, L. Zhang, and S. A. Li, Advance Materials, 17, 756-760, 2005.

Y, Xie, J. Yuan, P. Song, S. Hu, Journal of Materials Science: Materials in Electronics, 26, 3868-3873, 2015.

[24] S. Cho, S. Jung, and K. Lee, Journal of Physical Chemistry C, 112, 12769-12776, 2008.

[25] I. A. Siddiquey, T. Furusawa, M. Sato, N. M. Bahadur, Md. M. Alam, and N. Suzuki, Journal of Ultrasonic Sonochemical, 19, 750-755, 2012.

[26] A. M. Pourrahimi, D. Liu, V. Strom, M.S. Hedenqvist, R. T. Olsson and U. W. Gedde, Journal of Materials Chemistry A, 3, 17190-17200, 2015.

[27] K. M. Wong, Y. Fang, A. Devaux, L. Wen, J. Huang, L. De Cola, and Y. Lei, Nanoscale, 3, 4830-4839, 2011.

[28] P. Uthirakumar, Y. Lee, E. Suh, C. Hong, Journal of Luminescence, 128, 287-296, 2008.

[29] D. Bucheler, A. Kaiser, F. Henning, Journal of Composites Part B, 106, 218-223, 2016.

[30] S. Lee, Journal of Fiber Polymer, 10, 295-301, 2009.

[31] L. Roza, K. A. J. Fairuzy, P. Dewanta, A. A. Umar, M. Y. A. Rahman, M. M. Salleh, Journal of Materials Science: Materials Electronics, 26, 7955-7966, 2015.

[32] F. Salleh, K. Asai, A. Ishida, and H. Ikeda, Journal Applied Physics Express, 2, 071203 (1-3), 2009.

[33] M. G. Ambia, M. N. Islam, M. O. Hakim, Journal of Materials Science, 27, 5169-5173, 1992.

[34] B. Kucukgok, B. Wang, A. G. Melton, N. Lu, and T. Ferguson, Physica Status Solidi C, 3, 894-897, 2014.

[35] D Gautam, M Engenhorst, C Schierning, R Schmechel and M Winterer, RSC Journal Materials Chemical A, 3, 189 – 197, 2015.

Summary and Proposed Future work

7.1 Summary

In this work, we focused on wearable thermoelectric power generator since the performance of the device is recycling wasted heat energy, lower production cost, scalability, long-lived power source, no side effects or harm, free from gas emission, easy to dispose of and reliable source of energy. Herein, we have adopted the solvothermal method for the coating ZnO and rGO with various nanostructures such as nanorods, nanosheets, nanospheres, and nanoporous. The seed creation and growth condition, the concentration of precursors, growth time, have been systematically studied. The as-synthesized fabric sample of functional properties was analyzed by X-ray diffraction profile, Raman spectroscopy, X-ray photoelectron spectroscopy, field emission scanning electron microscopy with mapping, transmission electron microscopy, UV shielding properties and thermoelectric properties. Besides, two different composite (Sb and Ag) were used to study the efficiency of thermopower.

A facile solvothermal method was adapted to grow the mixed nanostructures like rods and sheets without any surfactant or amine additive. Due to the two-step process, the controlled growth and optimization of the ZnO mixed nanostructures, its functional properties were investigated. It revealed the highest UPF value of 183.84 and enhanced power factor of 22 $\mu W/m.K^2$. Additionally, it is possible to observe that the connection between grains appears poorer in the case of ZnO nanorods, which resultant high resistivity. In ZnO nanosheets, boundary scattering of charge carrier is reduced in the thin film, and hence, its electrical resistivity is decreased. However, when the nanorods surrounded by nanosheets possess the intergranular electron transport is expected to be easier than nanorod, which explains the lower value of the electric resistivity qualitatively.

We have also employed two-step solvothermal method for ZnO composite with Sb-/ Ag- the coating on the cotton fabric. The growth process of ZnO is disrupted, when the Ag composites are introduced, and the growth process is again favored positive effect on the charge separation efficiency due to Ag have recombined with the Zn material. It possesses the P-type highest value of 471.9 µ/K thermopower because of intergranular crystal structure, which plays a significant role in charge transport, and the UV shielding value of 83.9. The rGO-coated fabric was successfully by the one-step hydrothermal method and improved the performance of this system by forming reduced graphene oxide on the fabric surface. The high UPF values measured as high as 442 and 32 µV/K of thermopower. Finally, carbon fabric used instead of cotton fabric to realize the difference of nonconducting and conducting fabric response towards UPF and thermopower, in this sonochemical assisted hydrothermal process involved to coat the ZnO nanostructures. Due to time duration, we obtained nanorods and nanosheets for 1h and 5h growth period respectively. The bare carbon fabric shows the UPF value of 28.62 and ZnO coated nanosheets UPF value of 201.75 due to denser coverage on carbon fabric. Similarly, ZnO coated carbon fabric about -0.04 ~ 0.054 µV/K and for bare carbon fabric it was found to be about 0.08 µV/K. It is significant to note that there was a change of carrier type from P-type to N-type resulting due to the coating of ZnO on carbon fabric.

7.2 Proposed future work

We have synthesized ZnO nanosheets porous by hydrothermal growth conditions assisted by annealing process with tunable porous sizes by adjusting the molar ratio of zinc nitrate and precursor and hexamine; then we succeed it. For examples, the Fig. 7.1 (a) to (d) shown the well-defined porous nanosheets network obtained. The synthesized ZnO nanosheets and porous nanostructured were expected high thermopower efficiency. The thermopower of fabric material should evaluate both horizontally and vertically near room temperature and Fig. 7.2 illustrates the handmade measurement system.
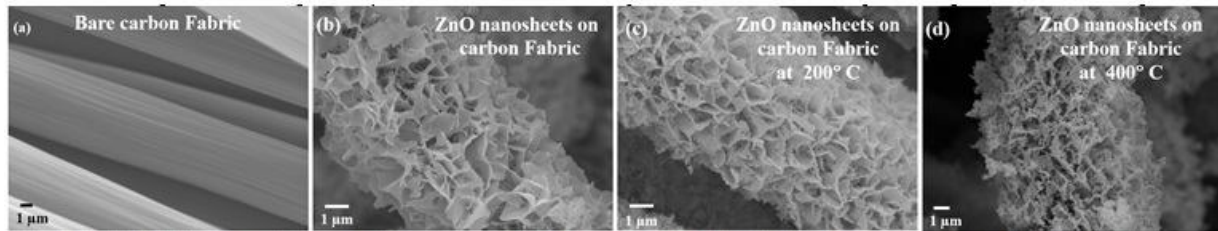
Fig. 7.1 FESEM images of bare carbon fabric (a), ZnO nanosheets (b), ZnO nanosheets with partial porous (c), ZnO nanosheets with porous network (d) coated on carbon fabric.
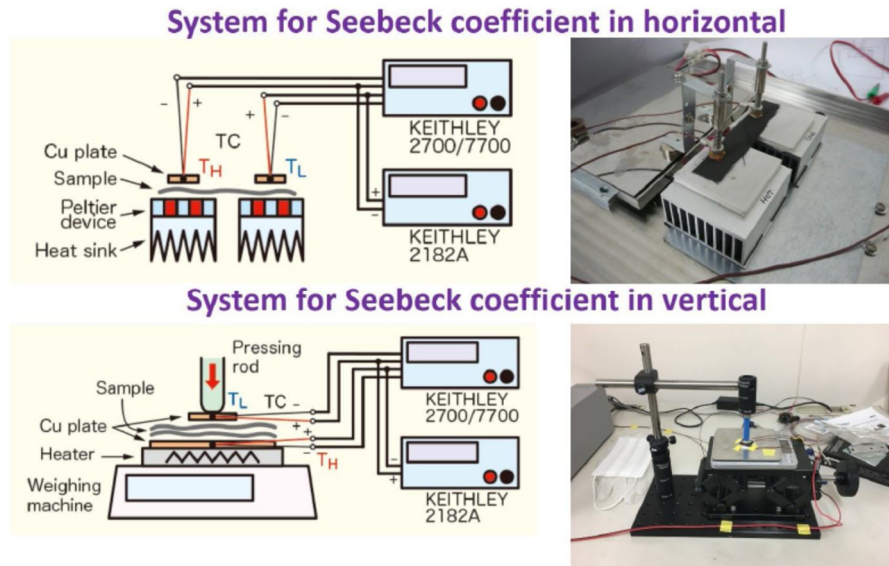
Fig. 7.2 Seebeck handmade measurement system

List of Publications and Conferences

(a) Journal Publications

1) <u>V. Pandiyarasan</u>, S. Suhasini, J. Archana, M. Navaneethan, M. Abhijit, Y. Hayakawa, H. Ikeda (2017) Fabrication of hierarchical ZnO nanostructures on cotton fabric for wearable device applications, Journal of Applied Surface Science 418: 352 – 361.

2) <u>Pandiyarasan Veluswamy</u>, Suhasini Sathiyamoothy, Faizan Khan, Aranya Ghosh, Majumdar Abhijit, Yasuhiro Hayakawa, Hiroya Ikeda (2017) Incorporation of ZnO and their composite nanostructured material into a cotton fabric platform for wearable device applications, Journal of Carbohydrate Polymers 157: 1801-1808.

3) <u>V. Pandiyarasan</u>, J. Archana, A. Pavitra, V. Ashwin, M. Navaneethan, Y. Hayakawa, H. Ikeda (2017) Hydrothermal growth of reduced graphene oxide on cotton fabric for enhanced ultraviolet protection applications, Journal of Materials letters 188: 123-126.

4) <u>Pandiyarasan Veluswamy</u>, Suhasini Sathiyamoorthy, Kalari Hanuman Chowdary, Omprakash Muthusamy, Karthikeyan Krishnamoorthy, Tsunehiro Takeuchi, Hiroya Ikeda (2017) Morphology dependent thermal conductivity of ZnO nanostructures prepared via a green approach, Journal of Alloys and Compounds 695: 888-894.

5) <u>Pandiyarasan Veluswamy</u> and Hiroya Ikeda (2016) Incorporation of polyaniline on graphene-related materials/cotton-fabric by interfacial polymerization pathway for wearable device, Asian Journal of Advance Basic Science 4(2): 94 – 97.

(b) Journal Publications (Unpublished articles)

1) <u>Pandiyarasan Veluswamy</u>, Logahewari Muniraj, Suhasini Sathiyamoothy, Faizan Khan, Majumdar Abhijit, E. Manikandan, M. Maaza, A. Umar, Yasuhiro Hayakawa, Hiroya Ikeda, Functionalization of carbon fabric with ZnO nanostructures and their wearable properties, Journal of Scientific Reports (Status: Under Review).

2) <u>Pandiyarasan Veluswamy</u>, Greeshma Girijakumari, Prashanth Kannan, Suhasini Sathiyamoorthy, Karthikeyan Krishnamoorthy, Hiroya Ikeda (2017) Investigation of functional properties of polyurethane foam with nanodispersions of carbon nanofiber, IOP Materials Research Express (Status: Under Revision).

3) <u>Pandiyarasan Veluswamy</u>, Suhasini Sathiyamoorthy, Yasuhiro Hayakawa, Hiroya Ikeda (2017) Surface engineered coating turns cotton fiber worthy for wearable properties (Status: To be submit).

4) <u>Pandiyarasan Veluswamy</u>, Suhasini Sathiyamoorthy, Hiroya Ikeda (2017) Efficiently suppressed thermal conductivity of Ag/ZnO nanostructures prepared by a facile solvothermal method (Status: To be submit).

5) <u>Pandiyarasan Veluswamy</u>, Suhasini Sathiyamoorthy, Pratik Lunagaria, Saranya T Shanmugam, D. W. Karolien, and Hiroya Ikeda (2017) Rapid surface functionalization of cotton fabrics by sonochemical synthesis of rGO/pani nanostructures with multifunctional properties (Status: To be submit).

6) <u>Pandiyarasan Veluswamy</u>, Santosh kumar Palaniamy, Suhasini Sathiyamoorthy, Chang Woo Lee, Hiroya Ikeda (2017) Rapid construction of porous ZnO nanoflowers on carbon fibers with thermally induced and their thermoelectric properties (Status: To be submit).

(c) Other Publications

1) <u>Veluswamy Pandiyarasan</u>, Jeyaram Archana, Mani Navaneethan, Salleh Faiz, Yasuhiro Hayakawa, and Hiroya Ikeda (2016) Evaluation of wearable thermoelectric power generators by Sb-/ Ag- doped ZnO nanocomposites and their properties, Journal of Institute of Electronics, Information and Communication Engineers Technical Report ED2015-122: 7-12.

2) Aamir Iqbal Waidha, <u>Veluswamy Pandiyarasan</u>, T. Anusuya, Kamran Manzoor Waidha, A. H. Shah (2015) Synthesis and characterization of silver nano rod like structures by green synthesis method using curcumin longa, International Journal of ChemTech Research 7: 1504-1508.

3) Jositta Sherine, Gnaneshwar. P. V, <u>Pandiyarasan Veluswamy</u> (2015) Synthesis and characterization of fabric coated with nano titanium oxide prepared using sol-gel, hydrothermal & sonochemical technique, International Journal of ChemTech Research 7: 1125-1134.

4) <u>V. Pandiyarasan</u>, P. Shanmugapriya, M.Y. Thanuja, T. Anusuya and P. Vairavaraja (2014) Synthesis and Characterization of ZnO Nanoparticles – A Green chemistry approach, Asian Journal of Advanced Basic Sciences 3: 94-101.

5) Annie Sujatha, <u>V. Pandiyarasan</u>, C. Muthamizhchelvan (2014) Optical and Morphological Studies of Cavity Shaped ZnS: Mn Surface Modified with L-Lysein, Procedia Materials Science 5: 592-597.

(c) Conferences

1) <u>Pandiyarasan Veluswamy</u>, Suhasini Sathiyamoorthy, Pratik Lunagaria, Saranya T Shanmugam, D. W. Karolien, and Hiroya Ikeda (2017) Rapid surface functionalization of cotton fabrics by sonochemical synthesis of rGO/pani nanostructures with multifunctional properties, 3rd Asia-Oceania Sonochemical Society Conference (AOSS – 3), Chennai, India 14th – 16th September 2017 [Poster Presentation].

2) <u>Pandiyarasan Veluswamy</u>, Faizan Khan, Shota Sakamoto, Aranya Ghosh, Manjumdar Abhijit, Masaru Shimomira, Kenji Murakami, Yusuhiro Hayakawa, and Hiroya Ikeda, High-performance multifunctional nanostructured ZnO and their composite fabric: Towards wearable device applications, 15th International Conference on Advanced Materials (IUMRS-ICAM), Kyoto, Japan 27th August – 01st September 2017 [Poster Presentation].

3) <u>Pandiyarasan Veluswamy</u>, Santosh kumar Palaniamy, Suhasini Sathiyamoorthy, Chang Woo Lee, Hiroya Ikeda (2017) Rapid construction of porous ZnO nanoflowers on carbon fibers with thermally induced and their thermoelectric properties, 4th International Conference on Nanoscience and Nanotechnology (ICONN), Chennai, India, 9th – 11th August 2017 [Poster Presentation].

4) <u>Pandiyarasan Veluswamy</u>, Faizan Khan, Shota Sakamoto, Yusuhiro Hayakawa, and Hiroya Ikeda, Porous-layered array of functionalized ZnO nanosheets on carbon fabric as a wearable material for the thermoelectric applications, 36th International Conference on Thermoelectric (ICT), California, USA 31st July – 3rd August 2017 [Poster Presentation].

5) <u>Pandiyarasan Veluswamy</u>, Faizan Khan, Shota Sakamoto, Yusuhiro Hayakawa, and Hiroya Ikeda, Selective patterned growth of ZnO nanorods/nanosheets on carbon fabric and their wearable properties, iPlasmaNano-VIII, Belgium, Europe 2nd – 6th July 2017 [Contributed Talk].

6) Faizan Khan, <u>Pandiyarasan Veluswamy</u>, Shota Sakamoto, Mani Navaneethan, Masaru Shimomura, Kenji Murakami, Yasuhiro Hayakawa, Hiroya Ikeda, Thermoelectric characteristics of nanocrystalline flexible materials for wearable power generator, 2017 Asia-Pacific Workshop

on Fundamentals and Applications of Advanced Semiconductor Devices - AWAD 2017, Gyeongju, Korea 3rd – 5th July 2017 [Oral Presentation].

7) <u>Pandiyarasan Veluswamy</u>, Greeshma Girijakumari, Suhasini Sathiyamoorthy, Manjumdar Abijit, Hiroya Ikeda, Carbon fabric functionalization @ ZnO nanostructures via solvothermal method, 8th International Conference on Advancements in Polymeric Materials APM 2017, Bangalore, India 10th – 12th February 2017 [Poster Presentation].

8) <u>Pandiyarasan Veluswamy</u>, Navaneethan M, Hayakawa Y, Hiroya Ikeda, Incorporation of polyaniline on graphene- related materials/ cotton-fabric by interfacial polymerization pathway for wearable device, 18th Takayanagi Memorial Symposium, Hamamatsu, Japan 15th & 16th November 2016 [Poster Presentation].

9) <u>Pandiyarasan Veluswamy</u>, Archana Jayaram, Navaneethan Mani, Hayakawa Yasuhiro, Hiroya Ikeda, Single step growth of ZnO nanostructures on carbon fabric by hydrothermal method for thermoelectric applications, 15th International Conference on Global Research and Education, INTER-ACADEMIA 2016, Poland, Europe 26th ー28^{th} September 2016 [Oral Presentation].

10) <u>Pandiyarasan Veluswamy</u>, Archana Jayaram, Navaneethan Mani, Hayakawa Yasuhiro, Hiroya Ikeda, Solvothermal growth of monodispersed ZnO nanostructures on carbon fabric for flexible thermoelectric applications, International conference on Flexible and Printed Electronics (ICFPE-2016), Yamagata, Japan 6th – 8th September 2016 [Oral Presentation].

11) Masaya Wanami, Selvaraj Shanthi, Yuhei Suzuki, <u>Veluswamy Pandiyarasan</u>, Faiz Salleh, Mani Navaneethan, Masaru Shimomura, Kenji Murakami, Hiroya Ikeda, Thermoelectric characteristics of flexible material with ZnO nanostructures for wearable power generator, International conference on Flexible and Printed Electronics (ICFPE-2016), Yamagata, Japan 6th – 8th September 2016 [Poster Presentation].

12) <u>Pandiyarasan Veluswamy</u>, Shota Sakamoto, Navaneethan Mani, and Hiroya Ikeda, Effect of growth time on the morphology of ZnO nanostructures on Carbon fabric for wearable device applications, SSSV and Sakura, Hamamatsu, Japan 31st August ー 5th September 2016 [Oral Presentation].

13) <u>Veluswamy Pandiyarasan</u>, Jayaram Archana, Mani Navaneethan, Salleh Faiz, Yasuhiro Hayakawa, Hiroya Ikeda, Facile preparation and thermoelectric properties of reduced graphene oxide, 63rd JSAP spring meeting, Tokyo, Japan 19th – 22nd march 2016 [Oral Presentation].

14) Wanami, Selvaraj Shanthi, Yuhei Suzuki, <u>Veluswamy Pandiyarasan</u>, Salleh Faiz, Shimomura, Kenji Murakami, ZnO Thermal diffusivity of the flexible thermoelectric material using nanostructures, 63rd JSAP spring meeting, Tokyo, Japan 19th – 22nd march 2016 [Oral Presentation].

15) <u>Veluswamy Pandiyarasan</u>, Jayaram Archana, Mani Navaneethan, Salleh Faiz, Yasuhiro Hayakawa, Hiroya Ikeda, Evaluation of wearable thermoelectric power generators by Sb-/ Ag-doped ZnO nanocomposites and their properties, Technical committee on Electron Device (ED), Hokkaido, Japan 03rd – 04th March, 2016 [Oral Presentation].

16) <u>Pandiyarasan Veluswamy</u>, Suhasini Sathiyamoorthy, Faiz Salleh, Yuhei Suzuki, and Hiroya Ikeda, Preparation and thermoelectric characterization of zinc oxide nanoflakes on In-Situ fabrication of cotton fabric, 23rd National Heat and Mass Transfer Conference and 1st International ISHMT －ASTFE Heat and Mass Transfer Conference, Kerela, India 17th － 20th December 2015 [Oral Presentation].

17) <u>Pandiyarasan Veluswamy</u>, Suhasini Sathiyamoorthy, Faiz Salleh, Yuhei Suzuki, and Hiroya Ikeda, Influence of Sb- and Ag- doping ZnO cotton fabric: Enhancement of Seebeck coefficient performance, International Conference on Advances in Functional, Smart and Innovative Textiles (AFSIT - 2015), Coimbatore, India 10th － 12th December 2015 [Oral Presentation].

18) <u>Pandiyarasan Veluswamy</u>, Kalari Hanuman Chowdary, Medapati Basivi Reddy, Anusuya Thangaraj, and Hiroya Ikeda, Retainability of ZnO Nanorods on In-Situ cotton fabric for UV-Protection, International Conference on Nanomaterials and Nanotechnology (NANO-15), Thiruchengodu, India 7th － 10th December 2015 [Poster Presentation].

19) <u>V. Pandiyarasan</u>, F. Salleh, and H. Ikeda, Ag doped ZnO nanocomposites with enhanced Seebeck effect, 17th Takayanagi Memorial Symposium, Hamamatsu, Japan 11th & 12th November 2015 [Poster Presentation].

20) <u>V. Pandiyarasan</u>, S. Faiz, Y. Suzuki, and H. Ikeda, Enhanced Room-Temperature Thermoelectric Performance of CGNs Cotton Fabric through Ultrasonically Assisted Hydrothermal Approach, 14th International Conference on Global Research and Education, INTER-ACADEMIA 2015, Hamamatsu, Japan 28th － 30th September 2015 [Oral Presentation].

21) <u>V. Pandiyarasan</u>, Y. Suzuki, F. Salleh, M. Omprakash, M. Navaneethan, Y. Hayakawa, and H. Ikeda, Preparation and Characterization of Polyethyleneimine Functionalized as Reduced Graphene Oxide for Thermoelectric Applications, The 76th JSAP Autumn Meeting, Nagoya, Japan 13th －16th September 2015 [Oral Presentation].

22) <u>V. Pandiyarasan</u>, F. Salleh, Y. Suzuki, J. Archana, M. Navaneethan, Y. Hayakawa, and H. Ikeda, Wearable Thermoelectric device with UV Protection, SSSV and Sakura, Hamamatsu, Japan 1st － 5th September 2015 [Oral Presentation].

23) Avik Ghosh, Akshay Borde, Jayabrata Das, and <u>Pandiyarasan Veluswamy</u>, In-Situ Synthesis of ZnO Nanorods on cotton fabric using hydrothermal route for UV-Protective, Antibacterial and Retainability studies, National conference on Biotechnological approach towards Environmental Sustainability and Conservation, Chennai, India 19th March 2015, Bharath University [Oral Presentation].